MSc Thesis in Civil Engineering and Geosciences

Effect of cyclic wetting and drying on soil erodibility

Alexey Dolgov

2024

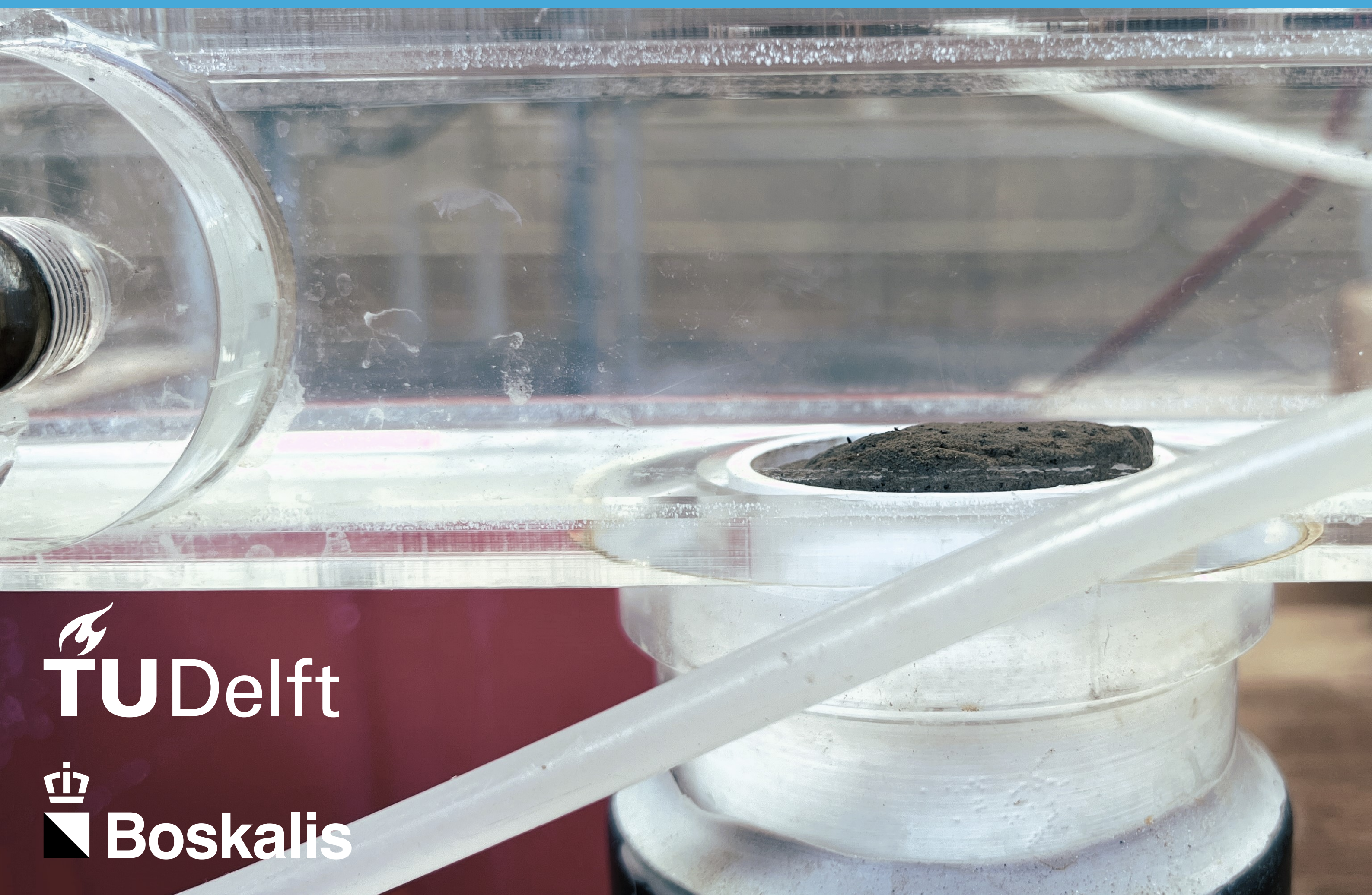

TU Delft

Boskalis

Master Thesis in Applied Earth Sciences

Effect of cyclic wetting and drying on soil erodibility

Alexey Dolgov

March 2024

A thesis submitted to the Delft University of Technology in partial fulfillment of the requirements for the degree of Master of Science in Applied Earth Sciences.

Alexey Dolgov: *Effect of cyclic wetting and drying on soil erodibility* (2024)

The work in this thesis was carried out in the:

Civil Engineering and Geosciences

Delft University of Technology

Royal Boskalis N.V.

Supervisors:	Prof. Cristina Jommi
	ir. Patricia Ammerlaan
Co-readers:	Dr. ir. Buu-Long Nguyen
	Dr.ir. Anne-Catherine Dieudonné
	Prof. Juan Pablo Aguilar-López

Abstract

Cyclic wetting and drying impact the integrity of cohesive clay materials in geotechnical engineering applications. Boom Clay, frequently used in erosion protective layers, presents a critical case study due to its widespread application and the environmental conditions it endures. This research delves into the effects of repeated wetting and drying cycles on Boom Clay's erodibility, a process that protective layers often undergo during construction and exposure.

Utilizing the Erosion Function Apparatus (EFA), performed experiments targeted changes in the structure and erosion resistance of Boom Clay under cyclic conditions. The test setup was adjusted, improved, and calibrated. It was observed that these cycles induce alterations in the clay's erodibility, contrasting with the behavior of untreated samples.

The results demonstrated cyclic wetting and drying increases the susceptibility of the material to erosion, and the rate of erosion, and decreases the threshold of the erosion process. This study enhances our understanding of how environmental stressors influence the long-term behavior of erosion protection materials. It provides engineers and environmental planners with insights for selecting and assessing materials for erosion protection, emphasizing the importance of considering environmental conditions in their design and application.

Contents

List of Figures

List of Tables

Acronyms

BET Borehole Erosion Test

CFD Computational Fluid Dynamics

EFA Erosion Function Apparatus

ESTD Ex Situ Scour Testing Device

FSOS Full-Scale Overtopping Simulator

HET Hole Erosion Tests

HR Homogenized Reconstitution Method

IR In-situ Retrieval Method

ISEEP In Situ Erosion Evaluation Probe

JET Jet Erosion Tests

LI Liquidity Index

LL Liquid Limit

NCHRP National Cooperative Highway Research Programs

PI Plasticity Index

PL Plastic Limit

RETA Rotational Erosion Testing Apparatus

SC Simulated Construction Method

SERF Subaqueous Erosion Rate Flume

SET Slot Erosion Test

SRICOS Scour Rate in Cohesive Soils (Model)

STD Scour Testing Device

1 Introduction

1.1 Background

Soil erosion impacts the stability and integrity of various civil infrastructures. The erosion protective layers are essential in safeguarding embankments, dikes, levees, and coastal structures against erosive forces. Their effectiveness depends on the erodibility of the materials used, typically assessed through established classifications. Such classifications guide the selection of appropriate materials for constructing erosion-resistant structures, balancing durability and environmental compatibility.

This research spotlights an uncertainty in geotechnical engineering: the potential discrepancy between the expected and actual behavior of materials post-construction. While clay materials are chosen for their known properties and anticipated erosion response, the extent to which repeated wetting and drying cycles alter these properties remains a question. Addressing this gap, the study investigates changes in the material's erodibility due to cyclic wetting and drying, aiming to provide a clearer understanding of what erodibility parameters can be expected in real-world conditions post-construction.

Boom Clay, is a material that is used for the construction of erosion-protective layers of dykes in the Netherlands. However, during the construction period and exploitation, clay material may be exposed to wetting and drying cycles due to natural precipitation or else, which can alter the erodibility of a material. Frequently, layers initially exposed undergo subsequent coverage by vegetation, yet the changes incurred during prior cycles remain a pivotal factor in their long-term performance.

While the effects of wetting and drying cycles on clay properties have been extensively studied, and laboratory tests on clay erodibility are well-documented, there remains a gap in research that combines these two areas. Few studies have thoroughly investigated the impact of wetting and drying cycles on the erodibility of clay in laboratory settings.

1.2 Research Significance

Understanding the impact of environmental factors like wetting and drying cycles on soil erodibility is vital, especially in the face of climate change and its associated impacts. This research seeks to address the crucial question:

"How do the erodibility of cohesive clay materials change during cyclic wetting and drying, and what causes these changes?"

By exploring this question, the study aims to contribute valuable insights into soil behavior under fluctuating moisture conditions, aiding in the development of more resilient geotechnical solutions.

1.3 Objectives

The overarching goal of this research is to conduct comprehensive wetting and drying cyclic experiments on different cohesive clay soils that are commonly used in anti-erosion protective layers. The study will evaluate changes in clay before and after these cycles. The goals of the study are:

1. Identifying the range of soils typically used as anti-erosion cover.
2. Studying the state-of-art approach to estimate and arrange soil erodibility.
3. Studying the effect of wetting and drying cycles on soil.
4. Experiencing the set-up and use of an Erosion Function Apparatus.
5. Processing the EFA output data.
6. Examining the accuracy and limitations of existing soil erodibility models.
7. Estimating the effect of cyclic wetting and drying on soil erodibility.

1.4 Methodological Approach

Laboratory erosion testing allows for studying soil erodibility, with the Erosion Function Apparatus (EFA) being commonly used in these studies. In this research, Boom Clay has been selected as the primary material for investigation. Its widespread use in erosion protection layers makes the findings highly relevant for practical applications. Additionally, Boom Clay's extensive study in previous research provides a robust knowledge base, complemented by the ample availability of the material for thorough examination.

The study also examines Kleirijperij clay, characterized by its high organic content and erodibility according to current classifications. This inclusion offers a comparative analysis with a significantly different soil type.

Sample preparation methods aim to mirror real-life construction practices, achieve sample homogeneity, and preserve the natural heterogeneity of clay. These techniques ensure a diverse range of samples for in-depth analysis.

Central to the research is the replication of wetting and drying cycles within a controlled laboratory setting, allowing for the precise observation of soil behavior under environmental stressors.

The EFA setup will be calibrated, followed by testing on clay samples subjected to wetting and drying cycles. The analysis of collected data will determine how these cycles affect soil properties and erodibility.

In conclusion, test outcomes will be evaluated through two models, providing a comprehensive data interpretation. This approach enhances the study's relevance to addressing practical engineering and environmental challenges.

1.5 Thesis Structure

This thesis is organized as follows:

Chapter 1 gives an introduction to the study, defining the research question and goals and highlighting the approach to achieve it.

Chapter 2 provides a detailed review of existing literature on soil erosion, emphasizing the influence of environmental factors on clay soil properties.

Chapter 3 outlines the methodology, focusing on the application of the Erosion Function Apparatus for testing Boom Clay under varied conditions.

Chapters 4 and 5 present observations and results from the erosion tests, illustrating the effects of cyclic wetting and drying.

Chapter 6 conducts a comparative analysis of the findings in the context of existing erosion prediction models.

Chapter 7 concludes with key insights and recommendations for future research, emphasizing the practical implications of these findings in geotechnical engineering.

Appendixes A - F provides raw data on sample preparation and erosion testing.

2 Literature Study

2.1 Erosion mechanism overview

Erosion is a group of processes that refers to the phenomena instigated by surface activities, like the movement of water or wind and temperature fluctuations, which dislodge and transport soil, rock, or solubilized material, depositing it at a different location. Geotechnical studies investigate the effect of erosion on the stability and integrity of infrastructure and earth structures among others (Julien [2010]).

Erosion triggered by the fluid flow, based on its occurrence in the environment, can be categorized into two main types (Briaud et al. [2019]:

1. Internal erosion, occurs when fluid flows within the soil mass or structure and leads to the progressive removal of soil particles. In engineering practice, it occurs in scenarios involving seepage through structures such as embankment dams, levees, and canal-side embankments.
2. Surface erosion, affects the surface layer of the soil due to the direct impact of flowing water or wave action, leading to soil displacement and changes in landscape or structure stability. In the built environment, this type should be addressed in bridge scour, overtopping of levees and dams, erosion of highway embankments, and the migration of river meanders.

In this study, the surface erosion and erodibility of cohesive materials triggered by a water flow will be reviewed. Water exerts normal stress or hydrostatic pressure on the surrounding soil particles, and at the same time, the flow applies the shear stress to the soil mass (Annandale [1995]). When water begins to flow over the cohesion material, three processes occur (Briaud et al. [2019]):

1. A drag force and corresponding shear stresses form at the interface between the soil particle and the flowing water.
2. The normal stress on top of the soil particle is reduced compared to the steady state due to the water flow. As the velocity around the particle or obstacle increases, the pressure drops by Bernoulli's principle to maintain energy conservation.
3. The normal and shear stresses at the boundaries experience time fluctuations because of water turbulence. These fluctuations, originating from the formation and dissipation of eddies, vortices, ejections, and sweeps in the flowing water, can significantly contribute to the erosion process, particularly at higher velocities.

The combination of these two forces - shear (drag) force and normal (uplift) force at a certain stage triggers the disassociation of soil particles from the soil body.

In the following equations:

$\dot{z}$- erosion rate $[mm/s]$ or $[g/s]$.

v - flow velocity $[mm/s]$.

v_c - critical velocity $[mm/s]$.

τ - hydralic shear stress $[Pa]$.

τ_c - critical shear stress $[Pa]$.

$\Delta\tau$ - change in hydralic shear stress $[Pa]$.

$\Delta\sigma$ - turbulent fluctuation of net uplift normal stress $[Pa]$.

ρ_w - mass density of water $[kg/m^3]$.

k - erodibility (detachment) coefficient $[\frac{m^3}{N \cdot s}]$.

$m, m', n, p, \alpha, \beta, \upsilon$ - model coefficients depending on the properties of the soil $[-]$.

Erodibility is defined as the relationship between erosion rate ($\dot{z}$) and flow velocity (v) at the soil-water interface (Equation 2.1).

$$\dot{z} = f(v) \tag{2.1}$$

In his article, Emmanuel Partheniades (Partheniades [2009]) revised the development of erosion studies, highlighting a shift from the initial concept of the predominant role of flow velocity in causing erosion to the shear stress applied by the flow. This transition occurred as researchers recognized that shear stress, rather than velocity, directly impacts soil particles' detachment and transportation. The following definition connects erosion rate to shear stress at the soil-water interface (Equation 2.2). Further researchers mentioned that the value of the mean flow velocity is less representative than the shear stress since the velocity varies within the flow (Shafii et al. [2016]).

$$\dot{z} = f(\tau) \tag{2.2}$$

Normalizing Equation 2.2, soil erodibility can be defined concerning the critical velocity (v_c), the value of shear stress applied by the flow ($/tau$), and critical shear stress, as proposed by Shafii et al. (Shafii et al. [2016]) in the Equation 2.3 as an attempt to represent the constitutive law for erosion, similar to a stress-strain curve for settlement problems.

$$\frac{\dot{z}}{v_c} = \alpha(\frac{\tau - \tau_c}{\tau_c})^m \tag{2.3}$$

The development of erosion models and equations typically adheres to a threshold-based framework, where erosion is initiated only upon surpassing a critical value, either of flow velocity or shear stress. Within this framework, no erosion is observed below this critical threshold, once exceeded, the rate of erosion increases in correlation with the increase in flow velocity or shear stress (Stein and Nett [1997]; Hanson and Cook [1997]; Simon et al. [2010]; Prooijen and Winterwerp [2010]; Shafii et al. [2016]; Briaud et al. [2019]). This framework may be illustrated by the erosion function curve (see Figure 2.1) with erosion rate plotted against the flow velocity or shear stress, obtained through laboratory tests of the same clay material in different flow conditions (Briaud et al. [2019]).

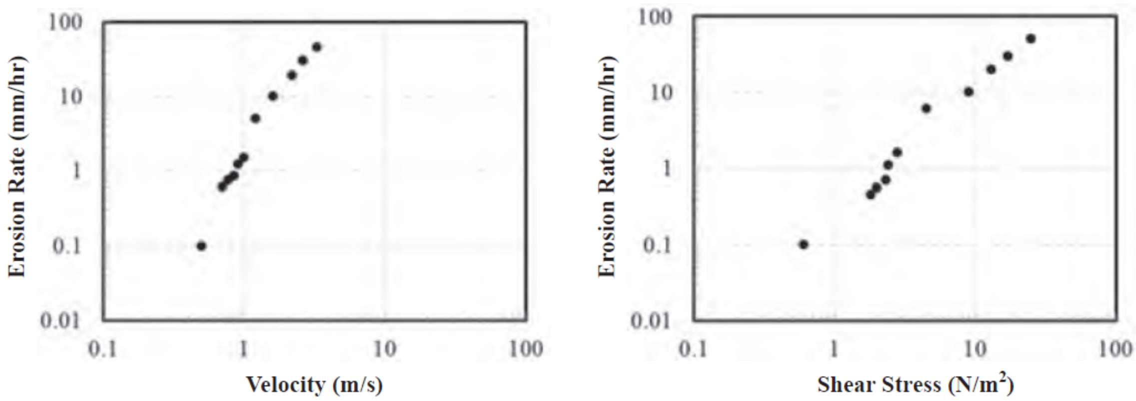

Figure 2.1: Examples of erosion function (Briaud et al. [2019]).

While the definition based on shear stress marks an advancement over velocity-based descriptions in understanding erosion mechanisms, it doesn't entirely capture the complexity of the process. The erosion rate is influenced not only by shear stress but also by normal stress fluctuations, intensified by turbulence within the flow. These fluctuations cause the disassociation of soil particles or aggregates that are then carried away by the drag force of the flow (Briaud [2008]; Shafii et al. [2016]; Zihan [2018]. This was expressed by Shafii et al. [2016] in the following Equation 2.4:

$$\frac{\dot{z}}{v} = \alpha(\frac{\tau - \tau_c}{\tau_c})^m + \beta(\frac{\Delta\tau}{\rho_w v^2})^n + \gamma(\frac{\Delta\sigma}{\rho v^2})^p \tag{2.4}$$

With:

- $\Delta\tau$ - turbulent fluctuation of the hydraulic shear stress [Pa].
- $\Delta\sigma$ - turbulent fluctuation of the net uplift normal stress [Pa].
- m, n, p - model parameters characterizing the material [-].

This model is comprehensive, but practical application is currently limited due to the extensive parameter requirements. The direct measurement of normal stress was addressed in several studies. Shan et. al. (Shan et al. [2012]) developed a direct force gauge as a part of an Ex-situ Scour Testing Device. The direct force gauge and a sensor disk were used to measure the horizontal and vertical stress on the surface of the sample during the erosion process caused by the water flow. Maali et. al. (Maali et al. [2012]) employed colloidal probe Atomic Force Microscopy (AFM) in a drainage experiment to measure the slip length and the drag force experienced by microstructured surfaces. Most methods involving the direct measurement of normal stress require a complex setup and equipment.

Currently, the equation 2.3 is widely recognized (Shan et al. [2015a]; Shafii et al. [2016]; Briaud et al. [2019] and will be used in this study.

2.2 Erodibility parameters

Transitioning from the soil erosion mechanisms, this section introduces and explicates parameters utilized in laboratory tests to quantify soil erodibility. It describes both measured and calculated parameters that allow quantifying the erosive behavior of materials under controlled conditions.

2.2.1 Erosion Rate

The erosion rate, represents the rate at which material is eroded. In different applications, it may be expressed as follows:

General Erosion Rate (Volume/Area/Time): quantifies the amount of material eroded from a given area in a specific time, typically expressed in units such as cubic meters per square meter per year (e.g., $m^3/m^2/hr$). This parameter originates from agricultural studies (Hudson [1993]) and is used in large-scale erosion models such as the Revised Universal Soil Loss Equation (RUSLE) and the Modified Universal Soil Loss Equation (MUSLE) (Morgan [2005]).

Linear Erosion Rate (Length/Time): In laboratory settings, especially when using test apparatus (Jet Erosion Tests (JET), EFA), linear erosion rate may be used, expressed in height of a soil sample eroded in a certain time (e.g. mm/s). This measurement focuses on the depth of material eroded over time, indicating how quickly the surface is being lowered due to erosion. This parameter is used in several laboratory researches on soil erodibility (Briaud et al. [2001]; Briaud [2008] along with studies on in-situ erosion tests (Hanson and Simon [2001].

Erosion Rate by Mass (Mass/Time): is another laboratory based measurement. The erosion rate is expressed in terms of the mass of material eroded per unit of time (e.g., g/s). This measurement provides a direct understanding of the quantity of material being lost due to erosion, regardless of the area it covers. It is used to quantify material erodibility in laboratory tests as RETA and EFA (Bloomquist et al. [2012].

Laboratory tests such as the EFA tests, JET, and Hole Erosion Tests (HET), as well as in-situ tests, are used to directly measure the erosion rate under controlled conditions. These measurements can then be used to calibrate and validate erosion models (Briaud [2008]; Simon et al. [2010]).

As a complex parameter that describes the process of erosion, it is influenced by a combination of various factors:

- **Soil properties**: The mineralogical composition, texture (proportion of sand, silt, and clay), structure, porosity, and organic matter content of the soil all play significant roles in determining its erodibility. Soils with high clay content, for instance, tend to be more resistant to erosion than sandy soils.

- **Water flow parameters**: The velocity and depth of the flow, as well as the hydraulic shear stress exerted by the water on the soil surface, are crucial factors. Higher flow velocities and shear stress levels can lead to an increased erosion rate.
- **Water and soil content**: The chemical composition of the water, including its pH and the concentration of various ions, can affect the erosion process. Certain ions can promote soil aggregation, thereby reducing erodibility, while others can have the opposite effect.
- **External conditions**: The temperature can influence the viscosity of water and the rate of chemical reactions, thereby indirectly affecting the erosion rate. Additionally, factors such as freeze-thaw cycles can also influence soil erodibility.
- **Characteristics of the flow**: These encompass not only the velocity of the flow but also its temporal fluctuations, notably cyclic loading that may occur due to repeated wetting and drying cycles. Such changes in hydraulic conditions can significantly impact the rate and nature of erosion, with potentially severe effects observed under conditions of rapid flow variations.

Furthermore, the characteristics of vegetation cover and land use practices can markedly impact the erosion rate in natural environments. These influences have been investigated in previous studies (Bijlard [2015]; Rinsum [2018]) and will not be researched in the current one, which focuses on erosion characteristics of clay material.

2.2.2 Shear stress and flow velocity

Shear stress τ is the force per unit area exerted by the moving water on the soil or sediment surface and is typically expressed in Pa. In erosion processes, the hydraulic shear stress causes detachment of soil particles and initiates erosion.

The initial approach to measuring hydraulic shear stress at the soil-water interface involved taking pressure readings before and after the soil sample, for example using standpipe manometers. However, due to the small and fluctuating differences in water levels caused by turbulent flow, these were replaced by a sensitive differential transducer for more accurate measurements. The method was accurate for coarse-grained soils, but the presence of a small protrusion during the testing of fine-grained soils on an EFA introduced significant errors in the calculations as it induced a roughness much larger than the natural roughness of the soil. An experiment conducted with an aluminum cylinder replacing the soil sample in the EFA showed the considerable influence of the protrusion on the calculated shear stress (Briaud et al. [2001]). Currently, the following methods are used within various lab and in-situ tests to assess the value of shear stress during the experiment:

1. Calculation from the flow velocity: As water flows over a surface, it exerts a force tangential to that surface. This force, divided by the surface area over which it's applied, results in a shear stress. Changes in pressure or velocity can indicate changes in this force, and hence in the shear stress. (Briaud et al. [2001])
2. Differential Pressure Transducer: To overcome the limitations of direct pressure measurements, a sensitive differential pressure transducer can be used. This method supplies more accurate measurements of the small and fluctuating differences in water levels caused by turbulent flow (Crowley et al. [2012]).
3. Computational Fluid Dynamics (CFD): CFD can also be used to estimate the shear stress on the soil sample. This method involves the numerical solution of the Navier-Stokes equations, which govern fluid flow, to predict the stress distribution on the soil surface. This method is computationally intensive and requires specialized software (Heijmeijer [2019]; Rook [2020]).

In EFA tests shear stress is calculated from the measured value of the flow velocity and is proved by Briaud (Briaud et al. [2001]) as acceptably accurate for fine-grained soils with a tendency to overestimate the value of shear stress when compared to Computational Fluid Dynamics (CFD) models (Briaud et al. [2019]). The shear stress τ is calculated as follows:

$$\tau = 1/8 f \rho v^2 \tag{2.5}$$

with:

τ - shear stress $[Pa]$.

f - roughness factor obtained from the Moody diagram $[-]$.

ρ - mass density of water $[kg/m^3]$.

v - mean flow velocity in the pipe $[mm/sec]$.

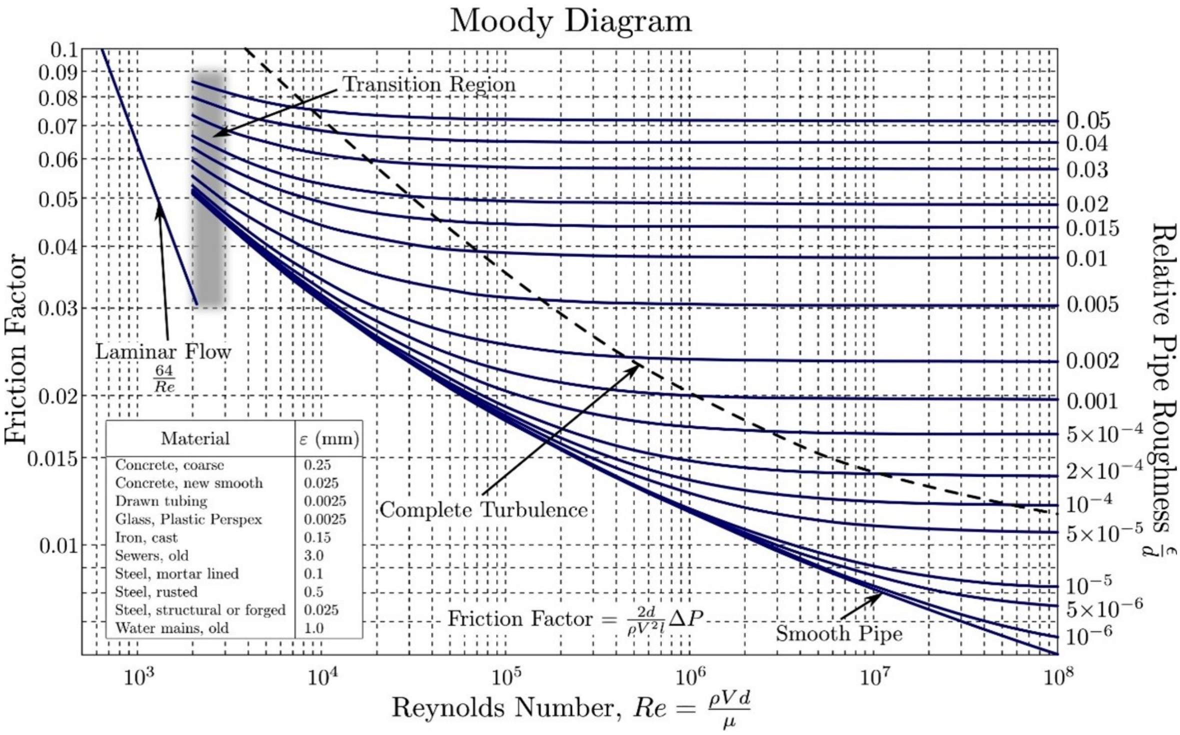

Figure 2.2: Moody diagram showing the Darcy–Weisbach friction factor f plotted against Reynolds number Re for various relative roughness ϵ/D

The value of the roughness factor is obtained from the Moody's chart (see Figure 2.2). The value of roughness elements ϵ is taken as $1/2D_{50}$ with the assumption that only half of the single soil particle is exposed to the flow. While the Moody diagram is primarily designed for circular pipes, it can be adapted for calculating shear stress in rectangular ducts like fumes. By using the hydraulic diameter in place of the actual diameter, the diagram's friction factor can be approximated for rectangular geometries. According to the series of laboratory tests, this approach results in an error of about 10% in the estimation of both shear stress and erosion rate during an EFA test (Briaud et al. [2001]).

From (Equation 2.3) it is possible to trace the direct dependency of τ on the flow velocity and depth along with the factors that affect the flow: the slope of the surface, fluid properties, etc., so it is characterized by the parameters of the flow (Ariathurai and Arulanandan [1978]). However, the roughness of the eroded surface, which may be described with D_{50} in the case of eroding soil also affects this parameter.

The group of laboratory rotating cylinder tests, such as Rotating Cylinder Apparatus (Moore and Masch Jr. [1962]), Improved Rotating Cylinder Test (Chapuis and Gatien [1986]) or RETA (Bloomquist et al. [2012]) utilize the calculation of shear stress on the soil surface from the value of torque applied to the rotating cylinder. Bloomquist et al. [2012] proposes the following equation (2.6) for the Rotating Erosion Testing Apparatus.

$$\tau = \frac{T}{2\pi R^2 L} \tag{2.6}$$

with:

τ - average shear stress acting on the sample surface $[Pa]$.

R - sample radius $[mm]$.

L - sample length $[mm]$.

T - torque $[N/m^2]$.

2.2.3 Critical shear stress

The critical shear stress, usually denoted as τ_c, represents the threshold shear stress required to initiate soil particle detachment or to start the erosion process and typically expressed in Pa. Below this value, the cohesive and frictional forces within the soil are strong enough to resist the hydraulic forces imposed by the water, and no erosion occurs. Above this value, the hydraulic forces exceed the soil's internal resistance, and erosion begins (Ariathurai and Arulanandan [1978]).

The studies first were conducted on a non-cohesive material. The equilibrium of a single particle of a non-cohesive material leads to the following equations that describe sliding (Equation 2.7) and rolling (Equation 2.8) mechanisms (White and Ingram [1940]). These mechanisms with the acting forces are schematically described in Figure 2.3 (a and b).

$$\tau_c A_e = W tan(\phi) \tag{2.7}$$

$$\tau_c A_e \alpha = W b \tag{2.8}$$

with:

A_e - effective friction area of the water on the particle [-];

W - submerged weight of the particle [g];

ϕ - friction angle of the interface between two particles [°];

α - ratio of the effective friction area of the particle [-].

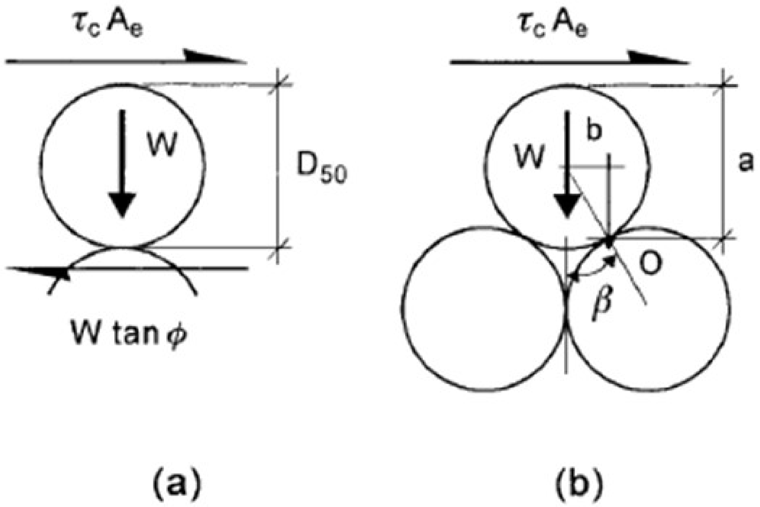

Figure 2.3: Forces applied to soil grain during scour: sliding (a) and rolling (b) (Briaud et al. [2001])

These basic conditions were then elaborated by Briaud (Briaud et al. [2001]) to the following equations for sliding (Equation 2.9) and rolling (Equation 2.10) mechanisms:

$$\tau_c = 2\frac{(\rho_s - \rho_w) g tan(\phi)}{3\alpha} \tag{2.9}$$

$$\tau_c = 2\frac{(\rho_s - \rho_w) g sin(\phi)}{3\alpha(1 + cos(\beta))} \tag{2.10}$$

with:

α - ratio of the effective friction area over the maximum cross-section of the spherical particle [-];

D_{50} - mean diameter representative of the soil particle size distribution [mm];

ρ_s and ρ_w - mass density of the particles and of water[g/cm^3];

g - gravitational acceleration [mm/s].

Briaud in his study also showed that the value of τ_c is proportional to D_50. This model presumes the following simplifications:

- The soil is non-cohesive.
- All grains are spherical.
- Electromagnetic, electrostatic, and chemical bonds between particles are neglected.

These simplifications make this model rather inapplicable for accessing the erodibility of fine-grain soils. However, it provides an understanding that the value of τ_c mostly depends (besides the acting shear force generated by a flow) on the granular composition of a material and bonding forces between these grains.

The common practice nowadays (Briaud et al. [2001], Hanson et al. [2005], Simon et al. [2010], Briaud et al. [2019]) is to determine the value of critical shear stress directly through laboratory tests such as the EFA or the HET, or in-situ tests such as the in-situ JET. During these tests, the hydraulic stress is gradually increased until the onset of erosion is observed, allowing for the determination of the critical shear stress.

The value of the critical shear stress is highly dependent on the soil's physical and mechanical properties, including its texture, structure, and organic matter content, among others. It is also influenced by environmental conditions and flow parameters. Therefore, this parameter can vary significantly from one soil to another, and within the same soil under different conditions (Rahimnejad and Ooi [2016]).

2.3 Laboratory and In-Situ Erosion Testing Methods

In the study of erosion processes, laboratory, and in-situ tests play a pivotal role in gathering essential data about the erodibility of soils. These tests fall into two broad categories: those measuring surface erosion and those assessing internal erosion. This section will describe several erosion tests with a focus on surface erosion laboratory tests.

2.3.1 Erosion Function Apparatus (EFA)

The Erosion Function Apparatus (EFA), initially developed at Texas A&M University in the early 1990s, is a widely used tool for assessing the erodibility of a broad spectrum of soils, ranging from cohesive to non-cohesive types, and even soft rocks. Soil samples, typically obtained via ASTM standard Shelby tubes, are subjected to water flow within a specially designed rectangular cross-section. The water flow's intensity is adjustable and measured by an in-line flow meter. The soil sample is methodically exposed to the eroding fluid by a piston which pushes it into the flow. The principal scheme of an EFA is depicted in Figure 2.4.

The EFA test procedure, as outlined by Briaud et al. [2001], starts with positioning one end of the tube on a circular plate piston and pushing it upward until it aligns with the bottom surface of the rectangular pipe. The pipe is then filled with water and left undisturbed for an hour. Following this, the water flow is initiated at a low velocity, typically $0.2m/s$, and the time recording starts. Throughout the test, it is crucial to maintain the soil surface flush with the pipe's bottom by continuously adjusting the piston as the water erodes the soil, thereby preserving a level interface. This process continues until 50 mm of the soil has eroded or 30 minutes have passed, whichever occurs first. The height of the erosion is determined by noting the change in the piston's bottom position. The entire procedure is then repeated for increasing flow velocities, ranging from $0.6m/s$ up to $6m/s$, in specified increments.

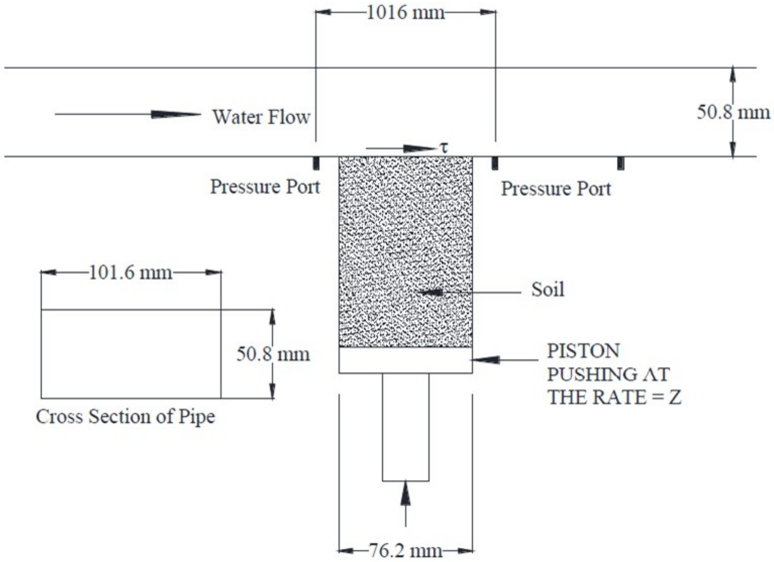

Figure 2.4: EFA schematic diagram Briaud et al. [2019]

The erosion rate is then plotted against flow velocity, and the shear stress exerted on the soil surface is determined using the Moody chart Briaud et al. [2001].

A variation of the EFA, **The Subaqueous Erosion Rate Flume (SERF)** developed by Sheppard and his team at the University of Florida and was used to assess the erodibility of both cohesive and non-cohesive sediments. The SERF is essentially a long, elevated rectangular channel equipped with two high-capacity parallel pumps that feed water from a large tank (see Figure 2.5). The dual pump system caters to harder soil samples that may require more force Crowley et al. [2012].

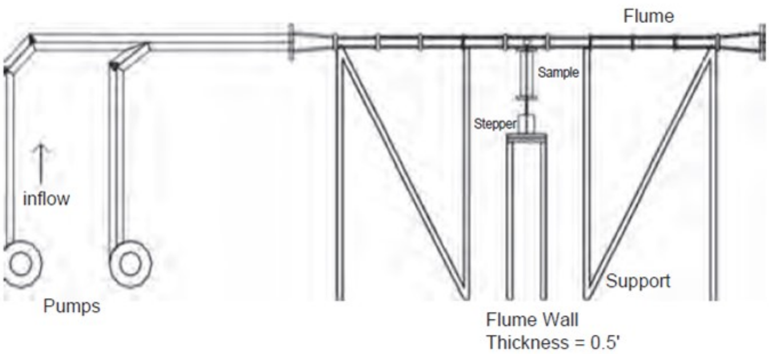

Figure 2.5: SERF apparatus at the University of Florida - a schematic diagram Crowley et al. [2012].

A key feature of the SERF is its automation: a control computer continuously monitors the erosion of the sample, aided by a video camera and an array of sonic transponders positioned over the test section. These transponders measure the mean elevation of the sample surface, informing the computer when to advance the piston and keep the sample surface flush with the flume base. The erosion rate is determined by the sum of the upward movements recorded for a specific flow velocity (shear stress) divided by the corresponding time period, and the pressure drop in the flume is also calculated (Briaud et al. [2019]).

Advantages

1. Soil samples may be obtained directly from the field to minimize its disturbance. Additionally, man-made samples may be also tested.

2. Direct readings of a flow (critical) velocity and direct assessment of erosion rate. Since the erosion function represents the erodibility of the soil at the element level, may be used to evaluate internal erosion.

3. A wide range of soils may be tested.

Disadvantages

1. The values of shear stress and critical shear stress are estimated from the average velocity according to the Moody chart and the average value of flow velocity is used.

2. The maximum size of particles is limited by the sample diameter.

2.3.2 Rotational Erosion Testing Apparatus (RETA)

The Erosion Centrifuge, also known as the **Rotational Erosion Testing Apparatus (RETA)**, is a globally used device for measuring erosion resistance. This instrument tests a cylindrical soil specimen by rotating water around it and assessing the sample's weight loss (see scheme on Figure 2.6).

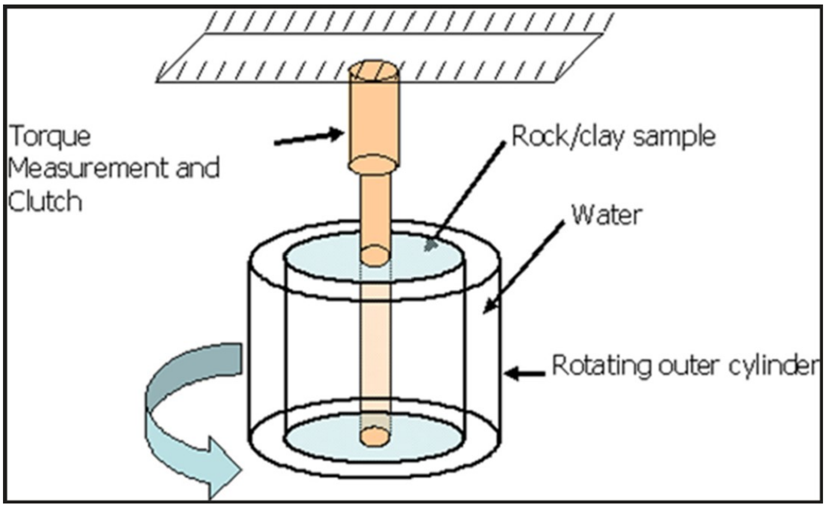

Figure 2.6: A scheme of a Rotational Erosion Testing Apparatus Bloomquist et al. [2012]

The outline of a test on an erosion centrifuge is as follows (Bloomquist et al. [2012]):

1. To account for potential surface disturbances from sampling, transport, and test preparation, a preconditioning run is carried out to remove any surface artifacts. The duration and torque depend on the estimated impact of erosion on the structure under consideration.

2. After the preconditioning run, the sample is rinsed, and returned to the cylinder, and the water in the annulus, containing eroded particles, is replaced.

3. A series of shear stresses are chosen for the test, with a minimum of three and preferably five tests performed. The RETA is then run at the lowest selected shear stress for a duration that depends on the type of soil or rock.

4. Once a test run is complete, the sample is carefully raised and rinsed into a container holding the eroded material. This container is then dried and weighed to determine the eroded mass.

5. The procedure is repeated for the remaining selected shear stresses until the testing sequence is completed. Each time, a new container is used, and the sample is refilled with water before the new shear stress is applied.

The primary measurements taken during the RETA test are the torque applied to the rotation cell and the mass loss of the sample. The value of the shear stress applied to the sample is then calculated according to the Equation 2.11 (Bloomquist et al. [2012]):

$$\tau = \frac{T}{2\pi R^2 L} \tag{2.11}$$

with:

τ - average shear stress on the sample surface $[Pa]$;

T - torque $[Nm]$;

R - sample radius $[mm]$;

L - sample length $[mm]$.

The measured change in sample mass is then used to obtain the value of the average eroded thickness 2.12 (Bloomquist et al. [2012]):

$$\Delta R = \sqrt{\frac{\Delta m}{2\pi \rho L}} \tag{2.12}$$

with:

ΔR - average eroded thickness $[mm]$;

Δm - change in sample mass $[g]$;

ρ - sample density $[g/cm^3]$;

L - sample length $[mm]$.

The rate of erosion may be calculated using obtained data as follows 2.13 (Bloomquist et al. [2012]):

$$\dot{z} = \frac{\Delta R}{\Delta t} \tag{2.13}$$

with:

$\dot{z}$ - linear erosion rate $[mm/sec]$;

ΔR - average eroded thickness $[mm]$;

Δt - test duration $[s]$.

Erosion rates of the same material, that were obtained at different rotation rates are then plotted against shear stress (see Figure 2.7. By extrapolating the erosion curve to the zero value of the erosion rate, the critical shear stress value can be determined. Bloomquist et al. [2012] proposed a linear fit based on multiple empirical and analytical studies for the cases when only a small number of tests are performed per sample. It is also mentioned that more complex functions may be used when more tests are conducted, and a clear nonlinear pattern emerges. The results are specific to the site and material tested and should not be extrapolated. It's crucial when performing a RETA test to cover the range of shear stresses relevant to the study.

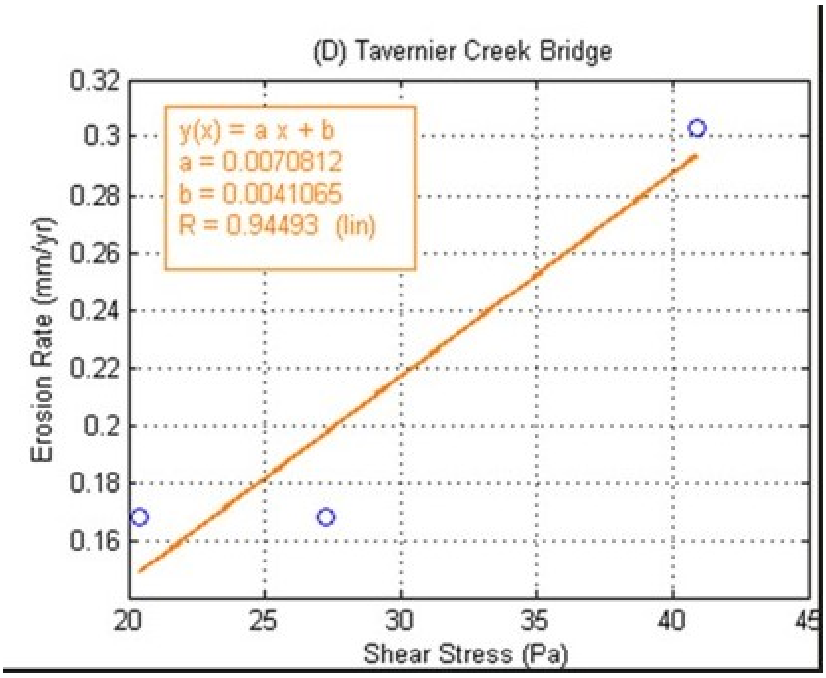

Figure 2.7: Sample RETA results Bloomquist et al. [2012].

Advantages

1. High speeds (and therefore indirectly shear stress) can be reached.
2. Continuously measured mass loss (discrete measurements in EFA and SERF).

Disadvantages

1. Indirect measurement of shear stress (calculations based on the centrifuge speed).
2. Boundary effects at the sample's top and bottom can cause it to assume an hourglass shape by the test's end.

2.3.3 Other erosion tests overview

Besides lab tests mentioned above a wide variety of tests both lab and in-situ have been developed and used to simulate an erosion process.

The Scour Testing Device (Scour Testing Device (STD)) is designed to simulate erosion under the impact of flowing water around structures like bridge piers or abutments. The STD has a hollow cylinder where the soil sample is placed and water is forced through the cylinder, simulating the water flow in a river. The process directly measures the amount of soil eroded, and indirectly, parameters like shear stress are calculated using the water flow velocity and the geometry of the apparatus. The STD is best used to study the localized scour around structures (Chiew [1992]).

Flume tests are versatile in their ability to simulate different types of erosion. A typical flume test involves flowing water over a soil sample placed at the bottom of a long, narrow channel, or 'flume.' The size of the flume and the velocity of the water flow can be varied to simulate different erosion environments. Flume tests can measure the direct impact of water flow velocity on the soil erodibility. They can also measure parameters like sediment concentration in the flow and changes in the soil surface. These measurements can then be used to estimate shear stress and the erosion rate (Julien [2002]).

The Jet Erosion Test (JET) uses a submerged jet of water to erode a soil sample. This test simulates the effects of high-speed water flows, as might be encountered in a flood event. The rate of soil erosion is directly measured by observing the depth of the hole created by the jet. From this, parameters such as the detachment rate, critical shear stress, and erodibility coefficient can be calculated (Hanson and Cook [2004]).

Hole Erosion Tests (HET) are used to measure the erodibility of soils when subjected to seepage forces, simulating internal erosion. A soil sample is placed between two reservoirs, and water flows from the higher-pressure reservoir through a hole in the sample to the lower-pressure one. The increase in the hole diameter over time is measured directly, and this can be used to calculate the erodibility coefficient and critical shear stress (Wan and Fell [2004]).

The Slot Erosion Test (Slot Erosion Test (SET)) is a flume-based test designed to simulate surface erosion. A soil sample is placed in a narrow slot at the bottom of a flume, and water is flowed over it. The erosion of the sample is measured over time, and this is used to estimate parameters such as the erosion rate and shear stress. SET provides a practical method to test the erodibility of thin layers of soil which can be critical in predicting the erosion stability of earthen structures (Wan and Fell [2004]).

The In Situ Erosion Evaluation Probe (In Situ Erosion Evaluation Probe (ISEEP)) is a device that assesses the erodibility of soil directly in the field by simulating the erosion forces of water flow. The ISEEP consists of a cylindrical chamber, which is pushed into the soil, and a mechanism to circulate water inside this chamber. The water flow's speed can be controlled to simulate different levels of shear stress. The amount of soil particles eroded, and the erosion rate can be directly measured, and these measurements can be used to estimate erodibility (Moore and Dwyer [2002]).

The Borehole Erosion Test (Borehole Erosion Test (BET)) is used to measure the erodibility of soil layers in the field by observing the growth of a hole over time. A hole is drilled in the soil, and water is flowed into it under controlled pressure. The changes in the hole's diameter over time are measured, and this information is used to calculate the erosion rate and the erodibility coefficient (Romkens et al. [2001]). BET is particularly useful for understanding internal erosion processes in earthen structures, such as embankments and levees.

The Full-Scale Overtopping Simulator (Full-Scale Overtopping Simulator (FSOS)) is a unique in-situ testing method designed to simulate the conditions when water overflows, or 'overtops,' a structure like a dam or a levee. The FSOS releases a controlled volume of water over the structure, and the resulting erosion is observed. Direct measurements include the volume of eroded material and the depth of the eroded area. These data are used to estimate parameters such as the erosion rate and critical shear stress under overtopping conditions (van der Meer et al. [2011]).

2.4 Effect of Wetting and Drying Cycles on Clay Structure and Properties

The following summarizes the studies on the impact of wetting and drying cycles on the structure and properties of clay. This includes a range of phenomena from the propagation of cracks to the micro-structural changes occurring within the clay matrix.

2.4.1 Cracks propagation

In clay soils, the mechanism of crack formation during wetting and drying cycles is a complex process influenced by soil suction and the resultant tensile stresses. As the soil dries, water is removed, leading to an increase in matric suction, which generates tensile stresses within the soil matrix Kodikara et al. [2000]. If these stresses surpass the tensile strength of the soil, cracks will form.

Fleureau et al. [2015] studied the appearance and propagation of cracks related to desiccation in clays with Digital Image Correlation. Authors argued that the initiation of cracks in clays is primarily linked to an increase in tensile stress. Figure 2.8 illustrates this mechanism at an early stage showing crack initiation as a result of an extension. The principal strain tensor, represented near a pre-crack stage, indicates that the major and minor principal strains are extensions (indicated in red), oriented in a way that shows the crack opening in mode I. As drying progresses, these extensions increase until a crack forms, leading to a relaxation of stresses and a decrease in strains. This process exemplifies the relationship between drying-induced tensile stress and crack formation in clays.

Further studies by Briaud et al. [2002]; Ahmadi et al. [2012]; Tu et al. [2022] highlight that once cracks occur, they are irreversible and alter the distribution of matric suction in subsequent drying

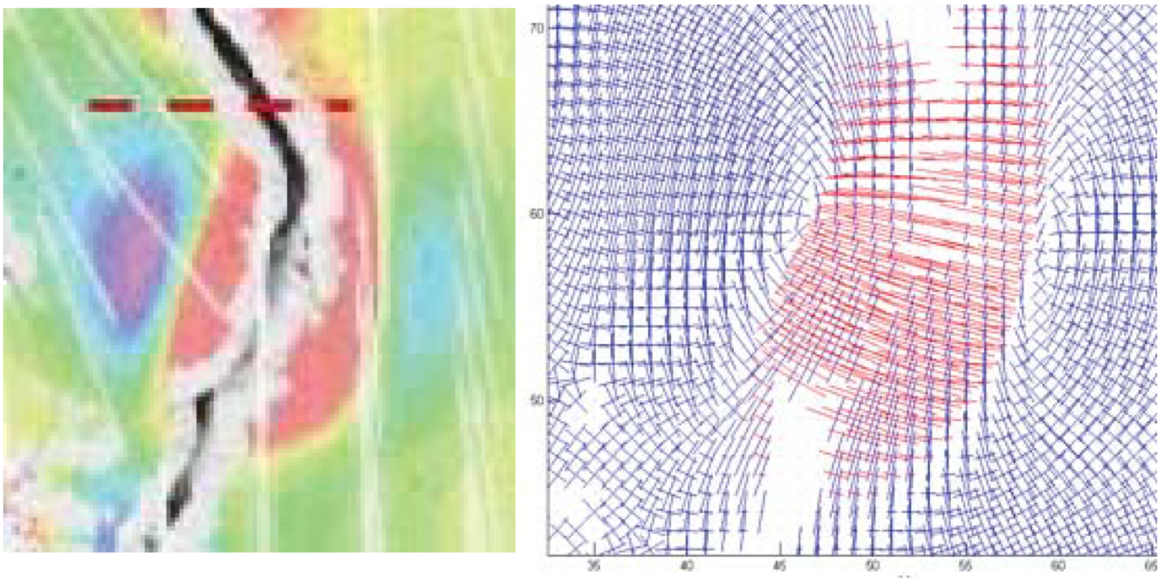

Figure 2.8: Crack initiation as a result of an extension mechanism Fleureau et al. [2015].

processes. Yesiller et al. [2000] studied the cracking behavior of three compacted landfill liner soils. Authors argued that for clay soils, the first drying cycle causes irreversible changes in the soil fabric, leading to weakening and reduced strength. Subsequent wetting partially seals the initial cracks, but these areas remain structurally weak. In repeated drying and wetting cycles, these weakened zones tend to reopen and further cracking occurs. This process is illustrated in Figure 2.9 with crack intensity factor (CIF) variation shown for several wetting and drying phases. After the first cycle, the structural rearrangement of the soil fabric diminishes, resulting in no significant change in the extent of soil cracking in subsequent cycles. This cracking notably decreases soil strength due to the development of desiccation cracks, impacting the overall structural integrity and properties of the clay soil.

The presence of cracks also changes the soil's hydraulic properties, such as permeability and water retention, as they provide pathways for water and air movement Tu et al. [2022]. Repeated wetting and drying cycles can exacerbate this cracking, leading to a deterioration of the soil structure and an increase in the size and number of cracks.

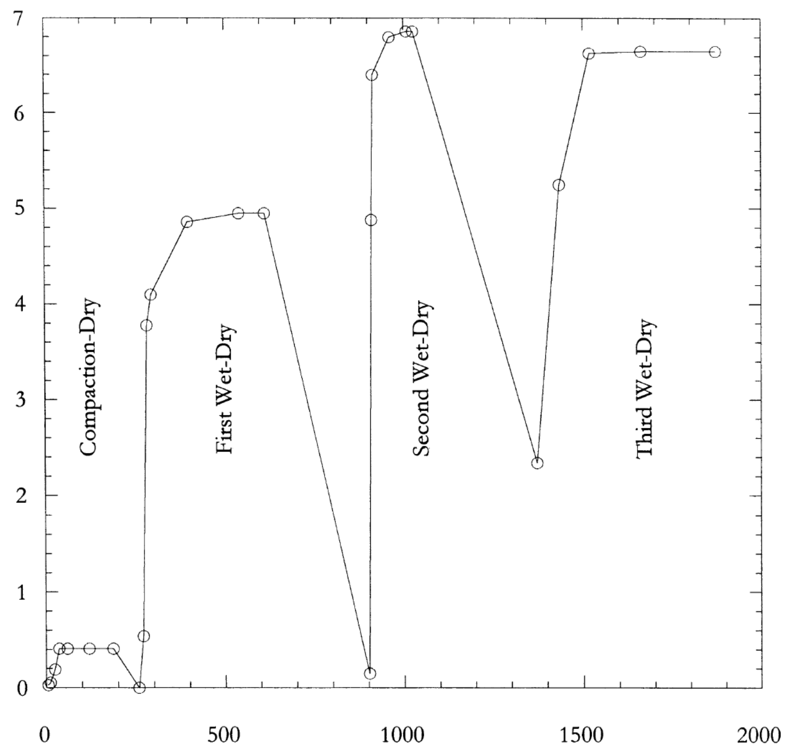

Figure 2.9: Variation of crack intensity factor (CIF) with time for Soil 2 in the multiple cycle tests Yesiller et al. [2000].

2.4.2 Micro-structural changes

Cyclic wetting and drying lead to changes in the microstructure of clay, including swelling-shrinkage behavior, particle reorientation, and porosity alterations. This impacts water absorption capacity and soil expansiveness.

Basma et al. [1996] tested reconstituted clay samples to study the swelling-shrinkage behavior of natural expansive clay. The authors used two drying schemes that followed the wetting phase. In this study "full shrinkage scheme" corresponded to drying samples below the shrinkage limit, while in the "partial shrinkage scheme" the sample was dried to the initial water content level. This study has demonstrated the distinctive behavior of these two groups of samples. Besides the deformation and change of the void ratio, changes in the samples were investigated using a Portable Ultrasonic Non-destructive Digital Indicator Tester, that measures the speed of ultrasonic pulses in the material. In the study, partial shrinkage of clay samples led to a decrease in void ratio and an increase in wave velocities, indicating a denser structure and reduced water absorption capacity, thus diminishing soil expansiveness. Conversely, full shrinkage increased void ratio and decreased wave velocities due to the separation of clay particles, enhancing the soil's swelling potential (see Figure 2.10). Microstructural analysis showed that repeated partial shrinkage cycles resulted in a turbulent microstructure, reducing water absorption and swelling. Full shrinkage favored a horizontal orientation of clay particles, increasing repulsion forces upon wetting and enhancing swelling (Basma et al. [1996]).

The study highlights that cyclic swelling processes gradually reconstruct and reorient clay microstructure, with specific changes depending on the initial microstructure and structural bonds.

Yanli et al. [2021] studied the mechanical properties of Red Clay under drying-wetting cycles and witnessed the alterations of clay microstructure due to these cycles. Specifically, an increase in pore size and significant structural damage to the clay, evidenced by holes and water flow traces on the surface. This process rounds the surface of particles and disintegrates larger soil particles, aligning them directionally. Figure 2.11 shows the evolution of clay microstructure with an increasing number of wetting and drying cycles. Quantitative analysis showed that drying-wetting cycles affect the geometric and spatial characteristics of particles and pores. There's a tendency for particles to align directionally after several cycles, with a shift in particle size content and shape, and similar changes

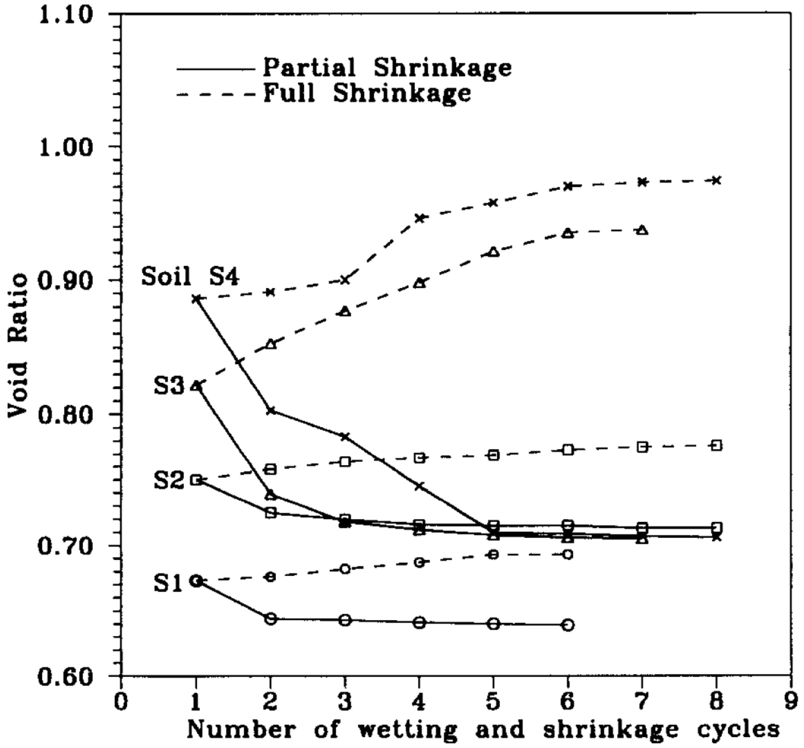

Figure 2.10: Change of void ratio with a number of cycles for partial and full shrinkage Basma et al. [1996].

in porosity. The particle size of the studied clay was predominantly below 2 μm. Following a cycle of drying and wetting, an increase in the proportion of particles sized between 2–10 μm was observed, while the fraction of particles larger than 10 μm decreased (see Figure 2.12.

Ma et al. [2015] in their research studied the microstructural evolution of expansive clay during wetting and drying cycles. According to the study expansive clay soils exhibit a complex structure with a bimodal pore size distribution, showing two distinct peaks for inter-aggregate macro-pores and intra-aggregate micro-pores Ma et al. [2015]. During drying, there is a significant reduction in macro-pores, compensated by an increase in micro-porosity. This trend reverses during the wetting process, where macro-porosity increases and micro-porosity decreases. Both macro-pores and micro-pores undergo irreversible changes during the drying-wetting cycles, impacting the soil's absorptive water content. This irreversibility is a critical factor in the soil's structural evolution Ma et al. [2020].

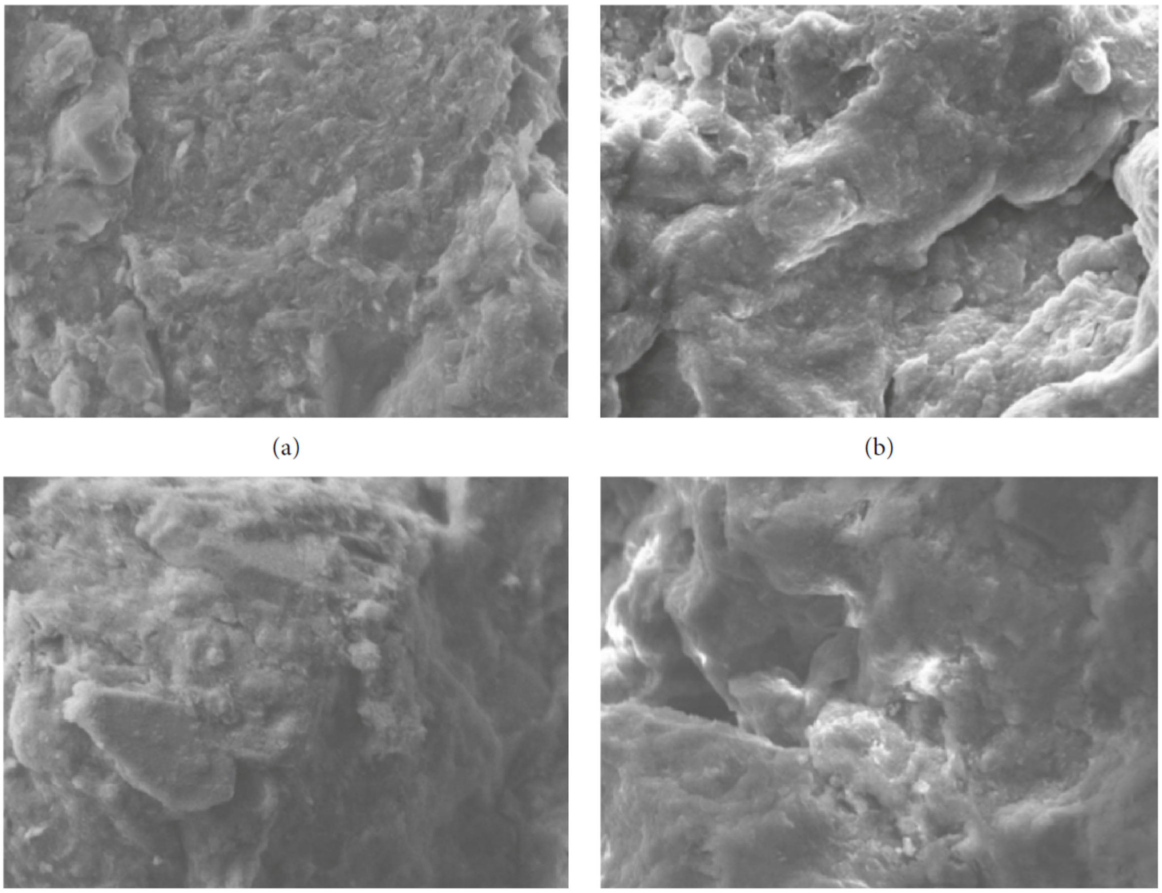

(a) (b) (c) (d)

Figure 2.11: Microscopic images of red clay at 1000x magnification under different wet and dry cycles. (a) 0 cycles. (b) 3 cycles. (c) 5 cycles. (d) 9 cycles Yanli et al. [2021].

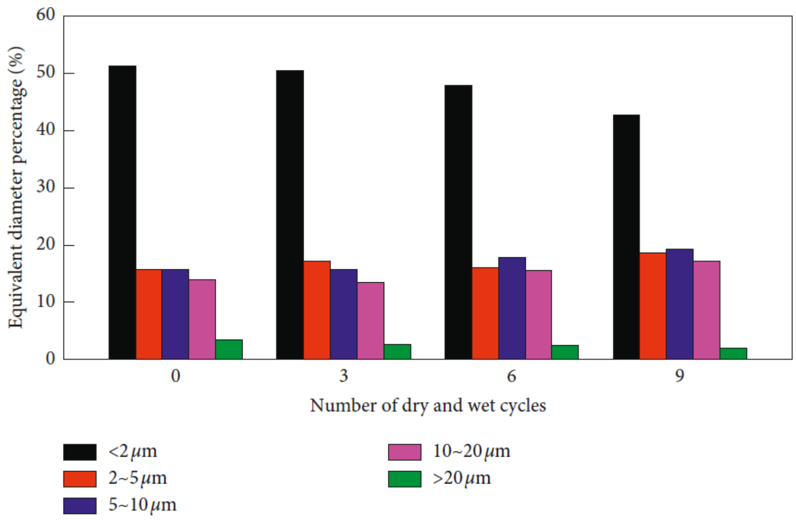

Figure 2.12: Distribution of the equivalent diameter of soil particles after different drying-wetting cycles Yanli et al. [2021].

2.4.3 Soil properties

Structural and microstructural changes affect clay's physical and mechanical properties, such as strength, hydraulic conductivity, and shear strength. Ahmadi et al. [2012] in their study investigated the effect of wetting-drying cycles on the free swell of clay samples from different regions. It was found that the free swell percentage is reduced after four to five cycles for all samples (see Figure 2.13). The study also observed a decrease in swelling potential after multiple wetting-drying cycles. The initial moisture content of the samples affected this behavior, with samples dried to a moisture content lower than the shrinkage limit showing an initial increase in swelling followed by a reduction in subsequent cycles.

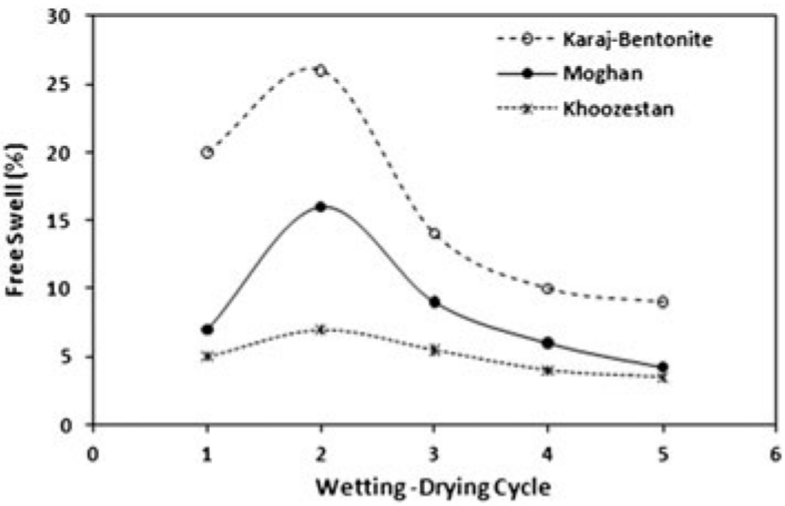

Figure 2.13: Free swelling after wetting and drying cycles (samples were dried to water content at shrinkage limit Ahmadi et al. [2012].

Kodikara et al. [1999] in their research studied how changes in clay structure due to wetting-drying cycles affect the hydraulic conductivity of clay. Saturated hydraulic conductivity can increase due to changes in the pore structure, with macropores (mostly cracks) being a key factor. However, unsaturated hydraulic conductivity is less affected by these macropores because they desaturate at low suction. Structural changes leading to intercluster pores can influence hydraulic conductivity over a wider suction range. Desiccation tends to increase the saturated hydraulic conductivity by enlarging pore sizes.

Goh et al. [2014] studied how changes in matric suction caused by cyclic wetting and drying result in changes in the shear strength of clay. Statically compacted sand-kaolin specimens, used by the authors exhibited hysteresis in shear strength during multiple drying and wetting cycles. Initially, specimens subjected to the first drying cycle exhibit slightly higher shear strength and greater axial strain at failure compared to those in later cycles. Specimens on their first wetting cycle demonstrate lower shear strength and smaller axial strain at failure than in subsequent wetting paths. After the second cycle, the specimens display consistent stiffness, ductility, and volume change characteristics during shearing. This was attributed by the author to the fact that the matric suction applied in these cycles does not exceed the maximum value experienced during the first cycle. Thus, the behavior during shearing does not significantly alter after the first two cycles.

Another study on the mechanical properties of a clay material was carried out by Yanli et al. [2021]. The specimens, both naturally obtained and reconstituted were prepared of Red clay, which is widely distributed in rainy areas in southern China. The changes in clay structure (see 2.11) resulted in a change in mechanical properties - both direct shear and triaxial tests show a decrease in shear strength parameters with an increasing number of cycles, most notably in the first cycle. The decline in strength becomes less pronounced in subsequent cycles. The resulting change in friction angle (ϕ) and cohesion (C) is demonstrated in Figure 2.13.

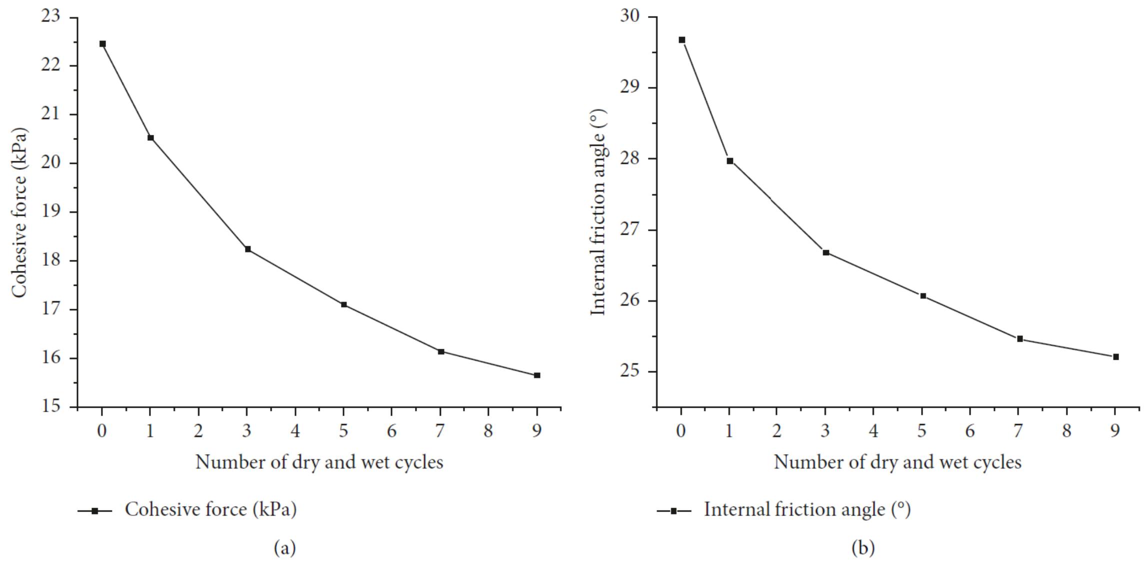

Figure 2.14: Relationship between cohesion (a) and friction angle (b) parameters and different dry and wet cycles Yanli et al. [2021].

2.4.4 Number of cycles

Some of the researches mentioned above (Basma et al. [1996], Yesiller et al. [2000], Goh et al. [2014], Ma et al. [2015], Yanli et al. [2021]) noticed that observed changes in clay structure and properties are stabilized with the number of wetting and drying cycles increases (Kodikara et al. [1999] or hysteresis effect becomes evident (Ahmadi et al. [2012], Goh et al. [2014]).

Basma et al. [1996] in their study observed how with increasing numbers of drying-wetting cycles, the large aggregates in the clay structure experience breakdown, and the initial structure of aggregates and particles is disturbed. With subsequent cycles, the breakdown of large aggregates and re-orientation of structural elements continue. By the fourth or fifth cycle, the magnitude of observed structural changes decreases, resulting in the stabilization of the clay's expansibility, meaning that no further significant changes are observed. That is evident from Figure 2.10 - the rate of decrease of void ratio diminishes after the second or fourth cycle of wetting and drying. It is worth mentioning that the study's conclusions on structural changes are inferred from measured changes in ultrasonic wave velocity and void ratio, without in-depth microstructural analysis.

Ahmadi et al. [2012] in their research pointed out that the reduction of free swell was maximal on the third or fourth cycle of wetting and drying with minimal to no change in the following cycles (see Figure 2.13).

Goh et al. [2014] in their study observed more diverse behavior - the difference in shear strength between drying and wetting paths of the clay specimens became less pronounced in later cycles compared to the first cycle. Specifically, the shear strength during the drying phase of the second and third cycles were slightly lower than the first cycle, while the wetting phase shear strength in these later cycles were higher than in the first cycle. This trend is attributed to the variations in the volumetric water content during the different cycles, influencing the shear strength of the specimens. Figure 2.15 presents the stress-strain relationships and the total volumetric strains experienced by the specimens during shearing (CD triaxial test). The data shown in these figures vary according to different matric suctions and cover both drying and wetting paths across various cycles.

Yanli et al. [2021] in their study observed that both the cohesion and internal friction angle of red clay decrease with an increasing number of drying and wetting cycles. The most significant decrease occurs during the first 1–5 cycles, followed by a more gradual decline in subsequent cycles (see Figure 2.14. Similarly, under constant confining pressure, the deviatoric stress of red clay decreases with each cycle, with the most notable reduction observed in the first cycle and a progressively weaker attenuation in later cycles as depicted in Figure 2.16.

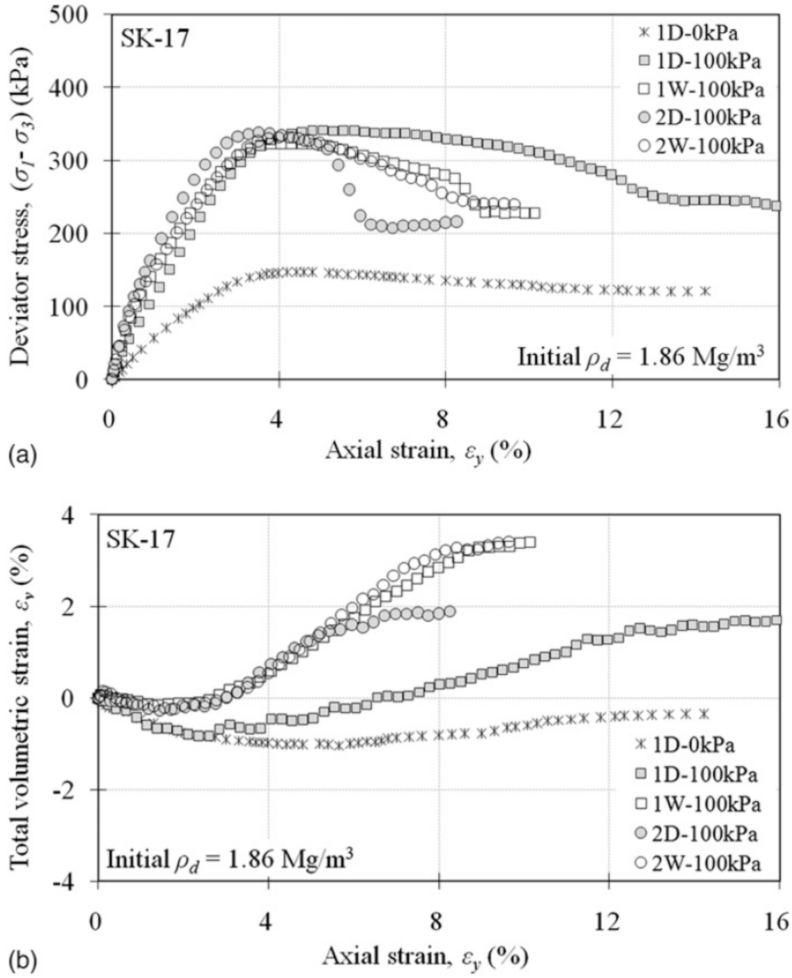

Figure 2.15: Stress-strain curves of SK-17 specimens at matric suction of 0 and 100 kPa in the first and second cycles of drying and wetting under net confining pressure of 50 kPa **(a)**.Total volume change characteristics of the SK-17 specimens during shearing at matric suction of 0 and 100 kPa in the first and second cycles of drying and wetting under a net confining pressure of 50 kPa **(b)** Goh et al. [2014].

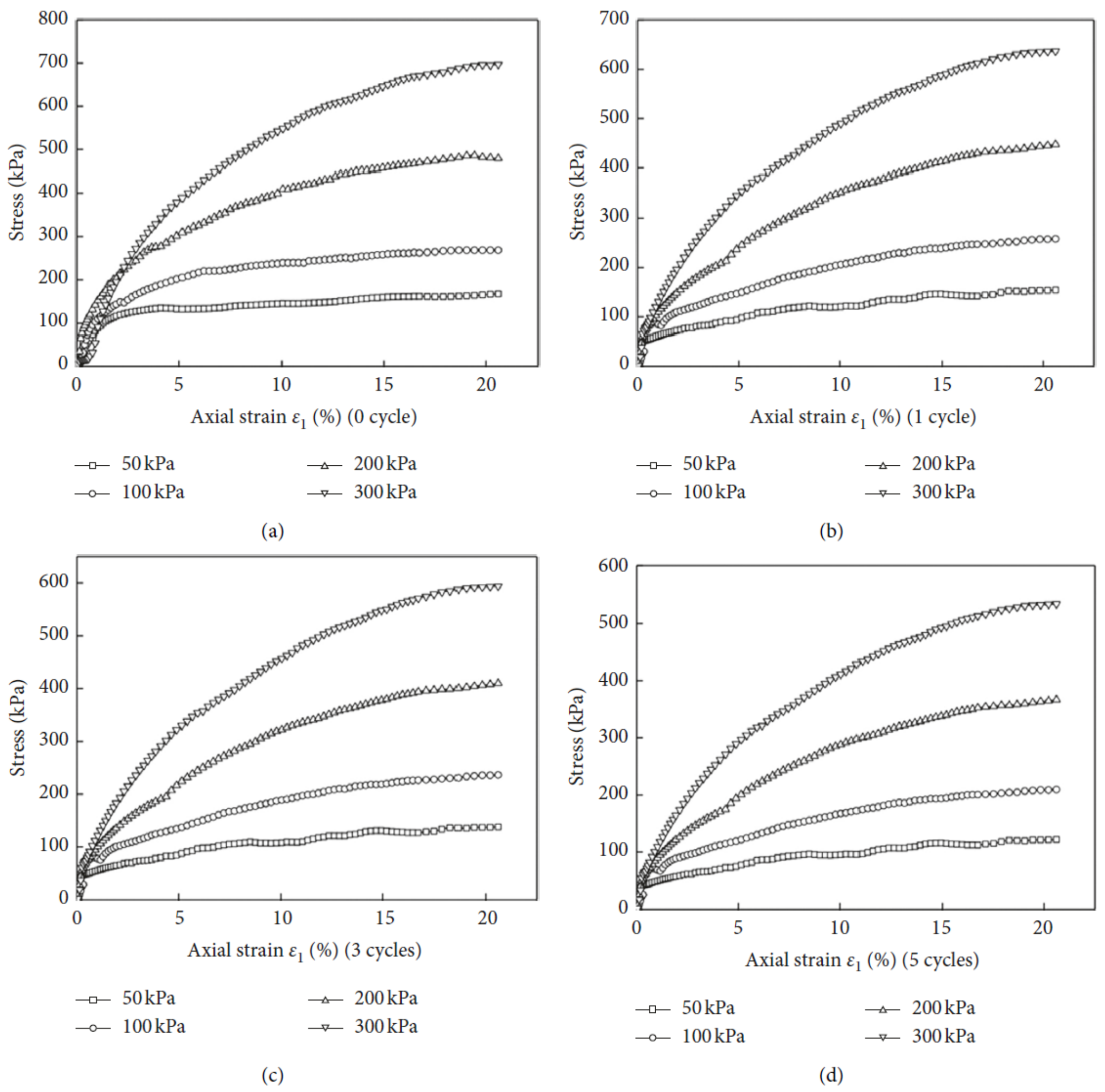

Figure 2.16: Deviatoric stress-axial strain relation curve of red clay under 0 (a), 1 (b), 3(c), and 5(d) wet and dry cycles Yanli et al. [2021].

2.5 Correlation of erodibility and soil properties

Surface erosion, as previously discussed, is a multifaceted process influenced by a range of external factors, including temperature, water's chemical composition, and flow parameters, alongside various soil properties. The resistance of cohesive materials is also driven by the nature and strength of the inter-particle bonds which makes it even more complicated.

The characteristics of soil - its composition, structure, organic content, moisture, and compaction - are fundamental in determining its erodibility. Through numerous studies, scientists have dissected these aspects to understand the complex mechanics underlying soil erosion. A soil's texture, primarily governed by the proportion of sand, silt, and clay it contains, significantly affects its erodibility. Clayey soils, with their smaller particle sizes and higher cohesion, typically exhibit lower erodibility compared to sandy or silty soils, a finding confirmed in various studies, such as those by Wischmeier et al. [1971].

Soil structure, particularly the arrangement and binding of soil particles into aggregates, plays a critical role in soil erosion. Le Bissonnais (Le Bissonnais [1996]) suggested that well-structured soils with larger aggregates have generally lower erodibility due to increased cohesion and reduced susceptibility to detachment by flowing water.

The organic matter content in soils has a direct bearing on their erodibility. Organic matter aids in the formation and stability of aggregates, thus reducing soil detachment.

Moreover, the moisture content within the soil can modulate its erodibility. Ellison (Ellison [1947]) found that soils with intermediate moisture content are generally more erodible than either very dry or very wet soils. Further studies, however, displayed a more complex inter-dependency of erodibility and water content - Briaud et al. [2019] in his research in an attempt to establish empirical correlations between soil properties and erosion characteristics concluded that higher water content in clay can lead to increased soil cohesion, which may reduce soil erodibility up to a certain point. However, when the water content exceeds the soil's liquid limit, the soil may lose its structure and strength, increasing its susceptibility to erosion. Therefore, the relationship between water content and erodibility in clay soils is complex and dependent on the balance between soil cohesion and structural integrity.

Rahimnejad and Ooi [2016] pointed out distinct relationships between critical shear stress and soil property parameters, such as moisture content, void ratio, unit weight, consolidation stress, and undrained shear strength. His study noted that critical shear stress increases with decreasing moisture content, decreasing void ratio, increasing unit weight, and increasing pre-consolidation stress. Additionally, it suggested that normally consolidated soils may exhibit a rise in critical shear stress with undrained shear strength, although the strength was not directly measured.

Erosion resistance, as several studies have established, is influenced by a myriad of soil properties, including antecedent moisture, clay mineralogy, proportion, density, soil structure, organic content, as well as pore and water chemistry (Grissinger [1982]). For instance, Arulanandan (Ariathurai and Arulanandan [1978]) observed a decrease in soil erodibility with an increase in the salt concentration of the eroding fluid, attributed to the consequent weakening of inter-particle bonds. Lastly, Briaud (Briaud [2008]) compiled results from laboratory testing on an EFA and literature, presenting a chart that represents critical shear stress as a function of mean grain size. This compilation further illustrates how critical erosion thresholds are linked to specific soil parameters (see Figure 2.17).

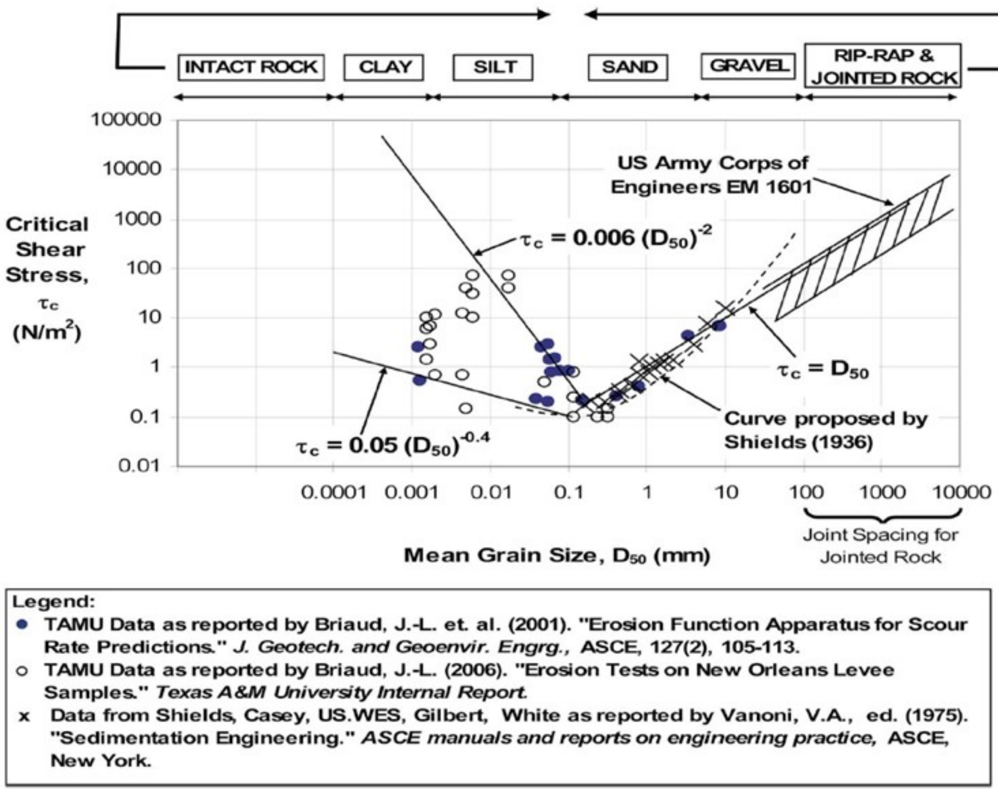

Figure 2.17: Critical shear stress as a function of mean grain size Briaud [2008].

2.6 Erodibility classifications

2.6.1 Erodibility classification used in The Netherlands

The Netherlands currently employs an assessment standard developed from the research on how clay properties such as water content, liquid limit (LL), and plastic limit (PL), influence soil erodibility. The research was carried out by Grondmechanica Delft in the 1980s (Kruse [1987, 1988]. It was based on erosion centrifuge tests, where soil samples were subjected to rotational water flow to measure mass loss at certain stress levels (see Section 2.3.2) along with the outcomes of full-scale overtopping experiments. These findings led to the establishment of the assessment criteria (voor Waterkeringen [1996]; CROW [2010]). The resulting guidelines are detailed in Table 2.1

	Erosion Class		
	I (erosion-resistant clay)	II (moderately erosion-resistant clay)	III (low erosion-resistant clay)
LL [%]	>45	<55	<0.73*(LL-20)
PI [-]	>0.73*(LL-20)	>18	<18
Sand content [%]	<40	<40	>40

Table 2.1: Dutch erosion guidelines (voor Waterkeringen [1996]; CROW [2010]).

The guidelines provide an additional list of requirements for the material used for dike construction (voor Waterkeringen [1996]; CROW [2010]):

Organic matter content ¡ 5%

Salinity ($NaCl$) ¡ 4 g/l

Lime content (HCl): ¡ 25 %

No extreme discoloration during excavation or drying

No unusual strong odor

2.6.2 Texas University and NCHRP Classification

Briaud Briaud [2008] and Hanson and Simon [2001] introduced category charts to simplify the classification of soil erodibility. These charts distinguish erosion categories through boundary lines on plots of erosion rate ($\dot{z}$) against flow velocity (v) and shear stress (τ), derived from extensive erosion testing at Texas A&M University. The categorization boundaries are defined by the critical velocity and critical shear stress.

To classify soil erodibility, several erosion rate measurements at varying flow velocities and the corresponding shear stress values are plotted on these charts. The erosion category (EC) is determined by the median point of the plotted erosion curve, which serves as the representative for EC (see Figure 2.19). The positioning of this median point on the curve directly influences the EC determination, thus acquiring multiple data points increases the accuracy in defining EC. Briaud in his studies (Briaud [2008]; Briaud et al. [2019] argues that erosion function is represented by an erosion curve rather than by a single value. However, the EC represents this curve into a single value that may be beneficial for engineering applications.

In summary, the erodibility of soil is a multifaceted process, influenced by an array of soil characteristics. These studies, along with ongoing research, contribute to a comprehensive understanding of soil erosion, providing crucial insights to guide effective soil management and conservation strategies.

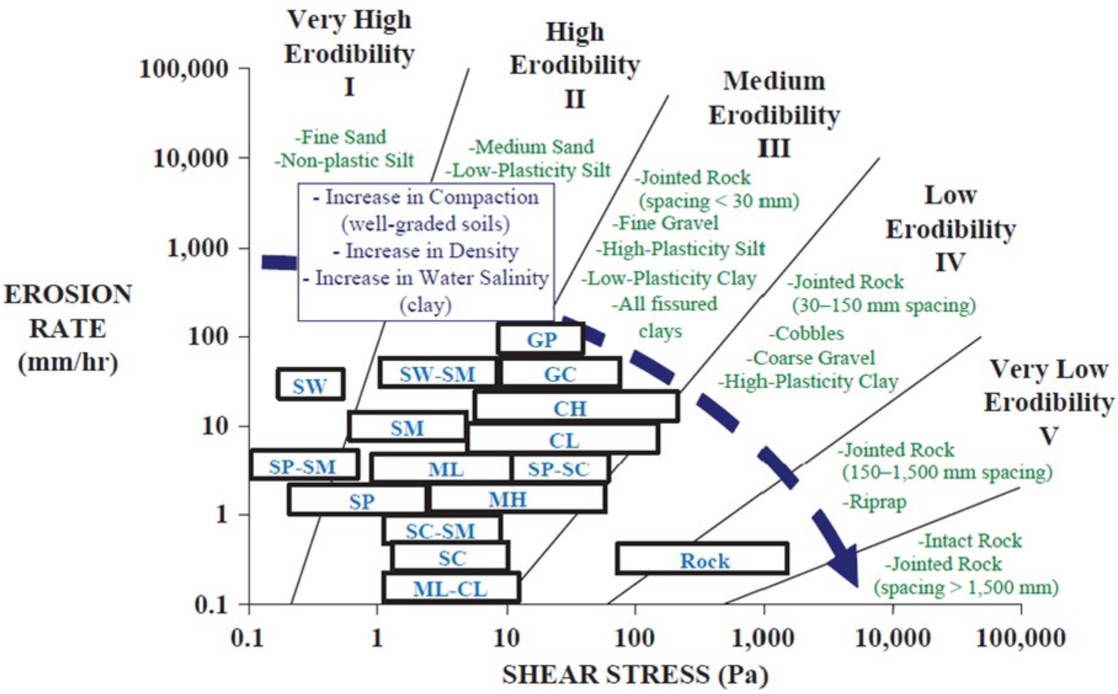

Figure 2.18: Erosion category charts with USCS symbols Briaud et al. [2019].

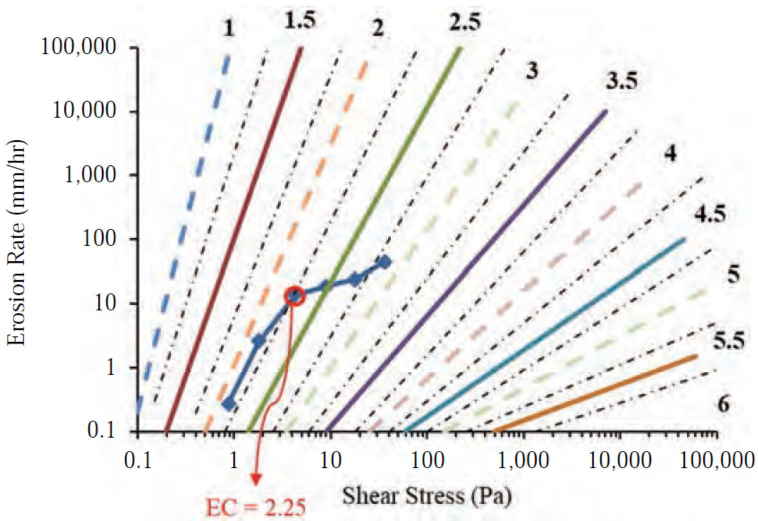

Figure 2.19: Example showing how EC is obtained for a sample erosion curve; the EC for this example is 2.25 Briaud et al. [2019].

3 Methodology

3.1 Introduction

The Boom Clay and Kleirijperij Clay were studied in this research. This chapter outlines the comprehensive methodology used to investigate the impact of cyclic wetting and drying on Boom Clay's and Kleirijperij Clay's erodibility. A series of erosion tests using the Erosion Function Apparatus (EFA) were performed to assess changes in soil erosion resistance. This approach aims to provide an in-depth understanding of environmental conditioning on soil erodibility, pivotal for designing and applying erosion protective layers effectively.

The Boom-Clay is classified as Category 1 in the Dutch erodibility classification (see Section 2.6.1). This material has been used by Boskalis on several projects for constructing an erosion-protective cover of dikes, including the ongoing project of Markermeerdijken. This material has been studied for its composition (Dehandschutter et al. [2004]) and structure (Romero et al. [1999]), which is beneficial since current research does not involve studying mineralogical and structural changes of the tested material. Additionally in his research Rook [2020] tested the Boom Clay specimens on a similar EFA setup.

The Kleirijperij Clay is classified as Category 3 in the Dutch erodibility classification (see Section 2.6.1) and is known for their higher compared to Boom Clay organic content (Kleirijperij [2023], Sittoni et al. [2019]).

The availability of these materials in sufficient quantities at the Boskalis laboratory and an ongoing dike construction project by Boskalis facilitated their selection.

The study involves detailed analyses of the soil's physical properties, using the following notations:

w [%] - moisture content - controlled before sample preparation and during wetting and drying cycles;

$\rho[g/cm^3]$ - bulk density - determined after sample preparation;

$\rho_d[g/cm^3]$ - dry density - calculated as $\rho_d = \rho/(1+W)$;

$\rho_s[g/cm^3]$ - soil particle density - determined by Boskalis [2023];

e [-] - void ratio;

LL [%] PL [%] - liquid limit and plastic limit determined during sample preparation;

PI [%] - plasticity index - calculated as $PI = LL - PL$;

LI [%] - liquidity index - calculated as $LI = (W - PL)/(LL - PL)$

The properties of the tested clay material are given in sections below, and a more detailed description of every sample along with soil properties are listed in Appendix A and Appendix B. The soil properties listed in this chapter refer to the originally prepared samples. Before erosion testing the values of moisture content ($W[\%]$) and density ($\rho[g/cm^3]$) were determined for each specimen to correctly calculate the mass loss. This data is given in Chapters 4, 6 and Appendixes A and B. It may slightly vary due to the loss of moisture during sample storage.

3.2 Tested Material Characteristics and Properties

3.2.1 Boom Clay: Material Origin

The choice of Boom Clay was driven by its widespread use in constructing erosion protective layers in The Netherlands, necessitating a detailed understanding of its erodibility (Wiseall et al. [2015], Haselsteiner et al. [2009]).

This clay material originates from the quarry of Schelle, Belgium, situated approximately 15 kilometers south of Antwerp, and was extracted from a depth of 25 meters below the surface. Samples were prepared either from disturbed clay material, stored at the Boskalis laboratory, or from sampling the constructed erosion protective layer of the ongoing Markermeerdijken project (see Section 3.3). The material stored in the Boskalis laboratory was received in a disturbed state and presented irregular chunks measuring approximately 1-4 cm (see Figure 3.1) with an initial moisture content (W) ranging between 7% and 10%.

The clay material used for an erosion-protective layer of the Markermeerdijken project originates from the same quarry. Samples were obtained from the top of the erosion protective cover after it had been constructed and compacted (see Appendix A) in pieces of approximately 10x10x15 cm (see Figure 3.1 with an initial moisture content (W) ranging between 24% and 26%.

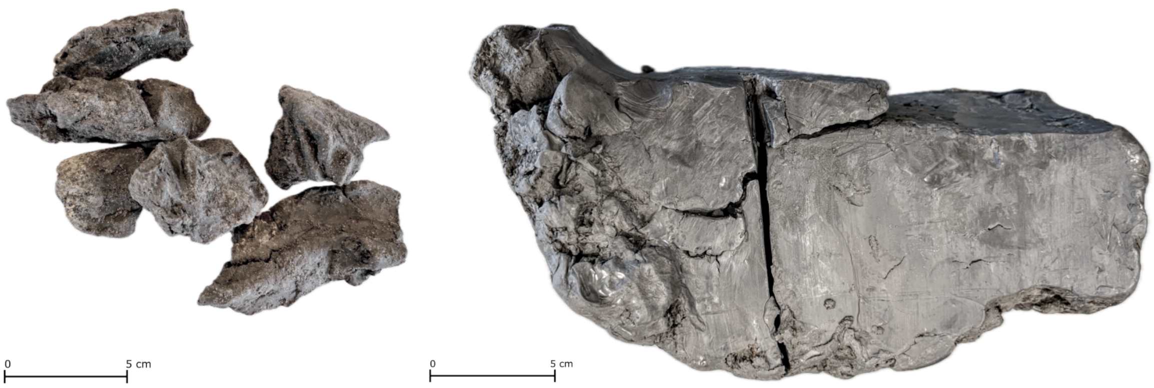

Figure 3.1: Initial clay material: Boom Clay. Left: material stored in the Boskalis laboratory; right: Sample obtained on the Markermeerdijken project site

3.2.2 Boom Clay: Mineralogical Composition and Structure

Boom Clay primarily consists of mixed clay and silt, with minor sand components. The clay fraction, varying between 23% and 60% of the bulk material, predominantly includes illite, smectite, and kaolinite (Dehandschutter et al. [2004]; Desbois et al. [2010]). The non-clay fraction mainly consists of quartz, also varying between 23% and 60%, along with feldspars, calcite, and pyrite Yu et al. [2012]. On a larger scale, Boom Clay is considered rather homogeneous, with similar qualitative mineralogical compositions found in different samples (Wiseall et al. [2015]).

Boom Clay's pore structure has been studied using methods like Mercury Injection Porosimetry (MIP) and Scanning Electron Microscopy (SEM) (Romero et al. [1999], Dehandschutter et al. [2004]. Key findings include a predominant pore radius of 0.01 μm to 0.09 μm (Dehandschutter et al. [2004]). Compaction studies show bi-modal and tri-modal pore size distributions at different densities (Romero et al. [1999]). Cryo-SEM analyses revealed an unimodal pore size distribution, with the majority of pores being less than 100 μm in radius. The total porosity was found to be 26.3% in dry samples and 20.4% in wet samples, with around 40% of the total porosity attributable to these ($< 100\mu m$) pore size (Desbois et al. [2010]).

3.2.3 Boom Clay: Properties

The soil properties of Boom Clay Were determined in the soil laboratory of Boskalis - either during this study or for the ongoing projects. The values of particle density (ρ_s), plastic limit (PL), and liquid limit (LL) were obtained from the test report of the clay material carried out by Boskalis in 2023 (Boskalis [2023]). The values of PL and LL for samples prepared according to Procedure 3 (see Section 3.3.3) were determined in the laboratory as a part of this study to ensure that the sample preparation process did not modify the properties. The values of the plasticity index (PI), and liquidity index (LI) were calculated.

The properties listed in this chapter refer to the originally prepared samples. Before erosion testing the values of moisture content ($w[\%]$) and density ($\rho[g/cm^3]$) were determined for each specimen to correctly calculate the mass loss. The values of plastic limit (Plastic Limit (PL)), liquid limit (Liquid Limit (LL)), and specific gravity (ρ_s) were obtained from the field report Boskalis [2023], except for the sample that has been prepared by complete reconstitution (BC-4) - the values of PL and LL were determined in the lab (see A). The values of dry density (ρ_d), void ratio (e), porosity (n), degree of saturation (Sr), plasticity index (Plasticity Index (PI)), and liquidity index (Liquidity Index (LI)) were calculated from the obtained parameters. This data is given in Chapters 4, 6 and Appendixes A and B. The value of moisture content for each specimen may slightly vary due to the loss of moisture during sample storage.

The properties of Boom Clay material:

- (ρ_s) 2.65 g/cm^3
- *LL* 63 - 69%*, **
- *PL* 21 - 22%*, **
- *PI* 41 - 48%*, **
- *LI* 0.09 - 0.24%*, **
- *Fraction* $< 63\mu m$ 93%**
- *Organic content* $<$ 5%***

* - determined during the research; ** - Boskalis [2023] *** - Durce et al. [2015]; Wiseall et al. [2015]

3.2.4 Kleirijperij Clay Characteristics and Properties

The second soil type is the Kleirijperij clay, originating from the Brede Groene Dijk demonstration project. This project undertakes comprehensive research into the feasibility of constructing a dike utilizing locally extracted clay from salt marshes and clay produced from dredging sludge. Anticipations surround the potential improvement of certain properties as the clay matures over time, accompanied by a reduction in organic content. This clay falls within the classification of Category III erosion clay having an average organic content higher than 5%.

This material was stored in the Boskalis laboratory in a disturbed state and presented irregular chunks measuring approximately 0.5-2 cm with an initial moisture content (W) ranging between 30% and 41%. Soil properties listed below were obtained during the index testing, as a part of the study of the material by Boskalis.

The properties of Kleirijperij Clay material:

- (ρ_s) 2.68 g/cm^3
- *LL* 105%
- *PL* 40%
- *PI* 65%
- *Fraction* $< 63\mu m$ 88%
- *Organic content* 10%

3.3 Sample Preparation

Three different sample preparation procedures were carried out. The first one aimed to replicate, on a smaller scale, the process of constructing erosion-protective covers on dikes. It involved compacting the clay material and simulating the conditions encountered during the construction of protective layers. The second sample preparation procedure was designed to achieve a higher level of homogeneity and uniformity within the sample. Lastly, the third procedure presumed preparing samples from the clay material obtained from the constructed erosion protective layer of an actual dike.

To ensure the accuracy and reliability of the laboratory testing, the samples underwent a preparation protocol to achieve consistent and homogeneous specimens. The list of all samples that were prepared with an indication of the preparation method is given in Appendix B. The procedures for each clay sample preparation method are illustrated in Figure 3.2, the detailed description is given below.

	Procedure 1 Simulated Construction Method (SC)	Procedure 2 Homogenized Reconstitution Method (HR)	Procedure 3 In-situ Retrieval Method (IR)
Goal	Mimic on a smaller scale construction of the erosion-resistant layer.	Obtain the most homogeneous samples that would yield repeatable results.	Compare material from the dike erosion protective layer
Material preparation	Crushing to pieces of 0.5 – 1.0 cm (W≈10%) → re-saturation (W≈27%) → compaction.	Crushing to the fine particles (W=0%) → re-saturation (W≈27%) → compaction.	Sampling the top layer on Markermeerdijken project site.
Compaction	Modified Proctor	Modified Proctor	-
+	Representation closer to real-world conditions. May incorporate construction-induced changes (e.g., layering)	High repeatability due to the homogeneous nature. Precise control during preparation.	Natural conditions.
-	The least control on sample preparation.	NC samples (original Boom clay is OC). Loss of internal structure.	Potential higher variability in samples due to natural heterogeneity

Figure 3.2: Clay Sample Preparation Procedures for EFA Testing.

3.3.1 Procedure 1: Simulated Construction Method

The first sample preparation procedure (**Simulated Construction Method (SC)**) was used for clay material stored in the Boskalis laboratory. The goal was to simulate on a smaller scale the construction of the erosion-resistant layer. The clay material was first mechanically crushed to reduce the chunk size to a uniform range of 0.5 - 1.0 cm (see Figure 3.3).

Once the desired size was achieved, the crushed clay was hydrated before the compaction by gradually adding water to the mix. This water addition was conducted incrementally while continuously mixing the sample to achieve uniform moisture distribution. Tap water at room temperature was used.

The target moisture range was set at 25-30%, higher than the optimum 20-25% (Rook [2020], Boskalis [2023]). This range was chosen to facilitate the study's wetting and drying cycles, aiming to reduce moisture to around 15% (see Section 3.4). This range also matched the moisture content of in-situ samples and allowed compatibility across laboratory-prepared and natural samples. Additionally, it provided a manageable variation in moisture content and aligned with similar properties in related research (Rook [2020]). This approach balanced research needs with practical considerations.

Following the saturation process, the moistened clay material was left in a sealed container for 24 hours. This time interval allowed the water to uniformly distribute throughout the sample.

The compaction process was carried out according to the Modified Proctor compaction procedure, a widely accepted and standardized method for determining the maximum dry density and optimum moisture content of soils and clayey materials. The procedure involved subjecting the prepared clay sample to 25 compaction blows using a modified compaction hammer with a compaction energy of 2.7 MJ/m^3. Each of the 5 layers of the sample was carefully placed in a mold and then compacted.

The initial moisture content of the material was checked right after the compaction procedure by completely drying three specimens. The mass of the obtained sample was registered and its density (ρ) was calculated with the known volume.

The samples ST-3, ST-4, BC-1, and BC-2 (Boom clay) were prepared according to this procedure (see Appendix B). Their properties are listed in Table 3.1. Figure 3.4 illustrates the compaction plane for

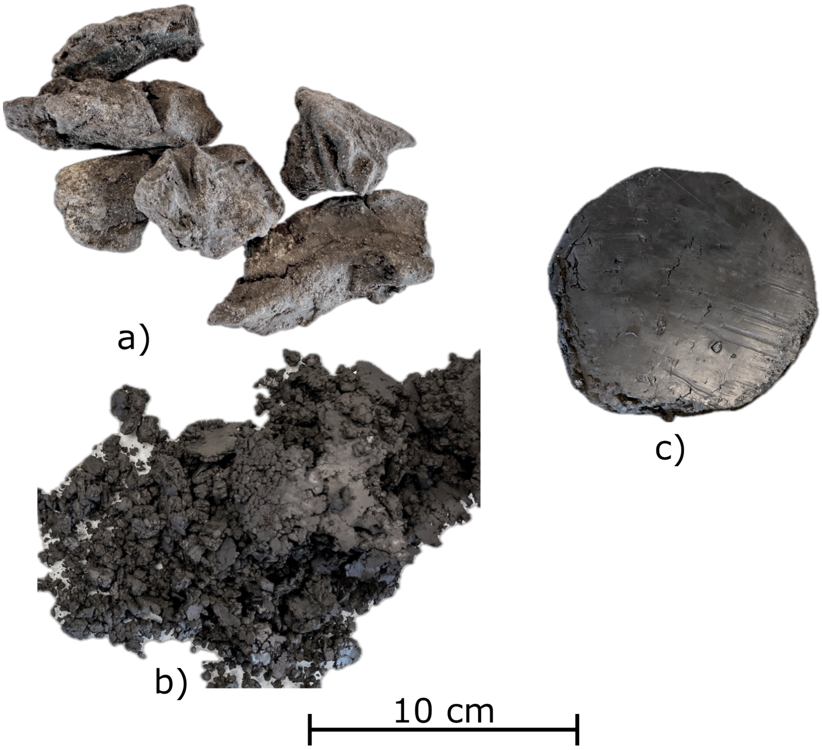

Figure 3.3: Stages of sample preparation (Boom Clay): a) material stored in the Boskalis laboratory; b) crushed and re-wetted material; c) prepared sample.

Boom Clay material, incorporating data from the current study as well as data from Rook's research (Rook [2020]). All information related to the compaction procedure can be found in Appendix A.

Sample	W	ρ	ρ_d	ρ_s*	e	Sr
	%	g/cm^3			-	
BC-1	32.31	1.85	1.40	2.65	0.89	0.96
BC-2	29.91	1.82	1.40	2.65	0.89	0.89
ST-2	6.89	1.74	1.62	2.65	0.63	0.29
ST-3	37.85	1.80	1.31	2.65	1.02	0.98
ST-4	30.71	1.82	1.40	2.65	0.90	0.91

Table 3.1: Boom clay samples were prepared according to procedure 1. * - Boskalis [2023]

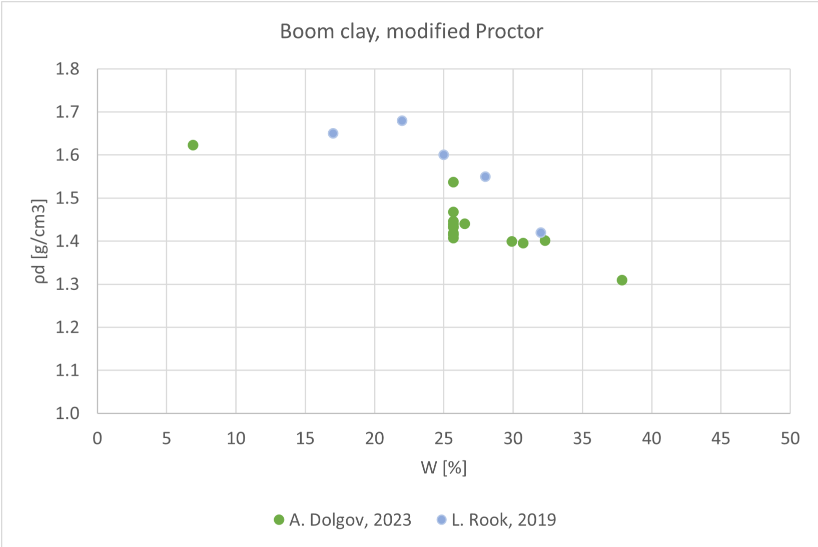

Figure 3.4: Compaction results for Boom Clay material performed in this research and by Rook [2020].

The samples prepared from the clay material of the Kleirijperij Project were created using the same method, aiming for a target moisture content of 30-35%, which corresponds to the highest recorded density (see Figure 3.5). This determination was based on the analysis of more than 200 Proctor compaction tests conducted by Boskalis in 2021-2022 (see Figure 3.5 and Appendix A). The soil properties of the Kleirijperij samples prepared according to this procedure are listed in Table 3.2.

Sample	W	ρ	ρ_d	ρ_s*	e	Sr
	%	g/cm^3			-	
CR-1	30.26	1.79	1.37	2.68	0.95	0.85
CR-2	32.47	1.82	1.37	2.68	0.95	0.91
CR-4	41.22	1.46	1.03	2.68	1.59	0.69

Table 3.2: Kleirijperij samples were prepared according to procedure 1.

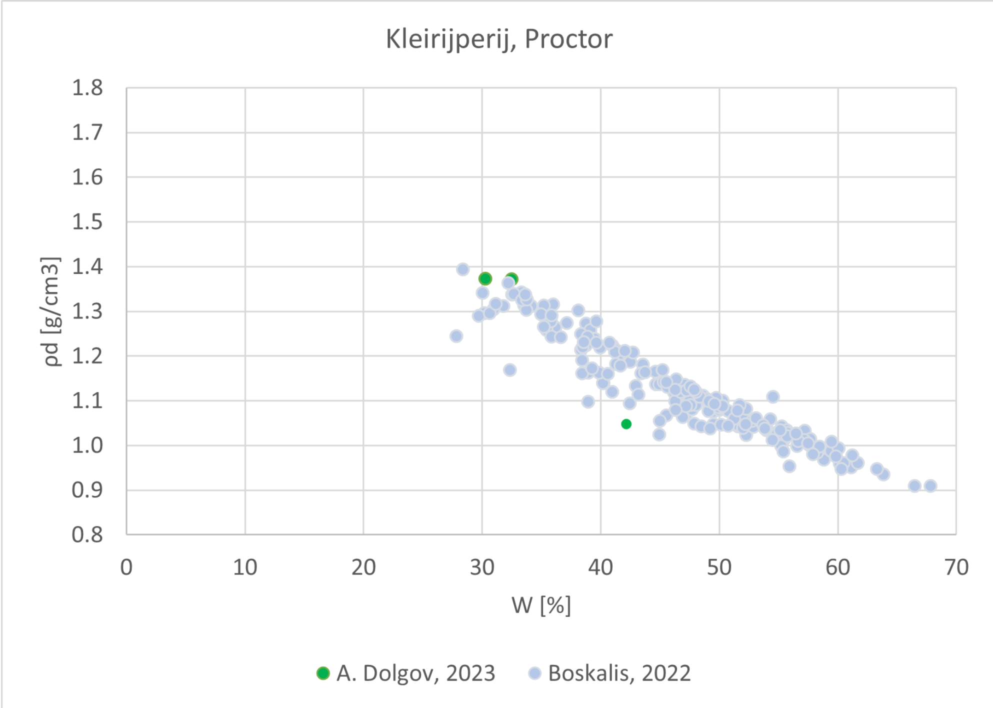

Figure 3.5: Proctor compaction data for Kleirijperij material.

3.3.2 Procedure 2: Homogenized Reconstitution Method

The second sample preparation procedure (**Homogenized Reconstitution Method** (HR) was also used for Boom clay material stored in the Boskalis laboratory with the goal of creating a homogeneous sample with more even structure and distribution of characteristics compared to the previous one. The clay material was first mechanically crushed to reduce the chunk size to a uniform range of 0.5 - 1.0 cm, then dried completely. The dried material was then crashed in a mortar to the fine particles, and then re-hydrated to reach the desired moisture content of 25-30%. Re-hydration was carried out incrementally adding tap water at room temperature while continuously mixing the sample to achieve uniform moisture distribution. Following the re-hydration process, the moistened clay material was left in a sealed container for 24 hours. This time interval allowed the water to uniformly distribute throughout the sample.

The Proctor compaction was carried out on the same condition as in the previous procedure. The initial moisture content of the material was checked right after the compaction procedure by completely drying three specimens. The mass of the obtained sample was registered and its density (ρ) was calculated with the known volume.

The samples BC-4 were prepared according to this procedure, its properties are listed in the table 3.3.

	W	ρ	ρ_d	ρ_s*	e	n	Sr
	%	g/cm^3			-		
BC-4	26.56	1.82	1.44	2.65	0.84	0.46	0.84

Table 3.3: Boom clay samples were prepared according to procedure 2. * -Boskalis [2023]

3.3.3 Procedure 3: In-situ Retrieval Method

The third procedure (**In-situ Retrieval Method (IR)**) involved utilizing Boom clay samples sourced from the Markermeerdijken project construction site near Warder, North Holland. In this project, Boom clay was employed to establish a protective erosion layer for a dike. It's noteworthy that the original clay material used in this phase of the research was sourced from the same quarry as the material employed in all other sample preparations, facilitating a comprehensive comparative study across different preparation methods. This layer was designed 1.0 m thick and was constructed according to current norms and regulations, which involved breaking up the initial clay material spreading, and compacting it in multiple layers over the existing dike structure. The goal is to create a durable, impermeable barrier which can withstand the elements and prevent erosion, ensuring the long-term stability and safety of the dike system.

The clay material was carefully obtained from the uppermost constructed layer of the dike, in pieces of approximately 10x10x15 cm. Following extraction, the material was securely sealed and transported to the laboratory. The initial moisture content of the material was checked by taking 5 samples from different pieces. Samples were then prepared by cutting them into the EFA molds, which allowed the calculation of the value of density.

The dyke was sampled approximately 1.5 days after the construction of the erosion protective layer. During this time, there was no precipitation on site. However, the transportation and storage of the original clay material were not controlled by the author and it may experience certain fluctuation in moisture content.

These samples were then either tested immediately or subjected to a series of wetting and drying cycles. The samples BC-5 were prepared according to this procedure, its properties are listed in the table 3.4.

	W	ρ	ρ_d	ρ_s*	e	n	Sr
	%	g/cm^3			-		
BC-5	25.70	1.82	1.45	2.65	0.83	0.45	0.82

Table 3.4: Boom clay samples were prepared according to procedure 3. * Boskalis [2023]

Prepared samples were denoted with a sample code (e.g. **BC-1**) with letters denoting initial material (**BC** and **ST** for Boom clay and **CR** for Kleirijperij clay). The overview of prepared samples is given in the table below:

Method	Material	Sample Code
SC	Boom Clay	ST-3, ST-4, BC-1, BC-2
	Kleirijperij	CR-1, CR-2, CR-3, CR-4
HR	Boom Clay	BC-4
IR	Boom Clay	BC-5

3.4 Wetting and Drying Cycles

Wetting and drying cycles were integral to this study, reflecting the real-life conditions of erosion protective layers exposed to environmental factors. Several studies discovered wetting and drying cycles may alter the soil structure and properties (Ma et al. [2015], Ma et al. [2020], Yanli et al. [2021]; see section 2.4 for a detailed overview). These cycles also occur in real-life practice - the erosion protective layers and earthwork structure being exposed to the surrounding experience periodical wetting due to precipitation, and drying. Even being covered by the grass cover, during the construction, several cycles of wetting and drying may occur. It is important to understand how and at what rate soil properties are changing - this will give insights into the performance of these structures, since the designer parameter of the materials may be altered by cycles of wetting and drying. The three-cycle approach, each drying to below the shrinkage limit, was based on literature suggesting significant changes in clay properties occur predominantly in the initial cycles (Basma et al. [1996], Yanli et al. [2021]).

In total 3 wetting and drying cycles were performed for each sample (by the scheme *D1-W1-D2-W2-D3-W3*). At each drying phase, a sample was dried below the plastic limit (**21%** for Boom Clay according to Boskalis [2023]) and below the shrinkage limit (**16%** for Boom Clay according to Assadollahi and Nowamooz [2020]). At each wetting phase, a sample was re-hydrated to the original moisture content. This methodology aimed to capture these changes while maintaining a balance with practical feasibility

3.4.1 Overview of Wetting and Drying Methodology

This study employs wetting and drying cycles to simulate the environmental conditions that soils used in anti-erosion layers typically endure. Understanding how these soils respond to moisture variations is crucial in assessing their suitability for such applications and in evaluating the accuracy of existing soil erodibility models. The methodology adopted here, involving dividing the samples post-Proctor compaction and subjecting them to cycles, directly addresses the study's goal to investigate the interplay between soil properties and environmental factors, providing key insights into the erosion processes.

Specific methodology was employed where clay samples underwent three cycles of wetting and drying, with each cycle designed to dry the samples to a water content lower than the shrinkage limit. This approach is grounded in the understanding that significant changes in clay's properties, particularly in terms of microstructure and shear strength, are most pronounced in the initial cycles Goh et al. [2014], Yanli et al. [2021]. Researches indicate that the magnitude of changes induced by cyclic wetting and drying tends to diminish after a certain number of cycles Basma et al. [1996], Ma et al. [2015]. Therefore, three cycles were chosen to adequately capture the significant changes while reflecting the stabilizing trend of properties observed in subsequent cycles. It also provided a reasonable time for each sample preparation, which allowed the preparation of the first batch of samples, observing its behavior during cycles and EFA tests. After these results were analyzed, the second batch of samples was prepared and tested.

3.4.2 Establishment of Wetting and Drying Procedure

The target moisture contents for the drying and wetting phases were chosen to reflect the study's focus on understanding changes in soil microstructure and erodibility due to environmental conditioning. This approach allows for a detailed analysis of how cyclic moisture variations affect the soil, contributing to a comprehensive understanding of soil behavior under real-world conditions and aiding in the development of effective erosion-resistant structures.

The choice of drying to a level below the shrinkage limit and plastic limit was based on studies suggesting that such conditions intensify changes in clay properties, including a reduction in void ratio and swelling potential Ahmadi et al. [2012], Goh et al. [2014]. Section 2.4 gives a more detailed overview of the studies that guided the chosen methodology.

The water content at the shrinkage limit for Boom Clay was obtained from the literature and equals 16% (Marinho [1994], Assadollahi and Nowamooz [2020]). The plastic limit (PL) for tested Boom Clay according to Boskalis research (Boskalis [2023]) and laboratory determination varies from 21% to 22%. Based on this, the target water content for the drying phase was set at 15% ± 5%. The target water content for the wetting phase was set at 27%.

Drying Procedure: Test samples were prepared in the same manner and subjected to drying, with intermediate checks of moisture content. Based on these tests, the following procedure was chosen:

1. The sample was sealed for 24 hours to ensure an even distribution of moisture.
2. It was then placed in a ventilated oven at 50°C for 1 hour.
3. Subsequently, the sample was exposed to air for 24 hours.
4. The change in mass was recorded, and the "dry" water content (W_d) was calculated.
5. Finally, the sample was sealed again for 24 hours to achieve even moisture distribution.

Wetting Procedure: Similarly, the wetting procedure was developed following a similar procedure:

1. The sample was placed between two saturated sponges in an enclosed container for at least 36 hours.
2. The change in sample mass was recorded every 8-12 hours to monitor the moisture content.
3. The process was stopped once the "wet" water content (W_w) equaled the original water content (W_0).
4. The sample was then sealed for 24 hours for even moisture distribution.

The duration of each step was determined using test samples prepared in the same manner and subjected to wetting and drying with intermediate moisture content checks. Once a test sample reached the desired water content and had been sealed for 24 hours, it was cut into pieces, and the water content was determined through complete drying. This procedure verified the homogeneous moisture change within the sample.

Figure 3.6 demonstrates moisture level fluctuation in wetting and drying cycles for a Boom Clay sample.

W [%]			
W_0	29.91		
W_{D1}	17.52	Dry	Cycle 1
W_{W1}	35.93	Wet	
W_{D2}	13.82	Dry	Cycle 2
W_{W2}	30.48	Wet	
W_{D3}	12.34	Dry	Cycle 3
W_{W3}	27.50	Wet	

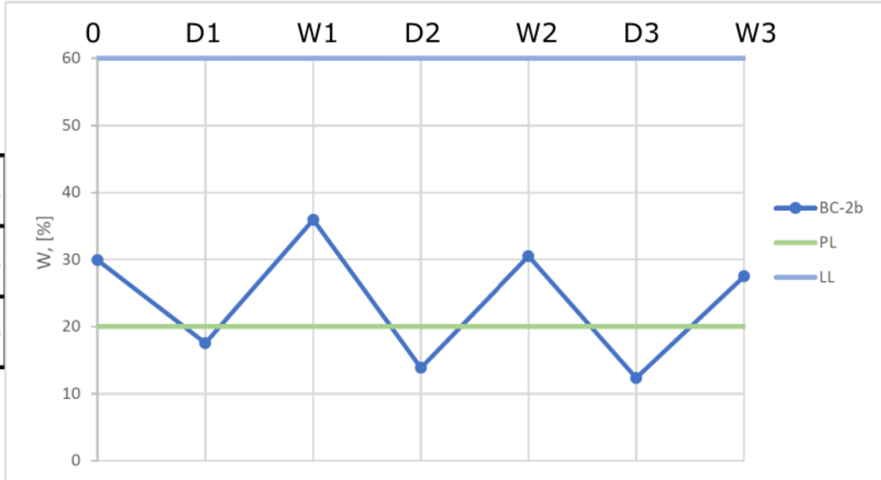

Figure 3.6: Moisture level fluctuation in wetting and drying cycles for Boom Clay sample prepared according to Procedure 1: Simulated Construction (BC-2).

3.4.3 Utilization of Test Samples in Establishing Cycle Duration

To optimize the wetting and drying routines, test samples played a crucial role in establishing the duration and efficacy of each step. These test samples were prepared from the same Boom Clay or Kleirijperij material, using the same Proctor compaction procedure as the main study samples, ensuring consistency across all tests.

Moisture Content Monitoring The moisture content of the test samples was closely monitored to guide the progression of the wetting and drying cycles. This monitoring involved hourly measurements of mass change during the cycles, with the final water content determined by completely drying the sample. This frequent and meticulous measurement allowed for accurate tracking of moisture changes, providing a reliable basis for adjusting the cycle duration.

Criteria for Cycle Progression The progression from one step of the cycle to the next was contingent upon reaching the predetermined water content for each phase. Achieving these moisture levels was critical in ensuring the validity of the cycles in simulating real-world environmental conditions.

Adjustments from Test Findings The duration of each phase in the wetting and drying cycles was fine-tuned based on the performance of these test samples. Notably, an attempt to accelerate the wetting process by fully submerging a test sample in water did not yield beneficial results (see Figure 3.7, reinforcing the chosen method of gradual moisture addition. These findings led to adjustments in the cycles' time frames, ensuring the most effective and realistic simulation of environmental conditions.

Validation and Confirmation of Procedures The test samples were instrumental in validating the 24-hour resting period between phases, confirming that this duration allowed for even moisture distribution within the samples.

3.4.4 Adjustment of Wetting and Drying Procedure

Initially, samples prepared according to Procedure 1, which involved compacting crushed material, were subjected to wetting and drying cycles as halves of a cylinder-shaped sample (72 mm in height

Figure 3.7: Boom Clay test sample (ST-4) lost its integrity after submerging into water.

and 105 mm in diameter) obtained from Proctor compaction. These samples, including **ST-1b, BC-1b, BC-2b, CR-1b, and CR-2b**, were treated in this manner. Upon completion of the last cycle, the EFA samples were prepared using the EFA mold (20 mm in height and 40 mm in diameter).

However, after running EFA tests and observing a slight difference in erosion performance between two groups of specimens, it was hypothesized that surface crack propagation might affect performance alongside structural changes in the soil. This led to a modification in the procedure: for samples prepared according to Procedure 2 (compacting homogeneous material) and Procedure 3 (obtained in situ), the EFA specimens were cut into molds (20 mm in height and 40 mm in diameter) after compaction and then subjected to the wetting and drying cycles. In these cases, the samples **BC-4b, BC-5b, and CR-4b** were processed with the top and bottom exposed, and the sides enclosed within the mold. A detailed description of the observed behaviors is given in Chapter 4, while a comparison of the results obtained from these different procedures is presented in Chapters 5 through 7.

3.4.5 Conclusion of Wetting and Drying Cycles Methodology

In conclusion, through meticulous planning and execution, the cycles were optimized to reflect real-world conditions. The use of test samples was instrumental in fine-tuning each step, ensuring accuracy in simulating the moisture changes that soils typically experience in anti-erosion applications. The scheme of the wetting and drying cycle routine is given in Figure 3.8. For a detailed description of every sample subjected to these cycles, including data on moisture content fluctuations, see Appendix C. This systematic methodology lays a solid foundation for the subsequent phases of the research, including erosion function apparatus testing and comparative analysis across various soil types.

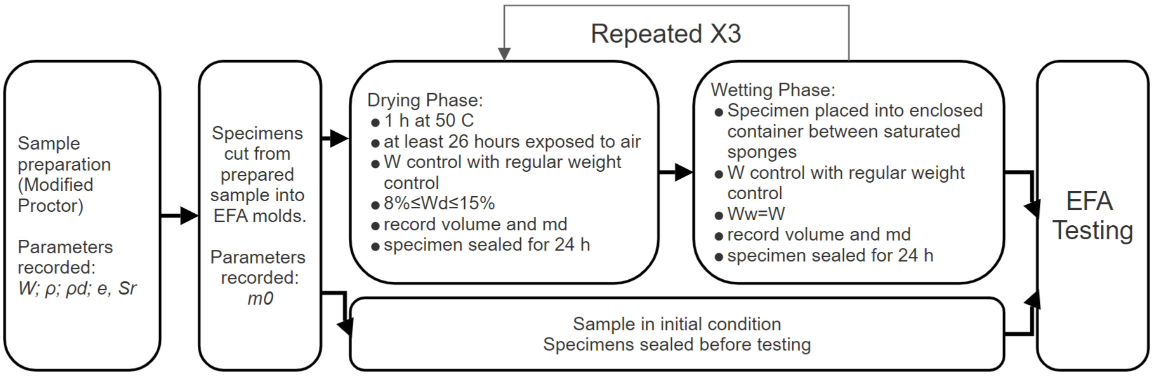

Figure 3.8: Scheme of the Wetting and Drying Cycle Routine

3.5 Erosion Testing Methodology

The erosion behavior of the tested clay material was investigated using the EFA setup. This section details the testing procedures and parameters.

3.5.1 EFA Description

The Erosion Function Apparatus (EFA) used in this study was assembled and tuned up in the Boskalis laboratory by Lars Rook as a part of his Master Thesis research (Rook [2020]) in 2020. It follows the traditional design of this kind of testing device (see Chapter 2.3). A 105 cm long plexiglas fume with a rectangular (6x5 cm) cross-section is connected to the pump that is submerged into the water and creates a flow in the fume (see Figure 3.9. The soil sample is protruded into the fume and exposed to the water flow that applies shear stress to the sample and triggers the erosion.

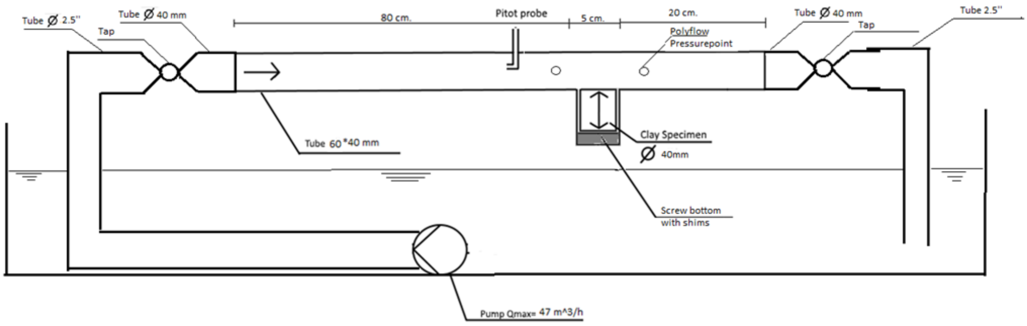

Figure 3.9: Scheme of the EFA (Rook [2020]).

The set-up is equipped with three Rosemount pressure difference sensors. The first one is connected to the pitot tube and allows logging and calculating the flow velocity; the second one is connected to the pressure points before and after the sample and provides readings of the pressure drop above the sample; the third Rosemount sensor provides readings of absolute pressure during the test. The following variables are controlled:

- Flow rate (adjusted by modulating the pump's operating frequency).
- Initial protrusion (fixed at 1 mm or 2 mm).
- Initial sample mass.
- Sample properties, which are standardized using either the Proctor compaction procedure or an EFA mold.

The following variables are measured:

- Flow velocity (measured with the pitot tube).
- Pressure drop in the sample area.
- Absolute pressure.
- Protrusion difference after the test.
- Sample mass loss during the test.

Flow velocities range from 2 m/s to 4.5 m/s, determined by the pump's capacity. This velocity has an accuracy of +/- 1.5% of the average recorded value. Erosion rate is then ascertained either by volume loss, considering the initial protrusion and test duration, or by mass loss. The range of measurable shear stresses is expansive, primarily due to the differential pressure sensor's precision and range (see Section 3.5.3 and Appendix D for detailed description). However, it doesn't register shear stresses below approximately 9 Pa due to the pump's velocity limitations. The maximum shear stress isn't specified as it significantly surpasses those linked with 4.5 m/s flow rates, and its deviation is around +/- 7%. The system can measure pressures from 0 bar to 4 bar. The EFA can detect erosion rates between 0 and 300 mm/hr. Tests shorter than 12 seconds, resulting from erosion rates above 300 mm/hr, aren't reliable. The expected accuracy of these rates is +/-10%, but it varies based on the specific clay under examination, as detailed in the Appendix. Further insights into the EFA design, full-page diagrams, result images, and proof-of-concept tests can be found in Appendices A B and D.

3.5.2 Testing Procedure

The erosion test commences with the preparation of the sample using a custom EFA mold, after which its mass is logged as m_0. After ensuring the setup is in proper working condition, the desired pump frequency is preset on the control unit. The sample is then positioned inside the erosion flume with the unique protrusion control mechanism adjusted to set a precise protrusion of either 1 mm or 2 mm. Once the flume is filled with water, the sensors are activated, time logging starts, and the pump is initiated to begin the flow. If deemed necessary, photo or video recording is initiated. The test operates consistently for an hour or until the entire protruded section erodes. After this, the pump is switched off, and the sample is retrieved from the flume. Logging operations cease, the mass of the sample is recorded as m_a, and the sample is moved to an oven for drying. Finally, once the sample has completely dried, its mass is noted as m_d.

3.5.3 Sensors interpretation

The set-up is equipped with three Rosemount pressure difference sensors that allow the calculation of flow velocity, pressure drop over the sample, and absolute pressure during the test.

The flow velocity was calculated based on the readings of the pressure difference sensor connected to the pitot tube. Logged pressure difference during the test was then recalculated to the flow velocity according to an equation 3.1 derived from Bernoulli's principle.

$$v = \sqrt{\frac{2(p_t - p_s)}{\rho}} \tag{3.1}$$

With

- v - flow velocity;
- p_t - stagnation or total pressure;
- p_s - static pressure;
- p - water density.

The average value of flow velocity during the test was then used in the calculation. The system was initially calibrated by running an empty fume at different pump frequencies and logging flow velocities.

That allows us to establish a correlation between pump frequency and flow velocity and examine the consistency of readings.

The value of shear stress during laboratory erosion tests is typically assessed by two main methods. The first one uses the Moody chart (see Figure 2.2), to obtain the value of friction factor based on flow type and roughness of the surface and calculating the the shear stress on the eroded soil surface with the formula 3.2. This method is used in EFA tests, JET tests, HET test, Sediment Erosion test at Depth Flume, and BET test (Briaud et al. [2019]).

$$\tau = \frac{1}{8} f \rho v^2 \tag{3.2}$$

With

- τ - shear stress [Pa];
- f - friction factor from the Moody chart[-];
- ρ - fluid's density $[kg/m^3]$;
- v - flow velocity $[m/s]$.

The equation is derived from the Darcy-Weisbach equation, which conveys the concept of head loss due to friction in fluid flow systems.

The friction factor f is determined by the Moody chart with the Reynolds number is calculated as follows:

$$R_e = \frac{\rho V D}{\mu} \tag{3.3}$$

With:

ρ - fluid density $[g/cm^3]$.

V - average flow velocity $[m/sec]$.

μ - dynamic viscosity $[Pas]$.

Relative roughness is the dimensionless ratio of roughness height ε, to the fume hydraulic radius. Based on these two parameters the value of the friction factor is determined on the Moody chart that incorporates both laminar and turbulent flow regimes.

The second method allows the calculation of shear stress on the bottom of a flow from the value of pressure drop over a certain length of flow. This method uses the Darcy–Weisbach equation to derive the formula 3.4 (for a rectangular channel). This method is used in SERF tests, Drill Hole tests, and Ex Situ Scour Testing Device (ESTD) (Briaud et al. [2019]).

$$\tau = \frac{(\Delta P \times A)}{(2a + 2b) \times L} \tag{3.4}$$

With

- τ - shear stress[Pa];
- ΔP - pressure drop [Pa];
- A - cross-section area of the channel $[m^2]$;
- $2a + 2b$ - hydraulic radius of the channel [m];
- L - distance between pressure reading spots [m].

Since the set-up had a sensor to measure the pressure drop over the sample the second method was initially used. However, due to sensor sensitivity, the fluctuations in the readings were very high. Also, after performing all tests a comparative analysis of the shear stress calculated by these two methods and the data obtained by L. Rook during the calibration of the set-up was carried out. Based on this analysis it seems that the value of shear stress calculated from the readings of pressure drop is systematically higher than values obtained by calculation from flow velocity and data of L. Rook (Rook [2020]). Based on this and the significant fluctuations of the pressure drop readings it was decided to use the value of shear stress calculated from the flow velocities. The other advantage is that this method of obtaining shear stress is typical for EFA tests, which makes obtained results comparable with other available data. A more detailed overview of shear stress calculation is given in Appendix D.

The setup incorporates an absolute pressure sensor capable of measuring pressures from 0 bar to 4 bar. While the sensor's primary function is to monitor potential excessive stress on the acrylic tube, its data also offers a potential reference point for cross-checking with results from Computational Fluid Dynamics (CFD) modeling, ensuring real-world test data is consistent with modeled outcomes. This modeling was performed by L. Rook during the initial build and calibration of the set-up(Rook [2020]). However, it should be noted that no modeling was conducted during the current study, and as such, the readings from this absolute pressure sensor were not utilized.

3.5.4 Test Results Interpretation

During the calibration runs of the EFA, certain specimens displayed atypical erosion patterns, particularly rapid erosion in large chunks within the first 5-10 minutes, followed by minimal subsequent erosion in the following hour. This phenomenon, likely due to weak zones in the samples, provided technical insights into soil structure but skewed overall results given the limited number of tests. To ensure data accuracy, tests showing significant erosion in 1-3 large chunks within the first 5 minutes and no visible erosion in the following hour were excluded from the final analysis. This exclusion criterion was adopted primarily due to a limited number of tests for each sample.

The following data was obtained or calculated during each test:

- v - flow velocity [m/s] - the average value is taken from the readings of the sensor connected to the pitot tube;
- τ - shear stress [Pa] - calculated from the average flow velocity as described in 3.5.3;
- dm [g] or dh [mm] - the difference in dry mass or height of the sample before or after the test;
- t [h] - duration of the test in hours;
- $\dot{z}(m)$ [g/h] or $\dot{z}(h)$ [mm/hr] - erosion rate by mass or by volume change, calculated as $\dot{z}(m) = dm/t$ and $\dot{z}(h) = dh/t$ respectively.

The values of $\dot{z}(m)$ and $\dot{z}(h)$ represent the average erosion rate with no differentiation by time during the test, which means that it was assessed under the hypothesis of a constant rate of erosion through the test. This is a common practice in laboratory erosion tests (see Section 2.3) and this allows comparing obtained results with data from the previous research (Rook [2020]).

At least three tests were run for each sample with the results plotted in the $\dot{z}/\tau$ plane (see Figure 3.10). In analyzing the data from the EFA tests, two models are used the most: the **SRICOS** and the **NCHRP Report Model**.

The **SRICOS (Scour Rate in Cohesive Soils) Model** functions more as a structured methodology than a strict model (Shan et al. [2015b]). It is characterized by its recommendation to plot shear stress against a "linear" erosion rate ($\dot{z}(h)$ [mm/h]) in arithmetic space, using a log function for the best fit (see Figure 3.10). Two primary properties are derived from this model:

- τ_c [Pa] - the Critical shear stress represents the shear stress at which erosion initiates - the crosssection of erosion curve and x-axis;
- Si [mm/hr/Pa]- detachment coefficient (share stress driven) - the linear slope of the early erosion curve when plotted against shear stress.

While the SRICOS model is valued for its simplicity and guarantee of yielding a result for critical shear stress and detachment coefficient, it has its limitations. The fit's quality is significantly influenced by the data points' quality and quantity. Additionally, presume to obtain the value of a critical flow velocity, even though the flow velocity is directly measured through the test. Generally, it has been observed that the SRICOS model produces higher critical shear stresses and detachment coefficients compared to the methodology in the NCHRP report.

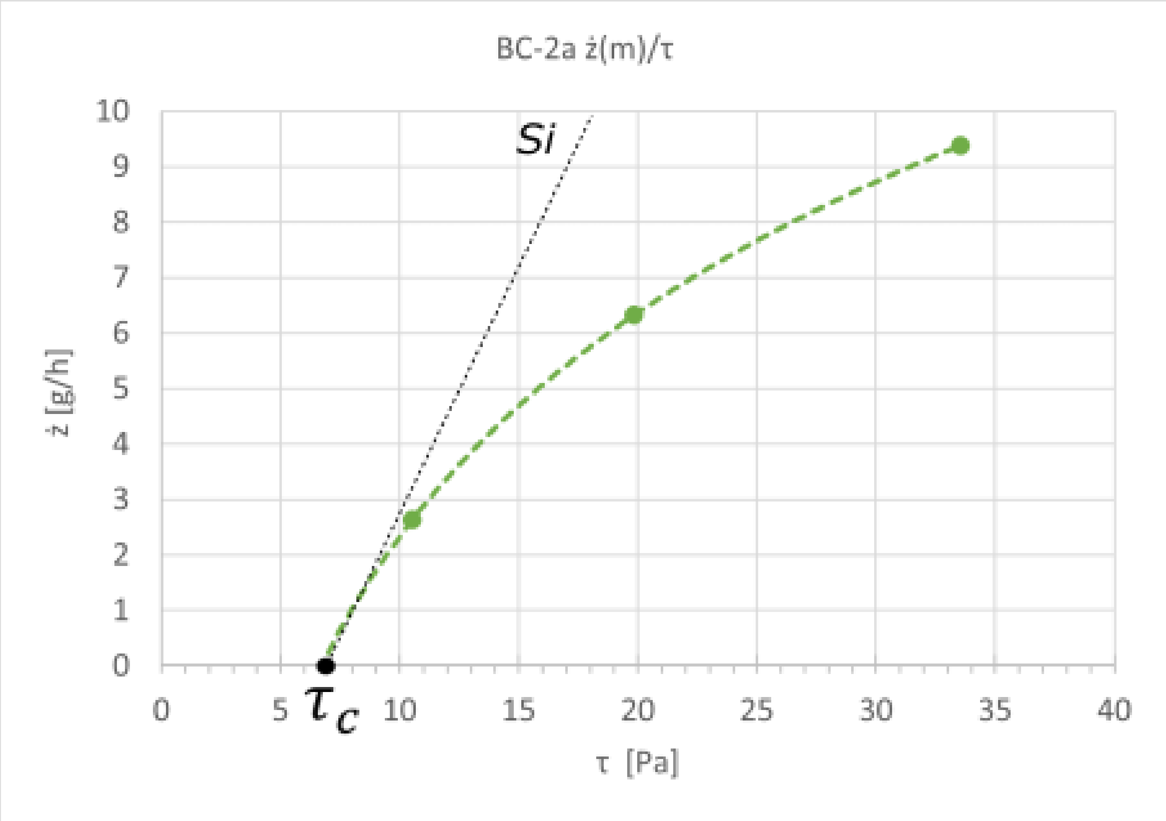

Figure 3.10: Test result of a Boom Clay sample (BC-2a) in SRICOS model presentation; $\tau_c = 6.71 Pa$.

The **NCHRP Report Model** based on the 2019 study carried out in Texas A&M Transportation Institute (Briaud et al. [2019]) takes a more holistic approach, encompassing a variety of tests, including but not limited to EFA and Jet erosion tests. This model suggests using two log-log space graphs for plotting erosion rate ($\dot{z}(h)$) versus shear stress and flow velocity (see Figure 3.11). From these graphs, equivalent erosion parameters are determined:

- v_c [m/s] - critical erosion velocity - the velocity where the erosion curve meets the horizontal axis;
- τ_c [Pa] - the critical shear stress represents the shear stress at which erosion initiates - the crosssection of the erosion curve and x-axis;
- Si [mm/hr/Pa]- detachment coefficient (share stress driven) - the linear slope of the early erosion curve when plotted against shear stress.
- Si_c [mm/hr/Pa]- detachment coefficient (velocity driven) - the linear slope of the early erosion curve when plotted against velocity.

The NCHRP model has the advantage of addressing the critical flow velocity, however, it often produces more conservative results compared to the SRICOS model, which is apparent in the lower predicted critical shear stresses and detachment coefficients.

Both these models along with Briaud et al. [2001], Hanson and Cook [2004] and other studies on EFA erosion tests usually utilize the value of the ”linear” erosion rate (often denoted as $\dot{z}$ $[mm/hr]$) that is calculated based on the time required to erode a specific amount of sample protrusion (usually 1.0 mm) in the erosion fume.

Also, the value of the weight erosion rate is used (often denoted as e_r $[g/hr]$) which is calculated based on the sample mass loss during the test. This approach is described in the literature (see Bloomquist et al. [2012], Crowley et al. [2012]). Briaud et al. [2001] in their study over the use of EFA tests for scour rate predictions argued that the linear erosion rate $\dot{z}$ is related to the weight erosion rate e_r which is determined using the rotating cylinder apparatus or the drill hole apparatus. This

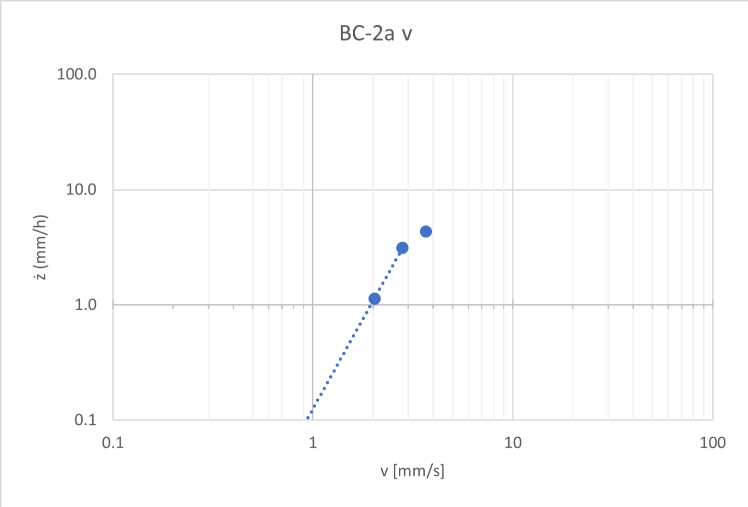

(a) $v_c = 0.93Pa$

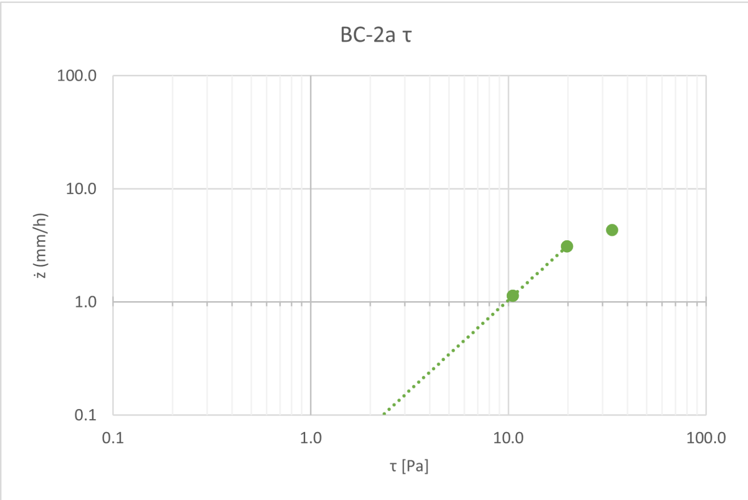

(b) $\tau_c = 2.31Pa$

Figure 3.11: Test result of a Boom Clay sample (BC-2a) in SRICOS model presentation the NCHRP Report Model presentation.

relationship may be expressed as follows:

$$e_r = \gamma \dot{z} \tag{3.5}$$

γ is the total unit weight of the soil.

For clarity, further in this study, the $\dot{z}(h)$ notation will be used for linear erosion rate and $\dot{z}(m)$ for erosion rate by mass.

During the erosion tests performed in this study, it became evident that the erosion pattern was not uniform across samples, especially for those subjected to wetting and drying cycles. Some areas of the sample can erode extensively, going below the 1 or 2 mm threshold, while other parts remain largely unaffected. This will be covered in detail in Chapter 4, the representative case is illustrated in Figure 3.12 which shows the Boom clay sample obtained from Markermeerdijken site and been subjected to 3 cycles of wetting and drying (BC-5bE2) after the erosion test.

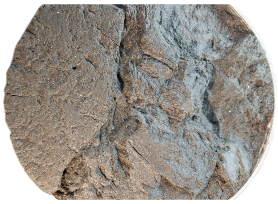

(a) BC-5bE2 top view

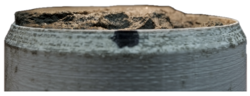

(b) BC-5bE2 side view

Figure 3.12: Boom Clay sample (BC-5bE2) after the erosion test.

The test ran for 78 minutes at a flow velocity of 2.10 m/sec; the dry mass loss recorded was 3.09 g, which corresponds with the erosion rate by mass ($\dot{z}(m) = dm/t$) of 2.38 g/h. It is evident from the photo (Figure 3.12b that while the right part of the sample (flow side) eroded completely and even below the mold border, the right side in some areas kept the original protrusion of 2.0 mm. The top view (Figure 3.12a) exposes numerous deeper-than-average erosion in the central part of the sample. After measuring the sample height with a precise caliper, the average height loss resulted in 3.35 mm, which corresponds with the linear erosion rate ($\dot{z}(h) = dh/t$) of 2.58 mm/hr. The linear erosion rate calculated according to equation 3.5 was 4.41 mm/hr. This higher value incorporates these deeper erosion regions and seems to be more representative.

Some EFA setups are equipped with a protrusion-controlling mechanism, which allows for the sample to protrude into the flow as its upper part gets eroded. This feature enables a larger soil volume to undergo erosion during the test, subsequently increasing the measurement's accuracy. However, the current setup lacks this mechanism, and retrofitting it poses significant technical challenges. Given these constraints, the reliance on linear erosion measurements alone can be misleading.

It was decided in this study to utilize erosion rate by mass as the primary determined value and recalculate it to the linear erosion rate to access the soil classification by the NCHRP Report Model. By weighing the sample both before and after the test and subsequently allowing it to dry completely, it's possible to calculate the loss in dry mass. With known initial density and moisture content, this loss in dry weight, when divided by the test duration, provides a more consistent measure of erosion rate in g/hr. This method captures the overall erosion impact without being skewed by localized uneven erosion.

3.6 Conclusion on Methodology and Experimental Plan

This research aimed to investigate how cyclic wetting and drying affect the erodibility of cohesive clay materials. The general changes that happen to the soil structure and properties during these cycles were studied from the previous research (see Chapter 2), and the main focus was on comparing the erodibility of samples in their original condition and after WD cycles using EFA testing.

Key Procedures and Controls:

- Material range: Two clays were tested: the first, Boom Clay, falls under Category 1 in the Dutch erodibility classification and is often used for constructing erosion protective layers. The second, Kleirijperij Clay, is classified as Category 3 and is generally considered unsuitable for such construction. Comparing these materials allows for a broader understanding of the spectrum of clay behavior in erosion contexts, from typically used to traditionally unsuitable materials.
- Sample Preparation: Ensuring comparable properties (water content, density) across all test samples was crucial. This involved controlled compaction of materials, consistent use of sample molds, and precise measurement of water content and densities.
- Wetting and Drying Cycles: The cycles were designed based on literature to induce structural changes in the clays, with controlled final water content for each cycle ensuring uniform treatment of samples. Three cycles of wetting and three cycles of drying were performed with water content going below the plastic and shrinkage limits to ensure the impact of drying on the soil structure and properties described in the literature.

- Erosion Function Apparatus Testing: EFA testing followed a standardized routine with calibrated equipment, ensuring consistent test conditions. At least 3 tests for each sample category were performed to enhance data reliability.
- Data Collection and Analysis: Data integrity was maintained through the use of calibrated laboratory equipment and the EFA setup.
- Challenges and adaptations: Several challenges were encountered during the study: the sample protrusion control mechanism in the EFA setup was redesigned, to improve the persicison of protrusion control. Sample molds for EFA testing were redesigned and produced with 3D printing technology, which allowed effective cutting and storing of samples and improved their repeatability. The absence of specialized humidity-controlling facilities for wetting and drying cycles led to the development of a custom moisturizing system. Additionally, consumer-level photography equipment was used for capturing sample images, which were then analyzed to gain a better understanding of the processes occurring during the wetting and drying cycles.

4 Sample Preparation and Tests results

The study employs three distinct clay sample preparation methods which when tested on the EFA. The procedures for each method are detailed in Chapter 3. Table 4.1 below gathers the soil properties of prepared samples before the wetting and drying cycles. All Boom clay samples have similar water content and dry density that allow comparing the EFA testing results.

Method	**W**	ρ	ρ_d	ρ_s	**e**	**Sr**	**LL**	**PL**	**PI**	**LI**
	%	g/cm3			-	-	%			-
Boom Clay										
SC	29.91	1.82	1.40	2.65	0.89	0.89	69	21	48	0.19
HR	26.56	1.82	1.44	2.65	0.84	0.84	63	22	41	0.14
IR	25.70	1.82	1.45	2.65	0.83	0.82	60	20	40	0.10
Kleirijperij Clay										
SC	41.22	1.46	1.03	2.68	1.59	0.69	105	40	65	0.02

SC = Simulated Construction Method
HR = Homogenized Reconstitution Method
IR = In-situ Retrieval Method

Table 4.1: Properties of soil samples prepared by different methods.

4.1 Observations during cyclic wetting and drying

The samples prepared according to the Simulated Construction Method were subjected to wetting and drying and then cut into the EFA molds and tested. Two other groups were subjected to wetting and drying within the EFA molds. In total three cycles of wetting and drying were performed with moisture content reduced below the plastic limit during the drying phase and re-saturation to the original moisture content during the wetting phase. The detailed procedure description was given in Chapter 3, and the detailed data on cycles and sample photos may be found in Appendix C. During drying phases, the emergence of surface cracks was a recurring phenomenon, attributed to the shrinkage of clay particles as the water was lost. This was observed more often and on a larger scale for Boom clay samples due to higher swelling potential. This behavior aligns with Boom clays' well-documented shrink-swell behavior, whereby the interactions between clay particles, moisture, and environmental conditions lead to volumetric and structural changes (Bernier et al. [1997]). Figures 4.1 and 4.2 show a sample of Boom clay in its original condition and after 1 cycle of drying.

In the subsequent wetting cycles cracks were partially sealed due to particle expansion upon water absorption. Figure 4.3 shows a sample of Boom clay after 1 cycle of wetting.

(a) BC-1 side view (b) BC-1 top view

Figure 4.1: Boom Clay sample prepared by Simulated Construction Method (BC-1) in initial state

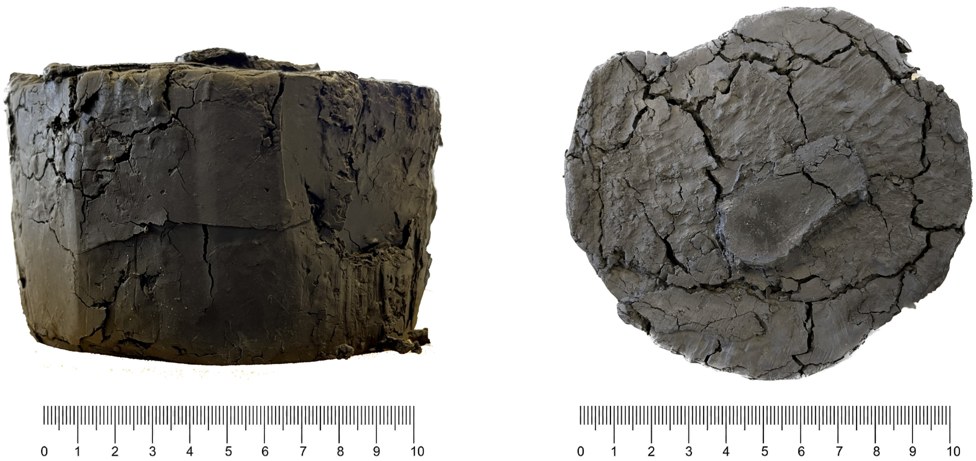

(a) BC-1 side view (b) BC-1 top view

Figure 4.3: Boom Clay sample prepared by Simulated Construction Method (BC-1) after the first wetting cycle

The samples that were prepared according to the HR method, and IR method were subjected to the cycles of wetting and drying in the EFA molds. As depicted in Figure 4.4, the HR sample (BC-4bE1) throughout its three drying phases displayed significantly fewer cracks in comparison to the IR sample (BC-5bE1), illustrated in Figure 4.5. The corresponding wetting cycles are not displayed in these photos.

This contrast becomes even more evident when observing the samples after multiple wetting and drying cycles. Figure 4.6 presents the HR sample (BC-4bE1) in its original state alongside the same sample after three cycles, revealing a marked ability for crack sealing, likely due to the clay's swelling attributes. In contrast, the IR sample, shown in Figure 4.7, does not exhibit a similar recuperative capacity after an identical number of cycles.

(a) BC-1 side view (b) BC-1 top view

Figure 4.2: Boom Clay sample prepared by Simulated Construction Method (BC-1) after first dry cycle.

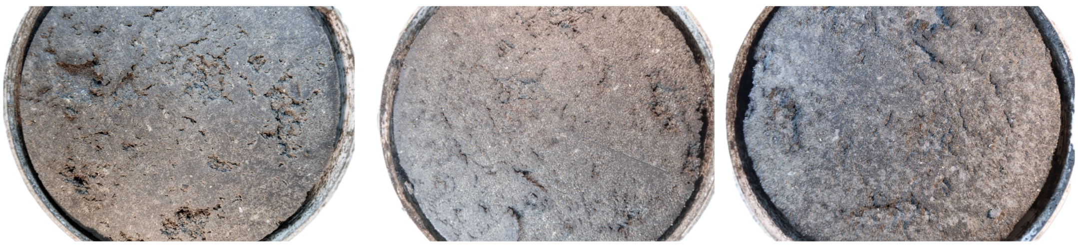

(a) Dry 1 (b) Dry 2 (c) Dry 3

Figure 4.4: Boom Clay sample prepared by Homogenized Reconstitution Method (BC-4bE1) after first (a), second (b), and third (c) cycles of drying.

(a) Initial condition (b) After 3 w/d cycles

Figure 4.6: Boom Clay sample prepared by Homogenized Reconstitution Method (BC-4bE1) in its initial condition (a) and after three cycles of wetting and drying (b).

(a) Dry 1 (b) Dry 2 (c) Dry 3

Figure 4.5: Boom Clay sample prepared by In-situ Retrieval Method (BC-5bE1) after first (a), second (b), and third (c) cycles of drying.

(a) Initial condition (b) After 3 w/d cycles

Figure 4.7: Boom Clay sample prepared by In-situ Retrieval Method (BC-5bE1) in its initial condition (a) and after three cycles of wetting and drying (b).

Subjecting specimens to wetting and drying cycles within the EFA molds also allows controlling the volume change during cycles. The measurements were made through the first two wetting and drying cycles since the specimen became rather brittle in the dried stage and there was a threat of damaging specimen.

The results demonstrated distinct swelling behavior of Boom clay and Kleirijperij clay samples. Both clays exhibited volume reduction upon drying; however, while Boom clay samples showed significant volume recovery and increase upon re-wetting, Kleirijperij samples did not regain their original volume. Table 4.2 demonstrates the average volume change of the different samples compared to the original volume. Kleirijperij clay, being an organic silt clay, consistently decreased in volume across all stages (by 21-22%) and did not regain its original volume during re-saturation, potentially due to the organic content influencing their swelling potential.

Sample	**Volume change from initial**			
	Dry 1	Wet 1	Dry 2	Wet 2
Homogenized Reconstitution	-19%	+3%	-12%	0%
In-situ Retrieval	-20%	+5%	-7%	+4%
Kleirijperij	-21%	-5%	-22%	-1%

Table 4.2: Average volume change in different clay materials due to cyclic wetting and drying.

Focusing on Boom clay, two categories of samples prepared differently displayed notable contrasts. The first category, HR samples, was created by drying and crushing the clay, while the second, IR samples, were obtained directly from the Markermeerdijken site. In this manner, IR samples are considered over-consolidated (OC), inheriting the stress memory of initial Boom clay material, while HR samples are normally-consolidated (NC) (Burland [1990]). The HR samples showed a less pronounced volume increase upon re-saturation and did not increase the initial volume on the second wetting cycle, while IR samples demonstrated an increase in volume of 4%.

The clay material for HR samples was initially dried at 105^oC and then crushed. This preparation should not affect the mineralogical composition or organic content. From the literature, it was not possible to establish a correlation of swelling behavior with the stress history of clay. With this said, the variance in swelling behavior between HR and IR Boom clay samples may be explained by differences in their microstructure. The HR samples, having undergone a process of drying and crushing, likely developed a more homogeneous and compacted structure that exhibits less swelling compared to the dispersed structure of IR samples, as the arrangement of soil particles influences the interaction with water. This hypothesis suggests that the preparation procedure significantly influences the swelling characteristics of clay, however, it was not verified by comparison of microstructure of different samples.

4.2 Erosion Tests Results

The range of samples were prepared and tested on an Erosion Function Apparatus (EFA) is given in Table 4.3.

Preparation	W/D	Specimen		ρ_d [g/cm^3]	W [%]	v [m/s]	τ [Pa]	$\dot{z}$(m) [g/h]	$\dot{z}$(h) [mm/h]	Valid
Simulated construction	N	BC-2a	E1	1.46	25.61	2.03	10.54	2.62	1.14	Y
	N		E2	1.44	25.61	2.81	19.84	6.32	3.13	Y
	N		E3	1.46	25.61	3.68	33.53	9.37	4.32	Y
	Y	BC-2b	E1	1.43	26.32	1.98	10.04	1.13	0.50	Y
	Y		E2	1.45	26.32	2.80	19.70	2.55	1.11	Y
	Y		E3	1.45	26.32	3.60	32.13	4.58	1.99	Y
	N	CR-4a	E1	1.52	41.20	1.77	8.07	3.98	2.08	Y
	N		E2	1.57	41.20	2.11	11.36	5.06	2.56	Y
	N		E3	1.51	41.20	2.43	14.96	7.62	4.01	Y
Homogeneous reconstitution	N	BC-4a	E1	1.44	27.00	2.04	10.64	7.82	3.41	N
	N		E2	1.45	25.70	2.83	20.12	1.75	0.78	Y
	N		E3	1.43	25.70	3.60	32.13	4.94	2.19	Y
	N		E4	1.42	27.00	1.91	9.36	5.41	2.42	N
	N		E5	1.40	27.00	2.03	10.54	4.40	2.01	N
	N		E6	1.40	27.00	2.51	15.93	5.01	2.24	Y
	N		E7	1.42	25.70	2.81	19.84	2.07	0.91	Y
	N		E8	1.38	27.00	3.55	31.26	7.50	3.26	Y
	Y	BC-4b	E1	1.40	27.00	3.91	37.72	11.15	4.80	Y
	Y		E2	1.46	27.00	1.84	8.70	2.01	0.87	Y
	Y		E3	1.45	27.00	3.67	33.35	7.34	3.29	Y
In-situ Retrieval	N	BC-5a	E1	1.42	25.70	2.02	10.44	0.46	0.21	Y
	N		E2	1.43	25.70	2.82	19.98	1.92	0.85	Y
	N		E3	1.43	25.70	3.62	32.47	2.35	1.05	Y
	N		E4	1.44	25.70	1.63	6.87	1.98	0.89	N
	N		E5	1.41	25.70	2.46	15.32	2.12	0.94	Y
	N		E6	1.42	25.70	3.89	37.35	2.12	0.93	Y
	Y	BC-5b	E1	1.47	29.04	1.98	10.04	4.62	1.94	Y
	Y		E2	1.45	29.34	2.10	11.26	2.38	1.02	N
	Y		E3	1.43	29.54	2.43	14.96	7.89	3.16	Y
	Y		E4	1.54	29.30	3.32	27.45	11.77	5.01	Y
	Y		E5	1.41	28.05	2.68	18.10	2.93	1.29	N

Table 4.3: Erosion tests results.

The table gives the list of all specimens that were prepared and tested according to the procedure described in Chapter 3. In total 33 tests were performed on Boom clay samples and 12 on Kleirijperij samples. Only 3 credible results were obtained for Kleirijperij, which is mostly caused by the limitations of the current test setup. Because of the pump and sensor limitations the lowest flow velocity that may be achieved is 1.65 - 1.70 m/s. From 12 Kleirijperij clay samples that have been tested, 9 samples were completely washed out of the mold within 5-10 minutes at a speed ranging from 1.65 - 2.20 m/s, so no credible evaluation of erosion rate may be performed. These samples were removed from the mold by the flow in almost their entire form, instead of gradual erosion aggregate by aggregate or particle by particle. The results from the erosion tests on Boom Clay were excluded due to the rapid loss of a large portion of the specimen within the first 5-10 minutes of testing, followed by a period of no observable erosion. This behavior is likely linked to pre-existing weak zones within the sample. Although the decision to exclude these results may seem arbitrary, it was necessitated by the limited number of tests conducted. The full list of tested samples including the ones that did not yield any results is given in the Appendix B.

During each test, flow velocity (v [m/s]) was measured and the corresponding shear stresses (τ [Pa]) were deduced from these recorded velocities. Additionally, the dry mass of the eroded clay material was recorded (dm [g]), facilitating the subsequent calculation of the erosion rate by mass ($\dot{z}(m)$ [g/sec]). This derived value was then utilized to compute the linear erosion rate ($\dot{z}(h)$ [mm/sec]). The obtained data was processed adhering to both the SRICOS and NCHRP Report Models' methodologies (see Section 3.5 for the detailed process). The last one was chosen as the primary since it allows the calculation of both critical shear stress (τ_c [Pa]) and critical velocity (v_c [m/s]). Nevertheless, for the sake of comprehensiveness, the results derived from the SRICOS model calculations have also been outlined in the subsequent section.

4.2.1 Test results - Boom Clay

Condition	**Method**	**Sample**	τ_c **[Pa]**	v_c **[mm/s]**
Original	SC	BC-2a	2.31	0.93
	HR	BC-4a	8.00	1.05
	IR	BC-5a	7.42	1.70
After w/d cycles	SC	BC-2b	2.57	0.98
	HR	BC-4b	0.98	0.60
	IR	BC-5b	0.89	0.57

SC - Simulated Construction
HR - Homogenized Reconstitution
IR - In-situ Retrieval

Table 4.4: Boom Clay: values of critical velocity and shear stress obtained according to the NCHRP Report Model.

Table 4.4 represents the numerical results of Boom clay tests that were processed according to the NCHRP Report Model to obtain the values of critical velocity (v_c) and critical shear stress (τ_c). The left column indicates whether or not these specimens were subjected to wetting and drying cycles and the preparation procedure. The samples prepared using the Simulated Construction Method (BC-2a and BC-2b) exhibited lower critical shear stresses, with a slight increase observed in the sample subjected to wetting and drying cycles (BC-2b). The Homogenized Reconstitution Method samples (BC-4a and BC-4b) showed a significant variation, with a noticeable decrease of critical values for samples that underwent wetting and drying cycles (BC-4b), when compared with samples in original condition (BC-4a). Samples from the In-situ Retrieval Method (BC-5a and BC-5b) displayed critical values close to HR samples and similar decrease after cyclic wetting and drying, even with a slightly higher magnitude. This data indicates that both the method of sample preparation and the effect of wetting and drying cycles significantly influence the erosion characteristics of Boom Clay. Figures 4.8 and 4.9, display the erosion curves for these tests and allow a comparison of the performance of each specimen and erosion rates.

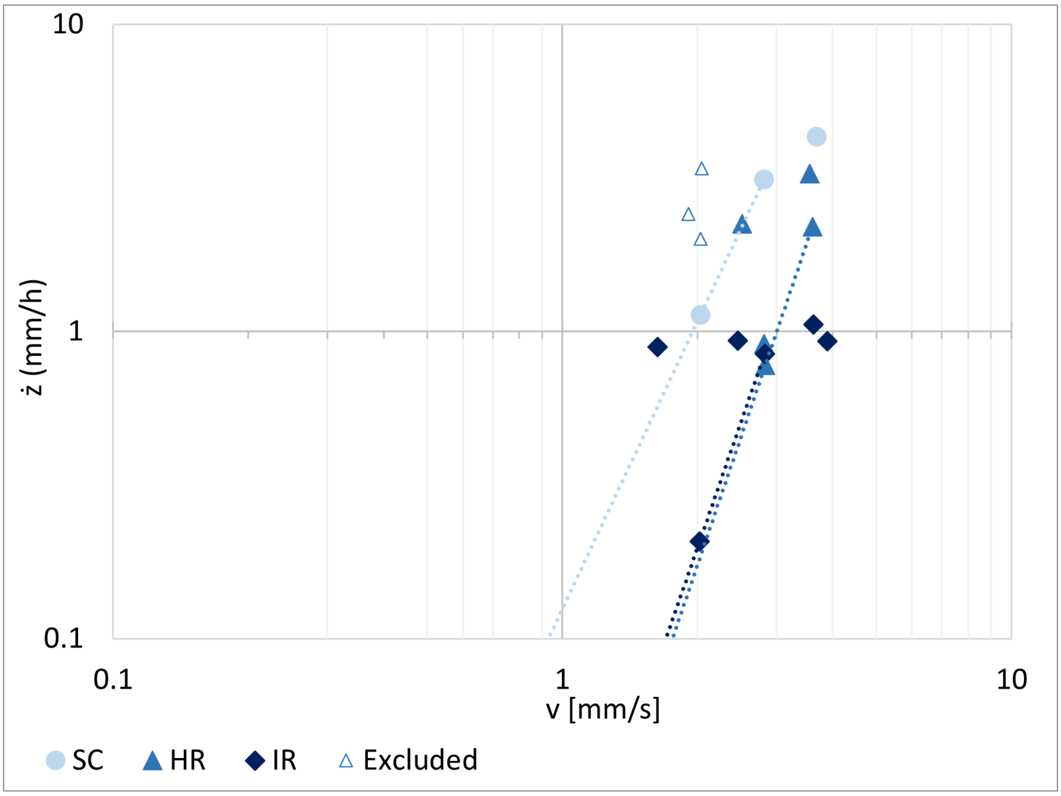

(a) $SC : \tau_c = 2.31Pa$; $HR : \tau_c = 7.43Pa$; $IR : \tau_c = 7.42Pa$

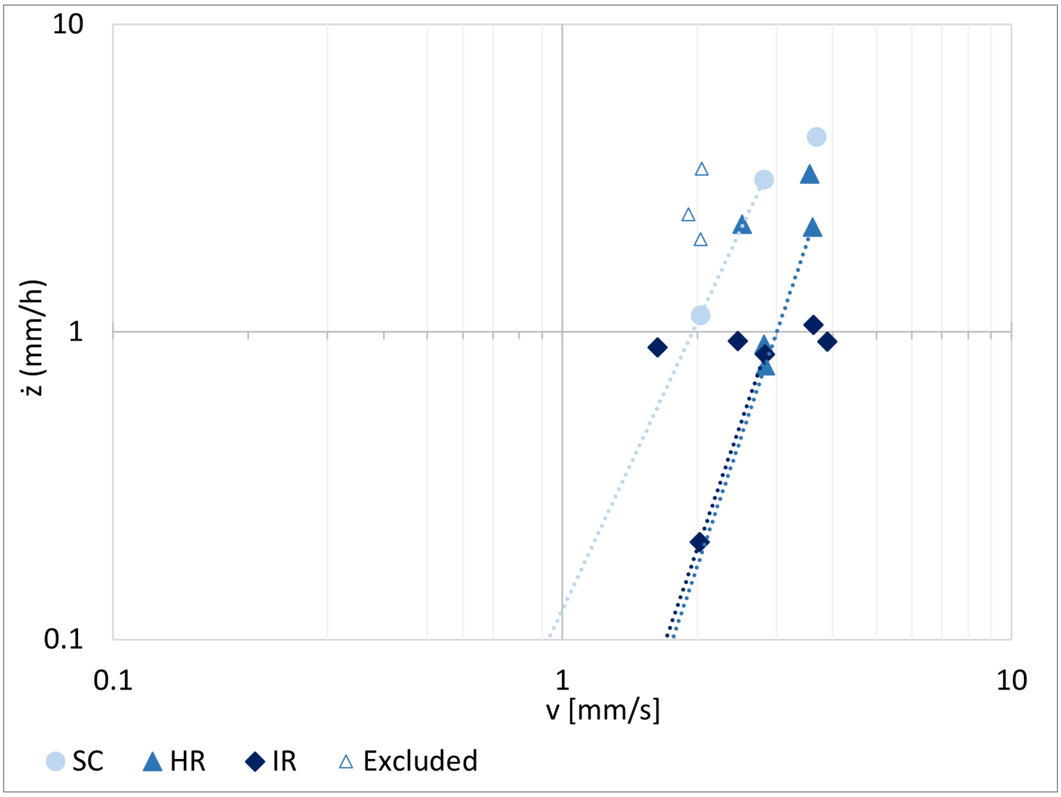

(b) $SC : v_c = 0.93m/s$; $HR : v_c = 1.05m/s$; $IR : v_c = 1.70m/s$

Figure 4.8: Erosion curves of samples in their original condition: based on τ_c (a) and based on v_c (b).

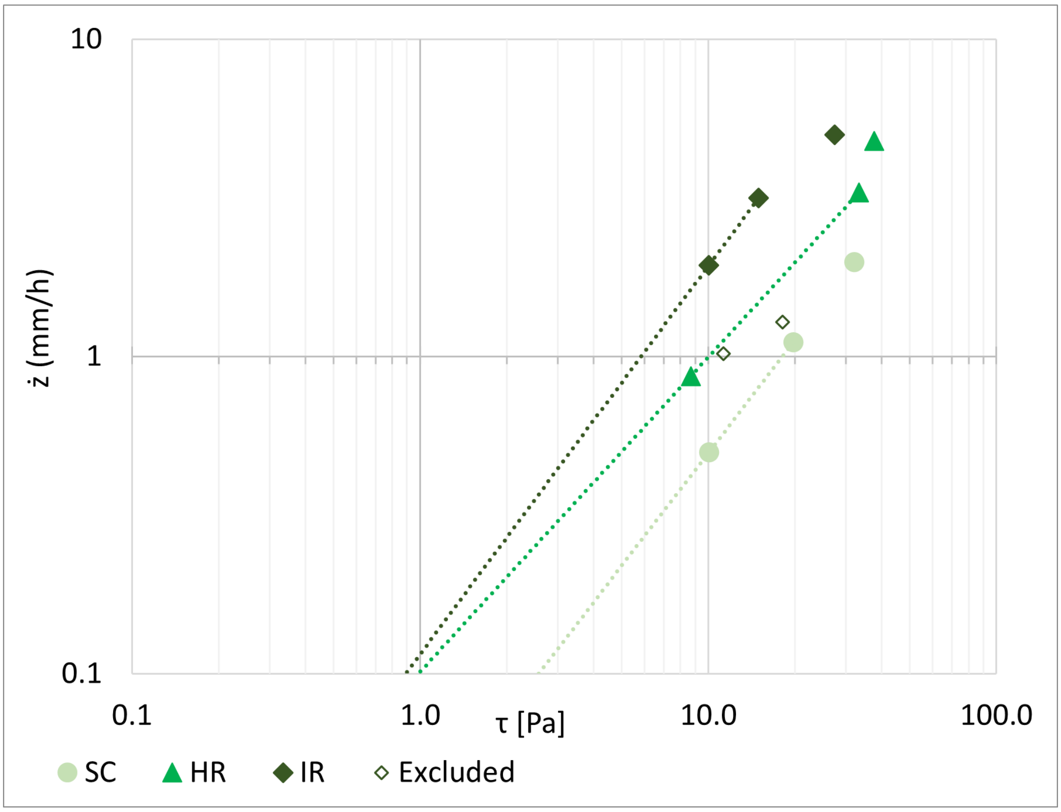

(a) $BC-2b : \tau_c = 2.57Pa$; $BC-4b : \tau_c = 0.98Pa$; $BC-5b : \tau_c = 0.89Pa$

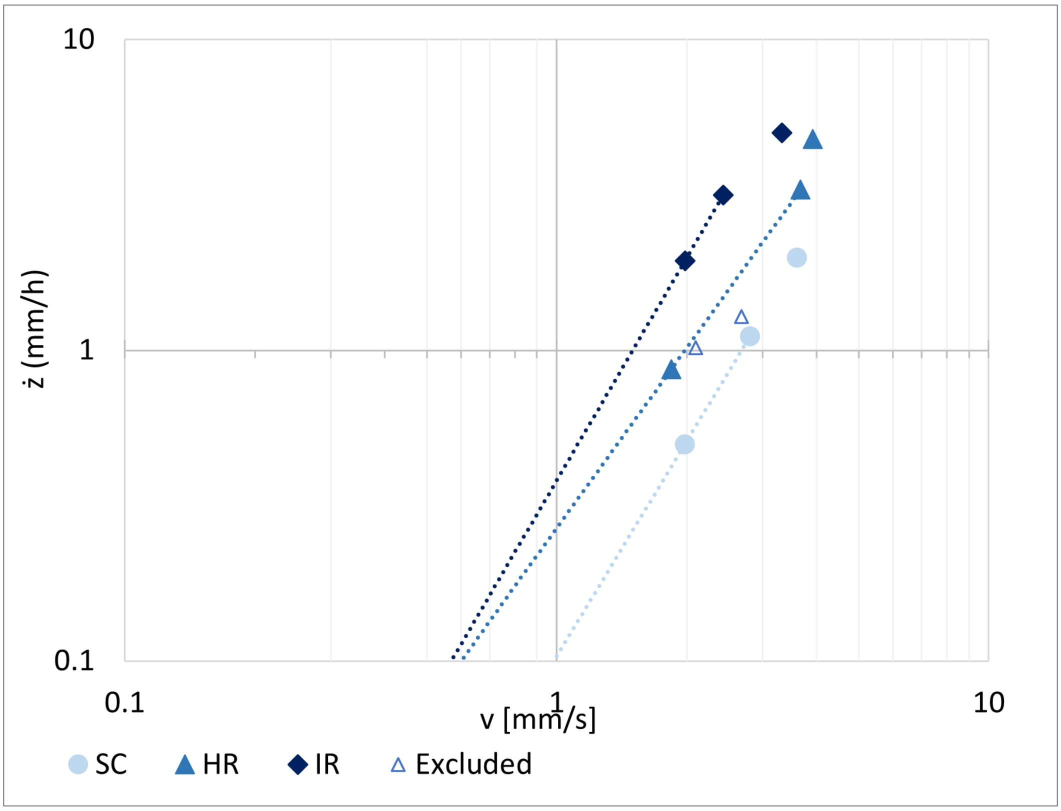

(b) $BC-2b : v_c = 0.98m/s$; $BC-4b : v_c = 0.60m/s$; $BC-5b : v_c = 0.57m/s$

Figure 4.9: Erosion curves of samples after wetting and drying cycles: based on τ_c (a) and based on v_c (b).

For Boom clay samples subjected to cycles of wetting and drying the erosion rates are generally higher than for samples in the original condition. Comparing samples prepared by different procedures, remolded homogeneous specimens (BC-4) and the ones prepared from soil samples obtained in situ (BC-5) demonstrate a general increase of erosion rates at relevant speed for specimens that were subjected to wetting and drying.

4.2.2 Test results - Kleirijperij Clay

The values of critical velocity and critical shear stress for the Kleirijperij clay are **0.14 m/s and 0.06 Pa** respectively — based on the NCHRP Report Model that are lower than those recorded for any of the Boom clay specimens, including those subjected to wetting and drying. The erosion rate is typically higher even at low flow velocity. Figure 4.10 shows erosion curves for the tested Kleirijperij sample.

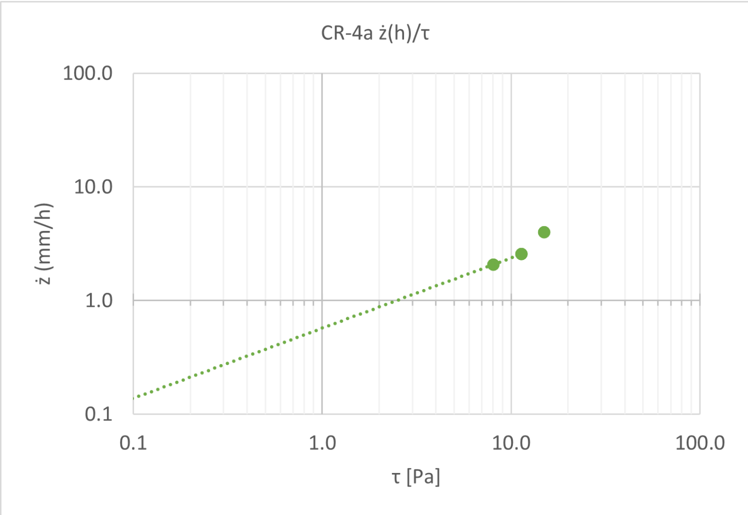

(a) $\tau_c = 0.06Pa$

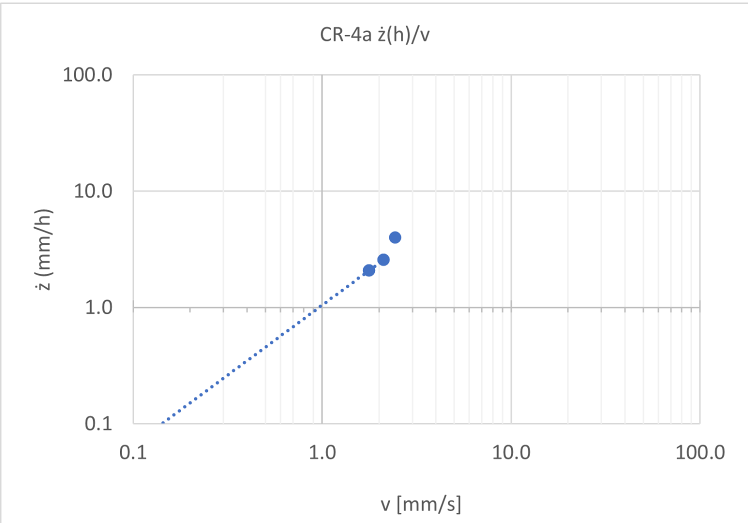

(b) $v_c = 0.14m/s$

Figure 4.10: Kleirijperij (CR-4a) specimens erosion curve.

5 Results Discussion

5.1 Influence of Preparation Method

Erosion test results for Boom Clay samples prepared according to different procedures highlight the differential erosion resistances of the materials. The Simulated Construction samples (BC-2) maintained their erosion resistances with critical velocities (v_c) and shear stresses (τ_c) of **0.93 m/s and 2.31 Pa** respectively. After cyclic wetting and drying only a slight increase to v_c=**0.98 m/s and** τ_c=**2.57 Pa** was observed. The Simulated Construction Method (SC) samples' resilience to wetting and drying could be attributed to the pre-existing microstructural configuration established during their preparation—where crushed chunks may create a matrix that mitigates the impact of moisture cycles commonly leading to soil weakening. This behavior underscores the significance of the initial soil preparation technique on the long-term erosion resistance of clay materials and warrants further investigation to fully comprehend the mechanisms at play.

Conversely, samples prepared by the Homogenized Reconstitution (BC-4) and In-situ Retrieval (BC-5) displayed a decrease in erosion resistance post-wetting and drying. For HR samples after wetting and drying v_c=**0.60 m/s and** τ_c=**0.98 Pa**, and for IR samples - v_c=**0.57 m/s and** τ_c=**0.89 Pa**. The erosion surface characteristics further differentiate the sample categories. HR samples, although eroded, show a smoother surface, while IR samples present more pronounced and irregular cavernous features, as may be observed in Figure 5.1.

(a) HR, original condition (BC-4aE8); v=3.55 m/s; τ=31.26 Pa

(b) IR, original condition (BC-5aE3); v=3.62 m/s; τ=32.47 Pa

Figure 5.1: Homogeneously reconstituted specimen (a) and In-situ retrieved (b) after erosion tests.

These features, however, were not observed on the initial samples, which had similar smooth surfaces as depicted in Figure 5.2.

Post-wetting and drying cycles, HR samples exhibited an increase in surface unevenness upon erosion, indicative of the method's initially homogenized structure becoming slightly more vulnerable to localized erosion. In contrast, IR samples presented more irregular erosion surface, both in their original state and after wetting and drying cycles.

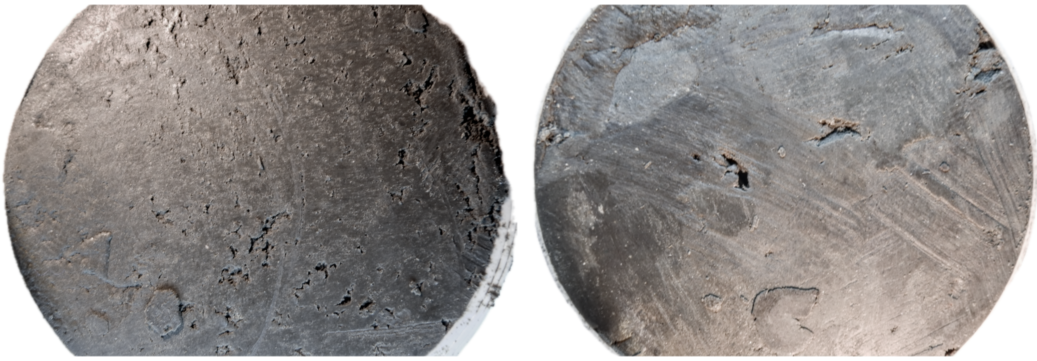

(a) HR, original condition (BC-4aE8) before the test.

(b) IR, original condition (BC-5aE3) before the test.

Figure 5.2: Homogeneously reconstituted specimen (a) and In-situ retrieved (b) before erosion tests.

5.2 Influence of Cyclic Wetting and Drying

The flow velocities in the tests range from 1.84 m/s to 3.91m/s with shear stresses corresponding to these velocities spanning from 8.70 Pa to 37.72 Pa. Obtained data allows to compare the behavior of samples in original condition to samples that were subjected to wetting and drying - the values of erosion rate by mass ($\dot{z}(m)$) and flow velocity (v) will be used in this analysis as primarily measured. Figure 5.3 shows the erosion rate plot at certain flow velocities. The Boom Clay results, included in the final calculation, were analyzed combined.

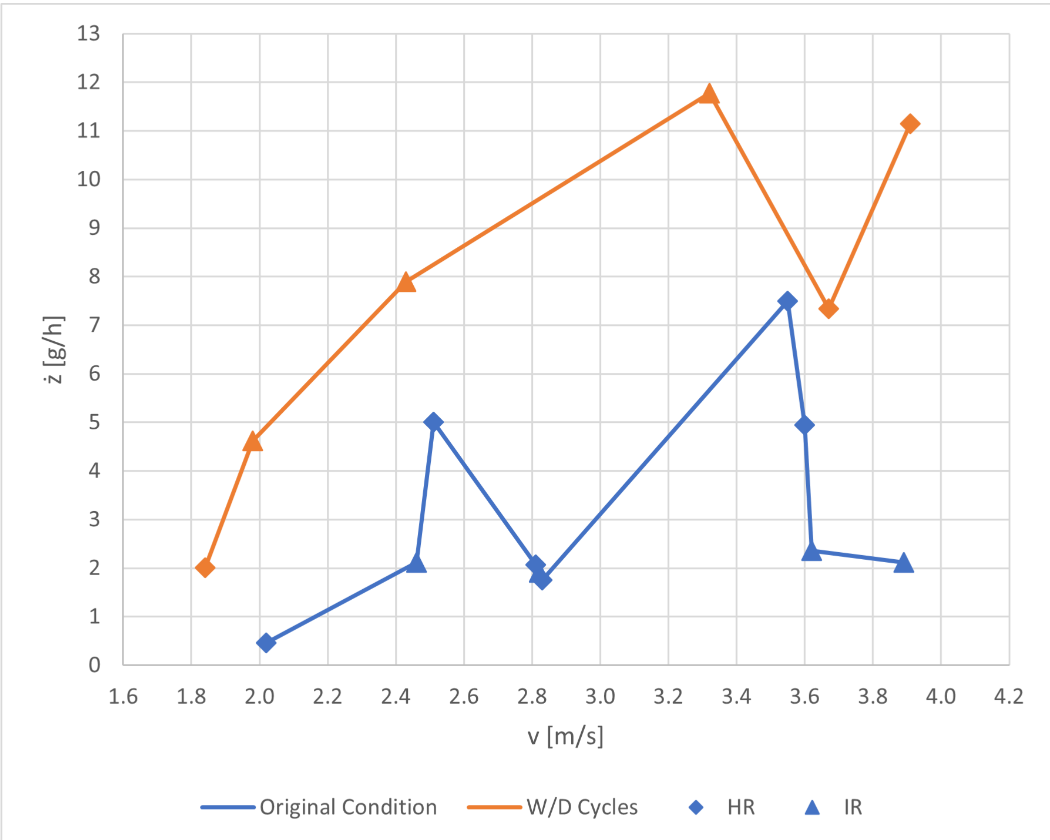

Figure 5.3: Erosion rate at certain flow velocities for Boom clay (HR and IR) in original condition and after cyclic wetting and drying.

For Boom clay samples that were subjected to cycles of wetting and drying the erosion rates are generally higher than for samples in the original condition. Comparing samples prepared by different procedures, HR specimens (BC-4) and IR (BC-5) demonstrate a general increase of erosion rates at relevant speed for specimens that were subjected to wetting and drying.

Examining the photos of the specimens after the test allows to compare the character of erosion. Samples in their original condition generally displayed a more uniform erosion profile, with the surface wearing away in a relatively even manner. In contrast, samples that had undergone cycles of wetting and drying exhibited slightly more irregular erosion patterns, characterized by deeper grooves and 'caverns' in the surface texture. This behavior is more common for homogeneously reconstituted specimens (BC-4). Figure 5.4 illustrates this contrast in the character of erosion between two specimens, BC-4aE4 (original condition) and BC-4bE2 (after wetting and drying cycles), following the erosion tests.

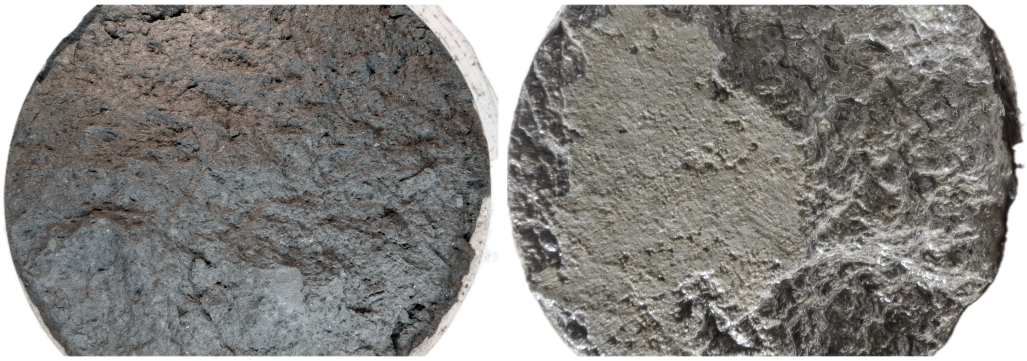

(a) HR, original condition (BC-4aE4); v=1.91 m/s; τ=9.36 Pa

(b) HR, w/d cycles (BC-4bE2); v=1.84 m/s; τ=8.70 Pa

Figure 5.4: Homogeneously reconstituted specimens in original condition (a) and after w/d cycles (b) after erosion tests.

This difference in erosion characteristics can be caused by the changes in soil structure and cohesion as a result of the wetting and drying cycles. Even though soil structure was not studied on a micro level, cracks propagation, and cyclic swelling, and shrinkage were observed for all samples. When erosive forces are applied during testing, these pre-weakened areas are likely to be more susceptible to erosion, leading to a less even surface and the formation of more pronounced features like caverns. The original condition samples, lacking this pre-established network of weaknesses, tend to maintain their cohesive integrity better under similar conditions, resulting in a more homogeneous erosion pattern.

5.3 Tests results discussion

5.3.1 Verification of methodology

EFA tests typically involve protruding the specimen into the flow, recording the time required to erode a set protrusion at various flow velocities, and then repeating the process with adjusted protrusions. While this method conserves time and minimizes specimen handling damage, it presents limitations in accurately calculating the erosion rate by mass, which was observed to be more reliable (see Chapter 3). An additional concern arises from the observed alteration in the moisture content of each specimen, which increased significantly during the testing duration (**ranging from 2% to 49% with an average of 18% of the initial value**). This finding implies that soil properties are altered from their original state post-testing.

In contrast, the approach of using smaller, individual specimens for each test not only facilitates the direct measurement of erosion rate by mass but also likely provides more reliable results in terms of material erodibility. This is because each test is conducted on a specimen with unaltered initial conditions, ensuring a more accurate representation of the soil's erosion characteristics.

5.3.2 Discussion of EFA Setup

The relatively high lower threshold for applicable flow velocity in the EFA setup restricted the ability to conduct tests near the calculated critical values for both Boom Clay and Kleirijperij Clay. As a result, the critical values were derived from the two models discussed earlier (see Sections 2.6, 6.1 and 6.2), as direct testing at these critical velocities was not feasible. This limitation particularly affected the outcome of Kleirijperij samples, as many tests had to be discarded due to the clay's higher erodibility, which was not adequately accommodated by the setup's lower flow velocity limit.

Additionally, the alternative approach to the calculation of shear stress was tested. The value of relative roughness, which is typically taken as $D_{50}/2$ (see Section 2.2) was calculated through digital analysis of photographs capturing the specimen's surface post-test. The average relative roughness value - pre and post-test, was then employed to derive the shear stress from the recorded flow velocity. This calculation procedure was rather complicated and time-consuming and resulted in an increase in the calculated value of shear stress by 1-7 Pa. However, the automation of this process could enhance the precision in estimating shear stress from measured flow velocity, compensating for the method's complexity.

While the measurement and calculation of applied shear stress conformed to methodologies used in previous studies, there is potential for improvement. These enhancements, which are detailed in the relevant chapters of the thesis (see Chapter 3 and Appendix D), could lead to more precise and reliable data, especially for soils with varying erodibility characteristics like Kleirijperij Clay.

5.3.3 Difference between Boom clay and Kleirijperij results.

The three Kleirijperij clay specimens that were tested long enough to yield credible results indicated a considerably higher erosion rate at lower flow velocities (up to 2 m/s) when compared to the Boom clay samples. This observation correlates with the physical characteristics of the Kleirijperij clay, which has a lower density and dry density ($1.46 g/cm^3$ and $1.03 g/cm^3$, respectively) higher moisture content (41.20%) and higher organic content, factors that generally contribute to increased susceptibility to erosion.

6 Erosion Models

This chapter presents a comparative evaluation of the SRICOS and NCHRP models based on the results of clay erosion tests conducted with the Erosion Function Apparatus (EFA). The SRICOS model, which plots shear stress against erosion rate in arithmetic space and applies a logarithmic function for curve fitting, is rather sensitive to the quality and quantity of data points and it overlooks flow velocity — a parameter that is often more readily measurable than shear stress. This approach typically yields higher estimates of critical shear stress and detachment coefficients. In contrast, the NCHRP report model utilizes dual log-log plots correlating erosion rate to both shear stress and flow velocity, deriving values for critical shear stress and critical flow velocity. This methodology tends to produce more conservative estimates, offering an alternate perspective on soil erodibility. The NCHRP report also proposes a soil erodibility classification based on the values of critical flow velocity and critical shear stress obtained during the tests. Table 6.1 gives the values of τ_c and v_c for all tested samples obtained according to NCHRP and SRICOS models. The values of the liquidity index (LI) are given alongside to prove the comparability of the results.

				NCHRP		**SRICOS**
State	**Method**	**Sample**	**LI**	v_c **[m/s]**	τ_c **[Pa]**	τ_c **[Pa]**
Orig	SC	**BC-2a**	0.10	0.93	2.31	6.71
	HR	**BC-4a**	0.14	1.05	8.00	8.40
	IR	**BC-5a**	0.14	1.70	7.42	4.22
	Kleirijperij, SC	**CR-4**	0.02	0.14	0.06	4.26
Cycl. Wet/ Dry	SC	**BC-2b**	0.11	0.98	2.57	7.18
	HR	**BC-4b**	0.17	0.60	0.98	6.21
	IR	**BC-5b**	0.20	0.57	0.89	5.08

SC = Simulated Construction Method
HR = Homogenized Reconstitution Method
IR - In-Situ Retrieval Method

Table 6.1: The values of τ_c and v_c that were obtained according to NCHRP and SRICOS models for different sample groups.

6.1 SRICOS Model

The SRICOS model results show a consistent trend where the critical shear stress values are generally higher compared to those from the NCHRP model across most of the samples. However, an exception is observed in sample BC-5a, where SRICOS reports a lower critical shear stress value than NCHRP. This discrepancy was due to a certain confusion during the result interpretation and will be addressed in the following section (see 6.2).

While the SRICOS model itself does not provide a specific soil classification system based on erodibility, its primary purpose is to predict erosion rates in cohesive soils under hydraulic stress. In this study, we intend to back-calculate erosion rates from the established logarithmic relationships between shear stress and erosion rate observed during testing. To perform the benchmark calculations and obtain values of erosion rate for the specified levels of overflow rates, the overflow rates (in l/s/m) were converted into corresponding shear stress levels (in Pa). Subsequently, the derived approximation of τ versus $\dot{z}$ was used to calculate the corresponding erosion rate values in mm/sec. The values **0.2 l/s/m, 2.0 l/s/m, and 200 l/s/m** were used as Low, Moderate, and High overflow rates, based on van Damme [2016]. This corresponds to the values of shear stress $\tau_L = 4$ **Pa;** $\tau_M = 9$ **Pa;** $\tau_L = 64$ **Pa**. The calculation will be performed based on the test results of the Boom clay sample in its original condition prepared by The Simulated Construction Method (BC-2a). The sample erosion curve is displayed in Figure 6.1 below; the value of critical shear stress is $\tau_c = 6.71Pa$.

The $\tau_L = 4$ Pa is lower than critical shear stress, which means that no erosion is expected at this stress level.

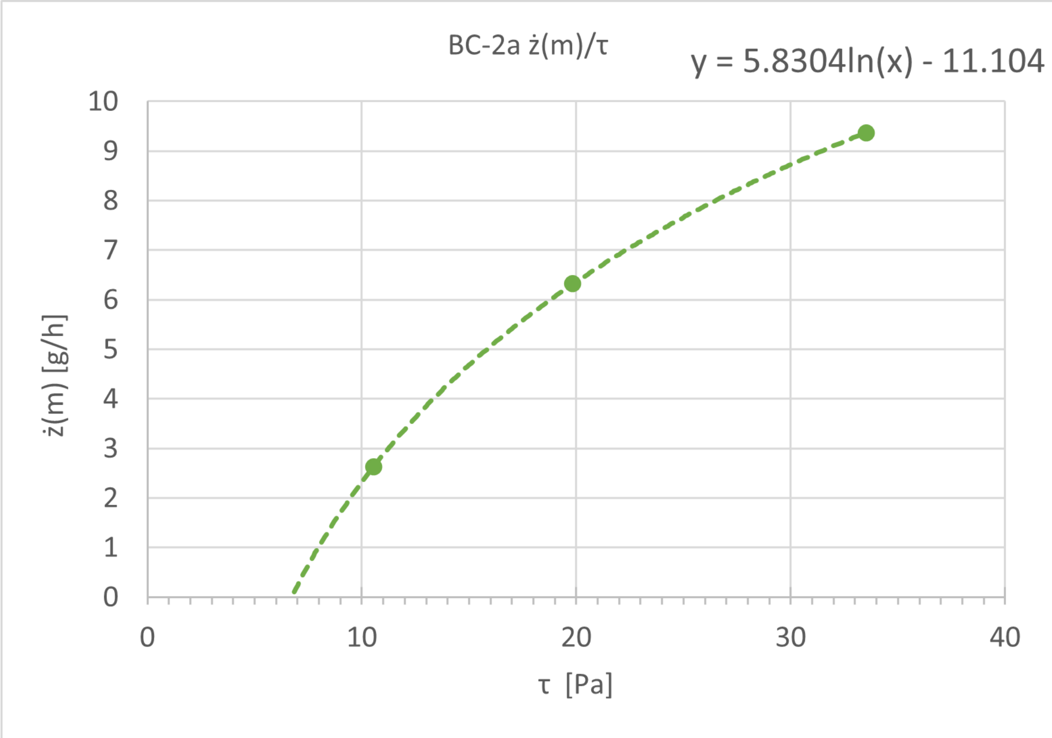

Figure 6.1: Erosion curve of BC-2a sample; $\tau_c = 6.71 Pa$.

- τ_L=4 Pa $\dot{z}$=0 mm/h;
- τ_M=9 Pa $\dot{z}$=0.93 mm/h;
- τ_L=64 Pa $\dot{z}$=7.14 mm/h.

6.2 NCHRP Report Model

The NCHRP Report Model provides consistent guidelines for determining the values of critical shear stress (τ_c) and critical flow velocity (v_c). The τ_c or v_c is determined by the point where the erosion curve intersects the horizontal axis, or, in the absence of such a data point, it is estimated by linearly extrapolating the line connecting the first two points of the curve to where it crosses the horizontal axis. During this study, the NCHRP Report Model proved useful for handling cases where unusual erosion patterns were encountered. In certain tests parts of the soil specimen were washed away within the first 10 minutes of the tests followed by an absence of visible erosion till the end of the test. Deciding whether to keep or discard these results can significantly impact the SRICOS model, making the erosion curve somewhat arbitrary. The NCHRP model's straightforward extrapolation rule for determining critical values is an advantage in this case.

This approach helps maintaining consistency across tests, as demonstrated in Figure 6.2. In this figure, an erosion curve of a Boom clay sample is given. The BC-5a is a sample obtained in situ that has not been subjected to wetting and drying. The value of τ_c included in the final evaluation according to the SRICOS is obtained from the erosion curve 6.2b with one test (namely BC-5a E4) results excluded. During this test, a large fraction of the specimen was washed away during the first 10 minutes followed by a lack of visible erosion during the following 55 minutes. This resulted in a relatively high erosion rate of 1.98 g/h, while the test BC-5a E1 performed on a relative speed resulted in $\dot{z}(m) = 0.46$ g/h.

If the results of all 6 tests performed on this sample are evaluated (see Figure 6.2a) an untypically low value of critical shear stress is obtained τ_c=**0.47 Pa**; with BC-5aE4 excluded τ_c=**4.22 Pa**. This last value was taken into evaluation and it is evident from Table 6.1 the critical shear stress value for BC-5a, as estimated using the SRICOS model (τ_c=**4.22 Pa**), was lower than that for the Homogenized

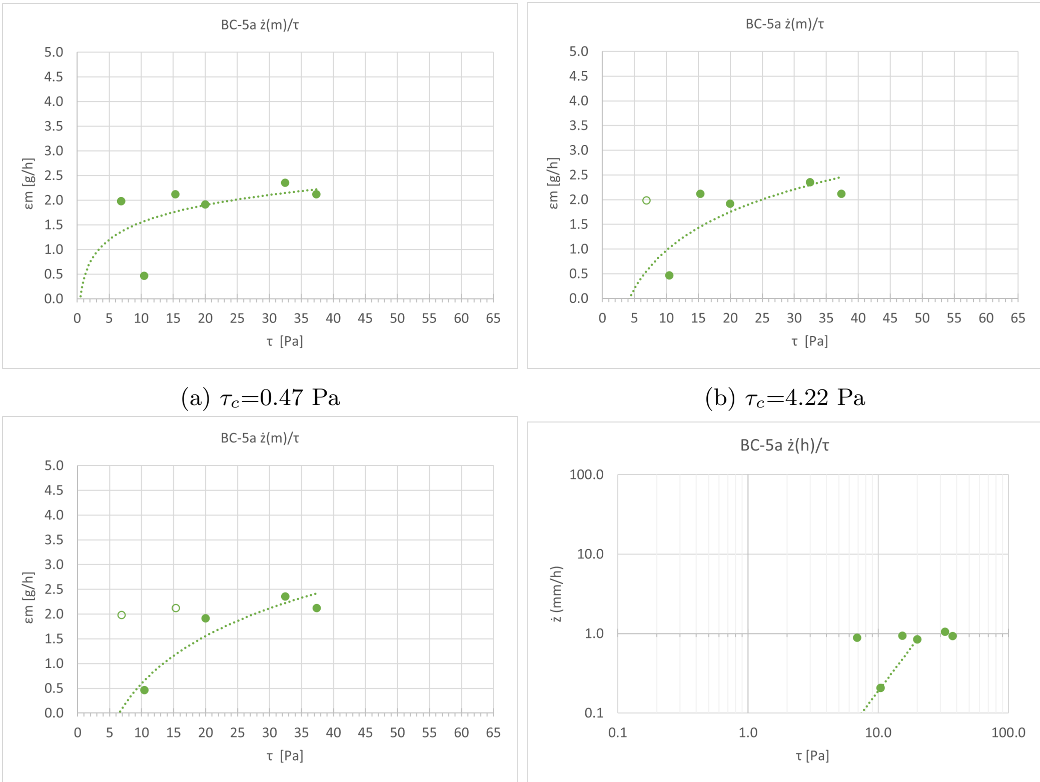

(a) τ_c=0.47 Pa (b) τ_c=4.22 Pa

(c) τ_c=6.49 Pa (d) τ_c=7.42 Pa

Figure 6.2: Erosion curve of a Boom Clay sample prepared by In-Situ Retrieval Method (BC-5a) with obtained values of τ_c according to SRICOS (a, b, c) and NCHRP (d) models.

Reconstitution (HR) sample (BC-4a; τ_c=**8.40 Pa**) and even lower than the In-situ Retrieval (IR) sample BC-5b, which had undergone wetting and drying cycles (τ_c=**5.08 Pa**). However, when the critical shear stress for BC-5a was calculated using the NCHRP model, it aligned more closely with the IR sample (BC-4a: τ_c=**8.00 Pa**; BC-5a: τ_c=**7.42 Pa**) and was notably higher than the BC-5b sample (τ_c=**0.89 Pa**). This contrast in outcomes between the SRICOS and NCHRP models underscores the variability in model sensitivity and response to unclear results.

Category	**Erosion Category Description**	v**(m/s)**	τ**(Pa)**
I	Very high erodibility geomaterials	0.1	0.1
II	High erodibility geomaterials	0.2	0.2
III	Medium erodibility geomaterials	0.5	1.3
IV	Low erodibility geomaterials	1.35	9.3
V	Very low erodibility geomaterials	3.5	62.0
VI	Nonerosive materials	10.0	500.0

Table 6.2: Threshold velocity and shear stress associated with each erosion category (Briaud [2008]).

The NCHRP model also provides a classification of the erosion category (EC) that is determined based on the median point of the erosion curve (the threshold values of v_c and τ_c are shown in Table 6.2). While the erosion function is better described as a curve rather than a single value, this approach allows a more clear estimate of material erodibility.

All the tested samples were classified accordingly. The Simulated Construction (SC) samples (BC-2a and BC-2b) were placed in the ”Medium Erodibility” category, both before and after undergoing wetting and drying cycles.

- **EC (BC-2a) =2.25**;
- **EC (BC-2b) = 2.5**.

The HR and IR samples, initially in the "Low Erodibility" category, were reclassified as "Medium Erodibility" after the environmental conditioning. The graphical representation of the classification is given in Figure 6.3.

- **EC (BC-4a) =2.5**;
- **EC (BC-5a) = 2.75**.
- **EC (BC-4b) =2.25**;
- **EC (BC-5b) = 2.0**.

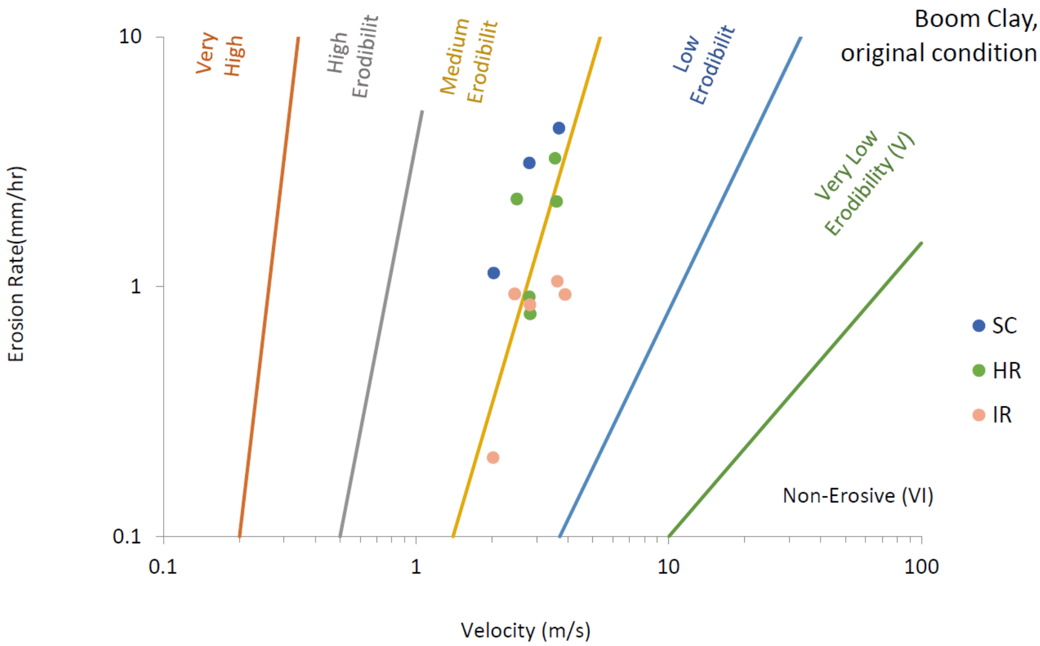

(a) Original condition.

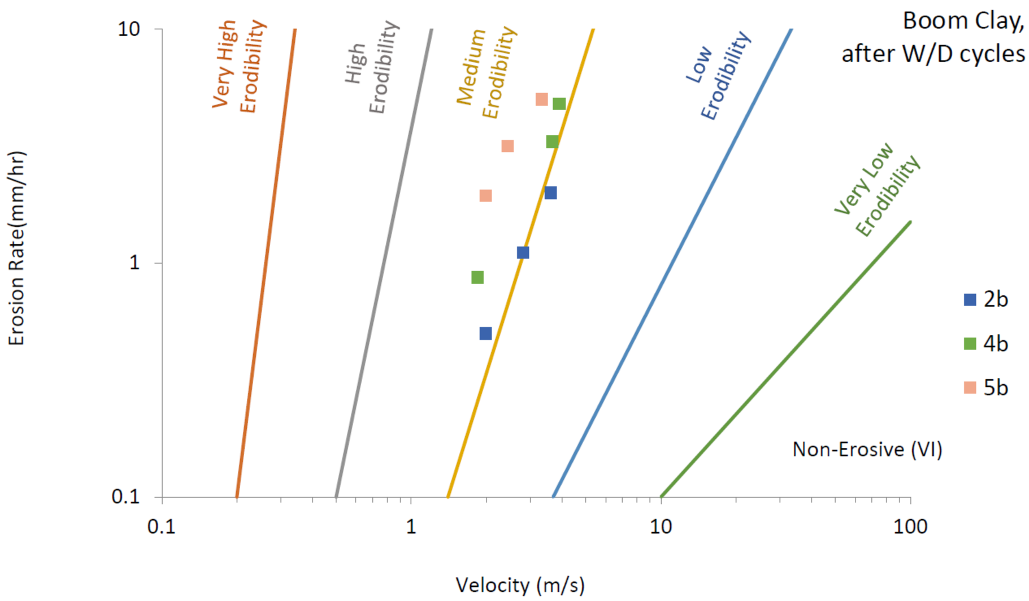

(b) After cycles of wetting and drying.

Figure 6.3: Erosion curves and categories of Boom clay samples.

The Kleirijperij samples may be attributed to the "Medium erodibility" category with **EC = 2.0** (see Figure 6.4).

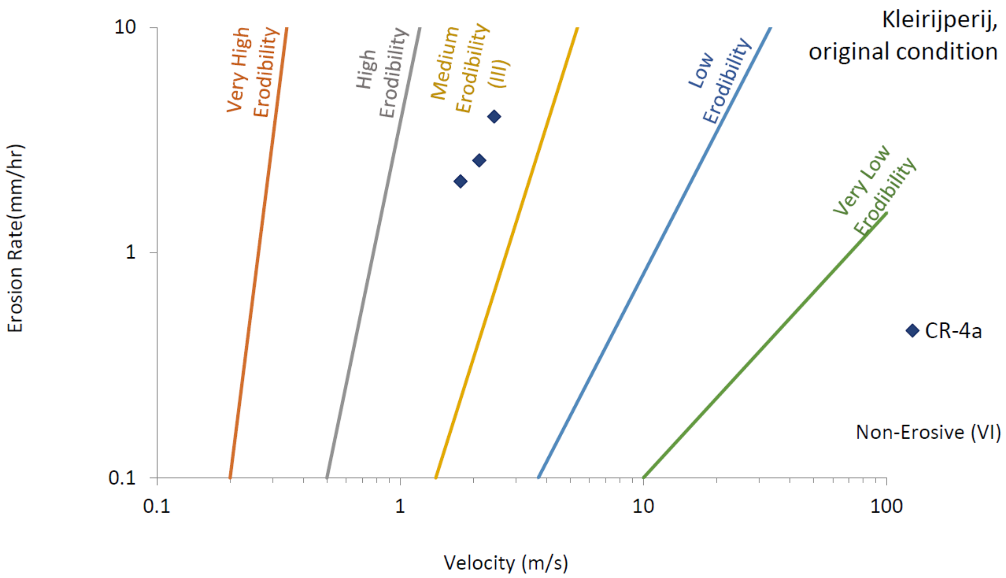

Figure 6.4: Erosion curves and category of Kleirijperij clay.

7 Conclusions and Recommendations

This research conducted a comprehensive study on clay erodibility, employing the Erosion Function Apparatus (EFA) to test clay samples prepared through different methods using Boom clay and Kleirijperij clay material. The study aimed to address the research question:

"How does the erodibility of cohesive clay-soil materials change as a result of cyclic wetting and drying?"

The findings indicate that erosion rates are generally lower for clay in its original condition, and the critical values are higher compared to the samples that underwent cyclic wetting and drying.

This chapter will present detailed conclusions drawn from the study, along with recommendations for further research.

7.1 Conclusions

1. **Effects of Wetting and Drying Cycles**:
   - **Structural and Microstructural Changes**: It was observed that cyclic wetting and drying impact the structure and swelling behavior of clay. Cracks propagated during drying phases and partially sealed during wetting, affecting soil erodibility. It was observed that the scale of these changes depends on the sample preparation procedure with homogeneously reconstituted samples displaying less crack propagation during drying.
   - **Erosion Resistance**: Due to observed changes and the changes in microstructure described in the literature, cycles of wetting and drying decreased the erosion resistance of clay samples except for a sample prepared in an attempt to simulate an erosion-protective layer on a certain scale.
2. **Impact of Preparation Methods on Erosion Behavior**: The Boom clay samples were prepared according to three different procedures.
   - **Simulated Construction Method (SC)**: This method resulted in lower erosion resistance, yet the samples remained stable against wetting and drying cycles. This suggests that the inherent structure that is a result of the preparation process plays a crucial role in defining the material's resilience to environmental changes. This could also be attributed to a different WD procedure that yielded EFA specimens less affected by surface cracking.
   - **Homogenized Reconstitution (HR) vs. In-situ Retrieval (IR)**: HR samples, are Normally Consolidated, they present a uniform and consistent structure. In contrast, IR samples, are Over-consolidated, and exhibit more heterogeneity, influencing their erosion characteristics and response to environmental conditioning. The erosion resistance of these sample categories is comparable, while the pattern of erosion process differs.
3. **Boom vs. Kleirijperij Clay**: two types of clay material were used to prepare samples - Boom clay, which is the most common material for dike erosion-protective layer construction, and clay material from the Kleirijperij project notable for its higher organic content.
   - Kleirijperij samples displayed higher erosion rates and lower erosion resistance compared to all Boom clay samples.
   - The Kleirijperij material has distinct properties when compared to Boom Clay - higher organic content and lower particle density along with lower bulk and dry density, of prepared samples. This, most likely, defines a lower erosion resistance demonstrated by these samples.
   - The limited lower range of flow velocities of this set-up did not allow testing Kleirijperij samples on velocities lower than 1.77 m/sec. This has most likely affected the fit of the erosion curve and, therefore, estimated critical values.

4. **Erosion Function Apparatus tests**: all tests were performed on the EFA setup that is a part of the Hydrodynamic laboratory of Boscalis. The set-up was first assembled and modified, then calibrated and 54 tests were performed in total.
   - The current setup is capable of performing erosion tests according to the most common guidelines and obtaining sufficient results.
   - The calculation of shear stress from flow velocity was proven as sufficient and easy to access, however, the alternative approaches, that might help to calculate the value of applied shear stress more precisely were studied and evaluated.
   - Opting for erosion rate by mass $\dot{z}(m)$ instead of linear erosion rate $\dot{z}(h)$ in EFA tests provides a more nuanced and precise measure of soil erodibility. This approach captures the actual material loss more accurately, reflecting the complex and variable pattern of erosion. By focusing on the mass eroded, the study accounts for the varying densities and compositions of the soil samples, which are critical factors in understanding erosion dynamics.
   - The use of smaller, individual specimens for each EFA test, as opposed to the typical method of repeated protrusions, allows for more accurate measurement of erosion rate by mass and ensures testing on soil samples with unaltered initial properties, leading to more reliable erodibility assessments.
   - The lower threshold of flow velocities most likely limits the accuracy of the results for materials with low erosion resistance.
5. **Model Implications in Erosion Prediction**: Results obtained through erosion tests were processed according to two models - Scour Rate in Cohesive soils (SRICOS) and the one that was proposed in the report of the National Cooperative Highway Research Program (NCHRP). The critical values of shear stress and flow velocity were calculated and classified.
   - **NCHRP Report model**: The NCHRP model provides a straightforward approach to determining the critical values (τ_c, v_c), that may be useful in engineering applications. It also proposes a soil erodibility classification (erosion categories) based on laboratory erosion tests along with the assessment of the value of critical shear stress.
   - **SRICOS Model**: The SRICOS model estimated higher critical shear stress values, suggesting a less conservative approach to predicting erosion resistance. It is currently widely used in the engineering practice.

7.2 Recommendations for Future Studies in Clay Erodibility

Future studies should focus on:

1. **In-depth Investigation of Structural Alterations**: Further research should focus on the microstructural analysis that could indicate changes that are happening as a result of wetting and drying cycles. The microstructural analysis post-erosion testing will help to understand how these changes affect the erosion mechanism on the particle and aggregate levels. This will provide a better understanding of change in erodibility, observed in this study.
2. **Consideration of Preparation Methods**: Further exploration of the SC method in simulating real-world conditions and its impact on erosion resistance is recommended. Additionally, studying the influence of soil particle arrangement and capillary effects on water interaction in HR samples could provide valuable insights.
3. **Enhancing Wetting and Drying Procedures**: Future studies should prioritize refining wetting and drying (WD) procedures. This research indicates that smaller samples exposed to WD cycles exhibit notable changes in erodibility. It's essential to align laboratory WD cycles more closely with real-life conditions to accurately simulate soil behavior. This will enable more accurate predictions and effective strategies for managing soil erosion in natural settings.
4. **Refinement of EFA Testing**: It's crucial to conduct tests at a broader range of velocities, particularly for materials like Kleirijperij clay. Enhancements in shear stress estimation and

sample preparation techniques, such as using smaller height molds, could improve the accuracy of erosion tests.

5. **EFA Set-up Adjustments**: In the current setup several components (e.g. absolute pressure sensor) are not used, so removing it may contribute to a more efficient design. Current flow velocity measurement with a pitot tube requires regular maintenance, additionally, the tube may clog during the test with the soil particles. Implementing a laser or ultrasonic non-contact flow velocity sensor may help to overcome it. The refinement of the specimen protrusion mechanism that would allow precise control of the protrusion of a sample that is installed into the flume could also benefit the testing process.

6. **Model Application and Verification**: Expanding soil testing to include a broader range of materials and correlating the results with local in-situ tests can enhance the practical application of erosion prediction models. Verifying correlations between erosion parameters and soil properties can provide efficient tools for preliminary assessments.

Bibliography

Ahmadi, H., Rahimi, H., and Rostami, M. E. (2012). Control of swelling of soil under canal lining by wetting and drying cycles. *Irrigation and Drainage*, 61:527–532.

Annandale, G. W. (1995). Erodibility. *Journal of Hydraulic Research*, 33:471–494.

Ariathurai, R. and Arulanandan, K. (1978). Erosion rates of cohesive soils. *Journal of the Hydraulics Division*, 104(2):279–283.

Assadollahi, H. and Nowamooz, H. (2020). Long-term analysis of the shrinkage and swelling of clayey soils in a climate change context by numerical modelling and field monitoring. *Computers and Geotechnics*, 127:103763.

Basma, A., Al-Homoud, A., Husein Malkawi, A., and Al-Bashabsheh, M. (1996). Swelling-shrinkage behavior of natural expansive clays. *Applied Clay Science*, 11:211–227.

Bernier, F., Volckaert, G., Alonso, E. E., and Villar, M. V. (1997). Suction-controlled experiments on boom clay. *Engineering Geology*, 47:325–338.

Bijlard, R. (2015). Strength of the grass sod on dikes during wave overtopping. *Delft University of Technology*.

Bloomquist, D., Sheppard, D. M., Schofield, S., and Crowley, R. W. (2012). *The Rotating Erosion Testing Apparatus (RETA): A Laboratory Device for Measuring Erosion Rates Versus Shear Stresses of Rock and Cohesive Materials*. ASTM International.

Boskalis (2023). Verslag bezoek groeve schelle 21/02/2023 bke-mmd.

Briaud, J.-L. (2008). Case histories in soil and rock erosion: Woodrow wilson bridge, brazos river meander, normandy cliffs, and new orleans levees. *Journal of Geotechnical and Geoenvironmental Engineering*, 134:1425–1447.

Briaud, J. L., Chen, I, S., and H, C. (2019). *Relationship Between Erodibility and Properties of Soils*. The National Academies Press.

Briaud, J.-L., Li, Y., Chen, H.-C., Nurtjahyo, P., and Wang, J. (2002). *Shear Stress Approach to Pier Scour Predictions*. Texas Transportation Inst., Publications Dept., College Station, Texas.

Briaud, J. L., Ting, F. C. K., Chen, H. C., Cao, Y., Han, S. W., and Kwak, K. W. (2001). Erosion function apparatus for scour rate predictions. *Journal of Geotechnical and Geoenvironmental Engineering*, 127:105–113.

Burland, J. (1990). Thirtieth rankine lecture: On the compressibility and shear strength of natural clays. *Geotechnique*, 40:329–378.

Chapuis, R. P. and Gatien, T. (1986). An improved rotating cylinder technique for quantitative measurements of the scour resistance of clays. *Canadian Geotechnical Journal*, 23(1):83–87.

Chiew, Y. (1992). Scour protection at bridge piers. *Journal of Hydraulic Engineering*, 118:1260–1269.

CROW (2010). Raw-systematiek 2010. Technical report, CROW.

Crowley, R., Bloomquist, D., Shah, F., and Holst, C. (2012). The sediment erosion rate flume (serf): A new testing device for measuring soil erosion rate and shear stress. *Geotechnical Testing Journal*, 35.

Dehandschutter, B., Vandycke, S., Sintubin, M., Vandenberghe, N., Gaviglio, P., Sizun, J.-P., and Wouters, L. (2004). Microfabric of fractured boom clay at depth: a case study of brittle–ductile transitional clay behaviour. *Applied Clay Science*, 26:389–401.

Desbois, G., Urai, J., and De, C. (2010). In-situ and direct characterization of porosity in boom clay (mol site, belgium) by using novel combination of ion beam cross-sectioning, sem and cryogenic methods.

Durce, D., Bruggeman, C., Maes, N., Van Ravestyn, L., and Brabants, G. (2015). Partitioning of organic matter in boom clay: Leachable vs mobile organic matter. *Applied Geochemistry*, 63:169–181.

Ellison, W. (1947). *Soil Erosion Studies - Part I, Agricultural Engineering.* Agricultural Engineering.

Fleureau, J.-M., Wei, X., Ighil Ameur, L., Hattab, M., and Bicalho, K. (2015). Experimental study of the cracking mechanisms of clay during drying. *XV Pan-American Conference on Soil Mechanics and Geotechnical Engineering.*

Goh, S. G., Rahardjo, H., and Leong, E. C. (2014). Shear strength of unsaturated soils under multiple drying-wetting cycles. *Journal of Geotechnical and Geoenvironmental Engineering*, 140:06013001.

Grissinger, E. H. (1982). Bank erosion of cohesive materials. *Gravel-bed Rivers*, pages 273–287.

Hanson, G. J. and Cook, K. R. (1997). Development of excess shear stress parameters for circular tests. *Transactions of the ASABE*, 40:993–999.

Hanson, G. J. and Cook, K. R. (2004). Apparatus, test procedures, and analytical methods to measure soil erodibility in situ. *Applied Engineering in Agriculture*, 20.

Hanson, G. J., Cook, K. R., and Hunt, S. L. (2005). Physical modeling of overtopping erosion and breach formation of cohesive embankments. *Transactions of the American Society of Agricultural Engineers*, 48.

Hanson, G. J. and Simon, A. (2001). Erodibility of cohesive streambeds in the loess area of the midwestern usa. *Hydrological Processes*, 15:23–38.

Haselsteiner, R., K., W., Heibaum, M., and Georg, H. (2009). Danger of flooding – new safety measures in dike construction by using geosynthetics. *17th International Conference on Soil Mechanics and Geotechnical Engineering (Alexandria).*

Heijmeijer, O. A. (2019). High velocity sand erosion.

Hudson, N. (1993). *Field measurement of soil erosion and runoff / by N.W. Hudson.* FAO soils bulletin ; 68. Food and Agriculture Organization of the United Nations, Rome.

Julien, P. Y. (2002). *River Mechanics.* Cambridge University Press.

Julien, P. Y. (2010). *Erosion and Sedimentation*, volume 1. Cambridge University Press, 2 edition.

Kleirijperij, P. (2023). Pilot kleirijperij: van slib tot dijk. wp 5.1 eindrapportage kleirijperij.

Kodikara, J., Barbour, S., and Fredlund, D. (1999). Changes in clay structure and behaviour due to wetting and drying. *8th Australian-New Zealand Conference on Geomechanics.*

Kodikara, J., Barbour, S., and Fredlund, D. (2000). Desiccation cracking of soil layers. In *Proceedings of the Asian Conference in Unsaturated Soil*, pages 693–698.

Kruse, G. (1987). Onderzoek van kleibekleding van dijken aan zout en brak water in friesland, zuid holland en zeeland voor het ontwikkelen van keuringseisen voor klei.

Kruse, G. (1988). Onderzoek naar het beoordelen van de geschiktheid van kleigrond voor de bekleding van dijken met grasbekleding.

Le Bissonnais, Y. (1996). Aggregate stability and assessment of crustability and erodibility: 1. theory and methodology. *European Journal of Soil Science*, 47:425–437.

Ma, R., Cai, C., Li, Z., Junguang, W., Xiao, T., Peng, G., and Yang, W. (2015). Evaluation of soil aggregate microstructure and stability under wetting and drying cycles in two ultisols using synchrotron-based x-ray micro-computed tomography. *Soil and Tillage Research*, 149.

Ma, T., Wei, C., Yao, C., and Yi, P. (2020). Microstructural evolution of expansive clay during drying–wetting cycle. *Acta Geotechnica*, 15:2355–2366.

Maali, A., Pan, Y., Bhushan, B., and Charlaix, E. (2012). Hydrodynamic drag-force measurement and slip length on microstructured surfaces. *Phys. Rev. E*, 85:066310.

Marinho, F. (1994). Phd thesis: Shrinkage behaviour of some plastic soils.

Moore, R. and Dwyer, J. (2002). Use of the in situ erosion evaluation probe in different soil types. *Transactions of the ASAE*, 45:1345–1351.

Moore, W. L. and Masch Jr., F. D. (1962). Experiments on the scour resistance of cohesive sediments. *Journal of Geophysical Research (1896-1977)*, 67(4):1437–1446.

Morgan, R. (2005). *Morgan, R.P.C. Soil Erosion and Conservation, 3rd edition.*, volume 56. Blackwell Publishing Ltd.

Partheniades, E. (2009). *Cohesive Sediments in Open Channels*. Butterworth-Heinemann, 1 edition.

Prooijen, B. and Winterwerp, J. (2010). A stochastic formulation for erosion of cohesive sediments. *Journal of Geophysical Research*, 115.

Rahimnejad, R. and Ooi, P. S. K. (2016). Factors affecting critical shear stress of scour of cohesive soil beds. *Transportation Research Record*, 2578:72–80.

Rinsum, G. (2018). Grass revetment reinforcements: A study into the effectiveness of measures applied during critical conditions. *Delft University of Technology*.

Romero, E., Gens, A., and Lloret, A. (1999). Water permeability, water retention and microstructure of unsaturated compacted boom clay. *Engineering Geology*, 54(1):117–127.

Romkens, M. J. M., Wang, X., and Tao, J. (2001). Soil erodibility parameters derived from borehole erosion tests. *Transactions of the ASAE*, 44:591–596.

Rook, L. (2020). Development of an erosion function apparatus for the assessment of the erosion resistance of compacted clay.

Shafii, I., Briaud, J., Chen, H., and Shidlovskaya, A. (2016). Relationship between soil erodibility and engineering properties. *Scour and Erosion*, pages 1055–1060.

Shan, H., Kornel, K., Junke, G., Shen, J. J., Wagner, A., and Xie, Z. (2012). An ex-situ scour testing device for characterizing erosion of cohesive soils. In *6th International Conference on Scour and Erosion*.

Shan, H., Shen, J., Kilgore, R., and Kerenyi, K. (2015a). Scour in cohesive soils. Technical Report FHWA-HRT-15-033, Genex Systems, LLC and United States Federal Highway Administration.

Shan, H., Shen, J., Kilgore, R., and Kerenyi, K. (2015b). Scour in cohesive soils.

Simon, A., Thomas, R. E., and Klimetz, L. (2010). Comparison and experiences with field techniques to measure critical shear stress and erodibility of cohesive deposits. *Federal Interagency Conference*.

Sittoni, L., Boer, J., van der Star, W., Heuvel, M., Baptist, M., van Eekelen, E., Groot, F., Nieboer, H., and Doets, I. (2019). Beneficial and nature-based sediment use-experiences from dutch pilots.

Stein, O. and Nett, D. D. (1997). Impinging jet calibration of excess shear sediment detachment parameter. *Transactions of the ASAE. American Society of Agricultural Engineers*, 40:1573–1580.

Tu, Y., Zhang, R., Zhong, Z., and Chai, H. (2022). The strength behavior and desiccation crack development of silty clay subjected to wetting–drying cycles. *Frontiers in Earth Science*, 10.

van Damme, M. (2016). Distributions for wave overtopping parameters for stress strength analyses on flood embankments. *Coastal Engineering*, 116:195–206.

van der Meer, J. W., Hardeman, B., Steendam, G. J., Schüttrumpf, H., and Verheij, H. (2011). Flow depths and velocities at crest and landward slope of a dike, in theory and with the wave overtopping simulator. *International Conference on Coastal Engineering*.

voor Waterkeringen, T. A. (1996). Technisch rapport klei voor dijken (tr17). Technical report, Rijkswaterstaat, Ministerie van Verkeer en Waterstaat.

Wan, C. and Fell, R. (2004). Investigation of rate of erosion of soils in embankment dams. *Journal of Geotechnical and Geoenvironmental Engineering*, 130:373–380.

White, C. M. and Ingram, T. G. (1940). The equilibrium of grains on the bed of a stream. *Proceedings of the Royal Society of London. Series A. Mathematical and Physical Sciences*, 174:322–338.

Wischmeier, W., Johnson, C., and Cross, B. (1971). A soil erodibility nomograph for farmland and construction sites. *Journal of Soil and Water Conservation*, 26:189–193.

Wiseall, A., Graham, C., Zihms, S., Harrington, J., Cuss, R., Gregory, S., and Shaw, R. (2015). *Properties and Behaviour of the Boom Clay Formation within a Dutch Repository Concept*. COVRA (Centrale Organisatie Voor Radioactief Afval).

Yanli, Q., Bai, M., Zhou, H., Shi, H., Pengxiang, L., and He, B. (2021). Study on the mechanical properties of red clay under drying-wetting cycles. *Advances in Materials Science and Engineering*, 2021:1–16.

Yesiller, N., Miller, C., Inci, G., and Yaldo, K. (2000). Desiccation and cracking behavior of three compacted landfill liner soils. *Engineering Geology*, 57:105–121.

Yu, H.-D., Chen, W.-Z., Jia, S.-P., Cao, J.-J., and Li, X.-L. (2012). Experimental study on the hydro-mechanical behavior of boom clay. *International Journal of Rock Mechanics and Mining Sciences*, 53:159–165.

Zihan, Z. (2018). Measurement of hydrodynamic forces on gravel particles in the erosion function apparatus. *Texas AM University Libraries*.

A Laboratory Data

A.1 EFA Tests Logbook: Boom Clay.

A.2 EFA Tests Logbook: Kleirijperij Clay.

A.3 Laboratory Report: Verslag bezoek groeve Schelle 21/02/2023 BKE-MMD.

A.4 Proctor Compaction: Boom Clay.

A.5 Proctor Compaction: Kleirijperij Clay.

A.1 EFA Tests Logbook: Boom Clay

BC-2a EFA 1				
ρd	1.46	g/cm3	**v [m/s]**	**2.03**
W0	25.61	%	**τ [Pa]**	**10.54**
ρ	1.84	g/cm3	**Freq [Hz]**	**25.37**
IL	0.10	-		
m1	46.48	g	mass	before the test
m1d	37.00	g	dry mass	
m2	45.88	g	mass	after the test
m2d	33.20	g	dry mass	
dm	**3.80**	**g**	**mass loss**	
t	87	min		
	1.45	h		
ż	**2.62**	**g/h**	1.14	mm/h
BC-2a EFA 2				
ρd	1.28	g/cm3	**v [m/s]**	**2.81**
W0	25.61	**%**	**τ [Pa]**	**19.84**
ρ	1.61	-	**Freq [Hz]**	**35.42**
IL	0.10	-		
m1	40.68	g	mass	before the test
m1d	32.39	g	dry mass	
m2	36.10	g	mass	after the test
m2d	26.80	g	dry mass	
dm	**5.59**	**g**	**mass loss**	
t	53	min		
	0.88	h		
ż	**6.32**	**g/h**	3.13	mm/h
BC-2a EFA 3				
ρd	1.37		**v [m/s]**	**3.68**
W0	25.61	**%**	**τ [Pa]**	**33.53**
ρ	1.73		**Freq [Hz]**	**45.81**
IL	0.10	-		
m1	43.66	g	mass	before the test
m1d	34.76	g	dry mass	
m2	33.85	g	mass	after the test
m2d	26.95	g	dry mass	
dm	**7.81**	**g**	**mass loss**	
t	50	min		
	0.83	h		
ż	**9.37**	**g/h**	4.32	mm/h
τ_C	**6.71**	**Pa**	**SRICOS Model**	
v_C	**0.93**	**m/s**	**NCHRP Report Model**	
τ_C	**2.31**	**Pa**		

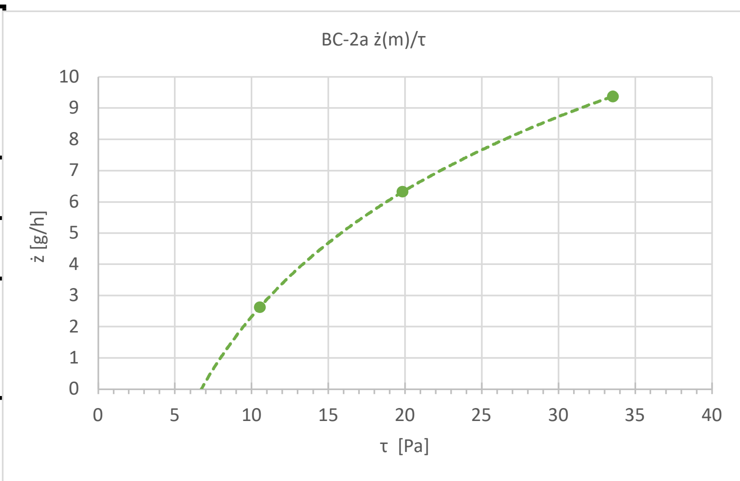

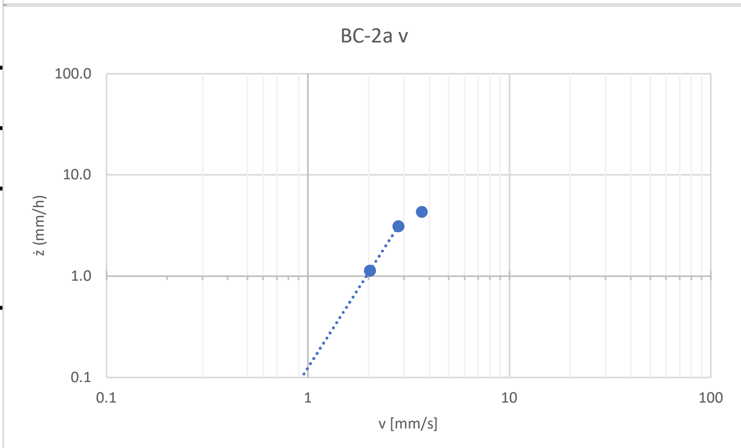

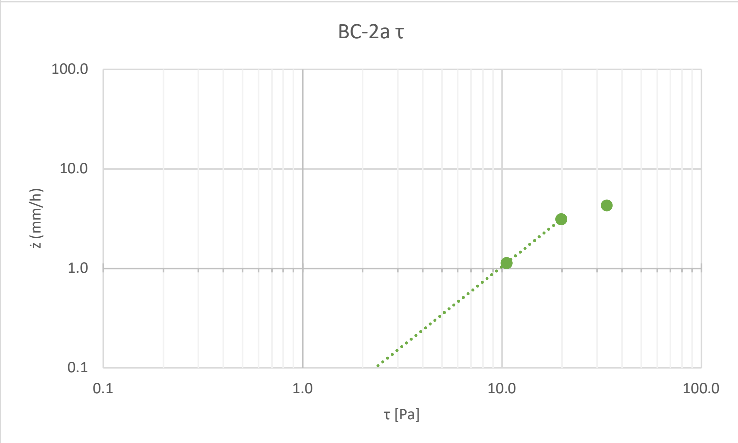

		BC-2b EFA 1		
ρd	1.43	g/cm3	**v [m/s]**	**1.98**
W0	26.32	%	**τ [Pa]**	**10.04**
ρ	1.81	g/cm3	**Freq [Hz]**	**22.00**
IL	0.11	-		
m1	45.71	g	mass	before
m1d	36.18	g	dry mass	the test
m2	42.47	g	mass	after the
m2d	34.35	g	dry mass	test
dm	**1.83**	**g**	**mass loss**	
t	97	min		
	1.62	h		
ż	**1.13**	**g/h**	0.50	mm/h
		BC-2b EFA 2		
ρd	1.45	g/cm3	**v [m/s]**	**2.80**
W0	26.32	%	**τ [Pa]**	**19.70**
ρ	1.83	g/cm3	**Freq [Hz]**	**35.00**
IL	0.11	-		
m1	46.33	g	mass	before
m1d	36.68	g	dry mass	the test
m2		g	mass	after the
m2d	33.91	g	dry mass	test
dm	**2.77**	**g**	**mass loss**	
t	65	min		
	1.08	h		
ż	**2.55**	**g/h**	1.11	mm/h
		BC-2b EFA 3		
ρd	1.45		**v [m/s]**	**3.60**
W0	26.32	%	**τ [Pa]**	**32.13**
ρ	1.83	g/cm3	**Freq [Hz]**	**45.00**
IL	0.11	-		
m1	46.33	g	mass	before
m1d	36.68	g	dry mass	the test
m2	39.30	g	mass	after the
m2d	32.63	g	dry mass	test
dm	**4.05**	**g**	**mass loss**	
t	53	min		
	0.88	h		
ż	**4.58**	**g/h**	1.99	mm/h
τ_c	**7.18**	**Pa**	**SRICOS Model**	
v_c	**0.98**	**m/s**	**NCHRP Report Model**	
τ_c	**2.57**	**Pa**		

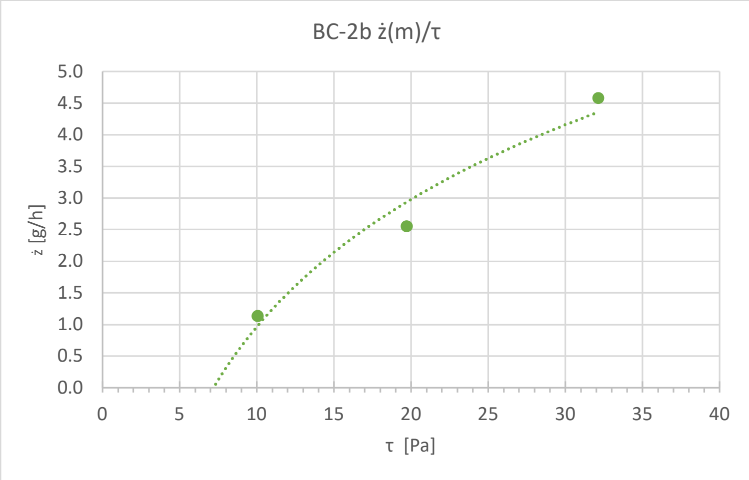

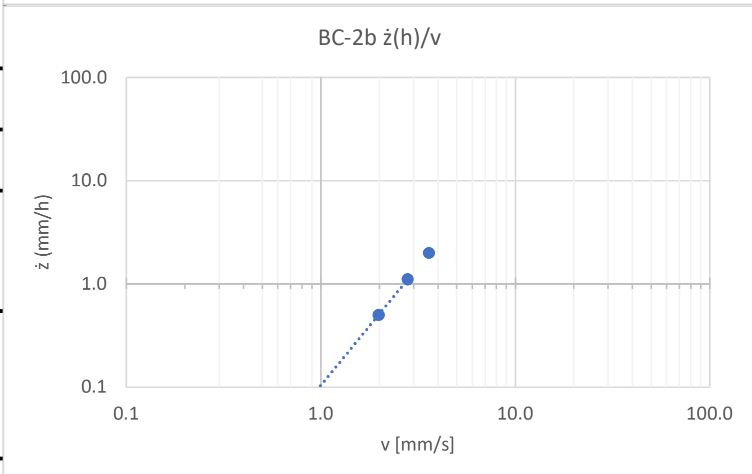

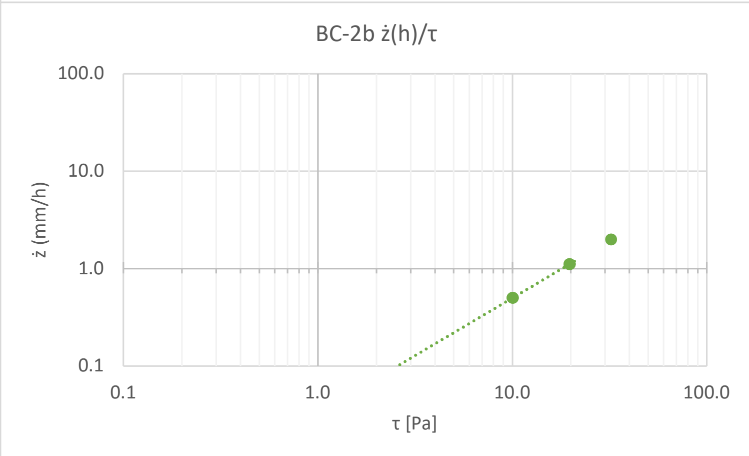

BC-4a EFA 1				
ρd	1.45	g/cm3	**v [m/s]**	**2.04**
W0	25.70	%	**τ [Pa]**	**10.64**
ρ	1.83	g/cm3	**Freq [Hz]**	**25.26**
IL	0.09	-		
m1	46.20	g	mass	before
m1d	36.75	g	dry mass	the test
m2	37.86	g	mass	after the
m2d	29.22	g	dry mass	test
dm	**7.53**	**g**	**mass loss**	
t	56	min		
	0.9	h		
ż	**8.07**	**g/h**	3.51	mm/h

BC-4a EFA 2				
ρd	1.42	g/cm3	**v [m/s]**	**2.83**
W0	25.70	%	**τ [Pa]**	**20.12**
ρ	1.79	g/cm3	**Freq [Hz]**	**35.10**
IL	0.09	-		
m1	45.24	g	mass	before
m1d	35.99	g	dry mass	the test
m2	44.38	g	mass	after the
m2d	34.24	g	dry mass	test
dm	**1.75**	**g**	**mass loss**	
t	60	min		
	1.00	h		
ż	**1.75**	**g/h**	0.78	mm/h

BC-4a EFA 3				
ρd	1.43	g/cm3	**v [m/s]**	**3.60**
W0	25.70	%	**τ [Pa]**	**32.13**
ρ	1.79	g/cm3	**Freq [Hz]**	**45.00**
IL	0.09	-		
m1	45.32	g	mass	before
m1d	36.05	g	dry mass	the test
m2	40.39	g	mass	after the
m2d	31.11	g	dry mass	test
dm	**4.94**	**g**	**mass loss**	
t	60	min		
	1.00			
ż	**4.94**	**g/h**	2.19	mm/h

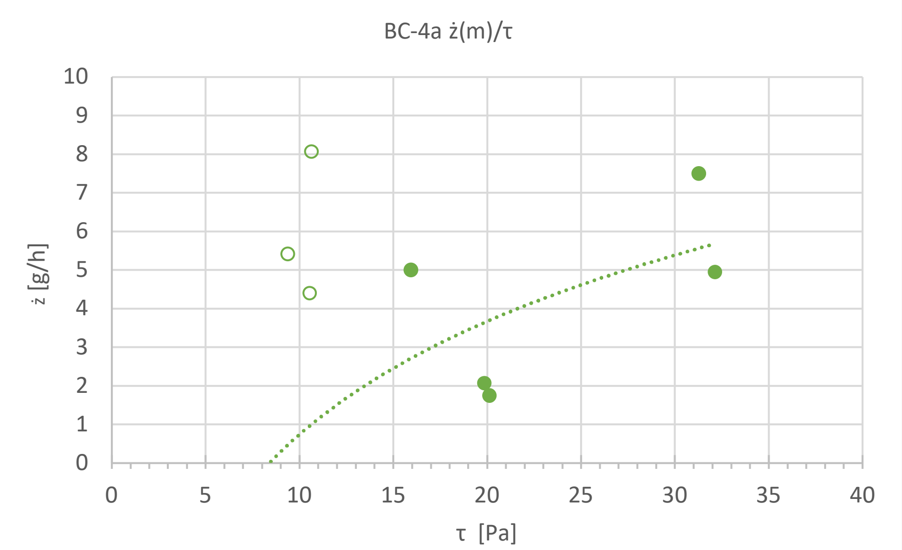

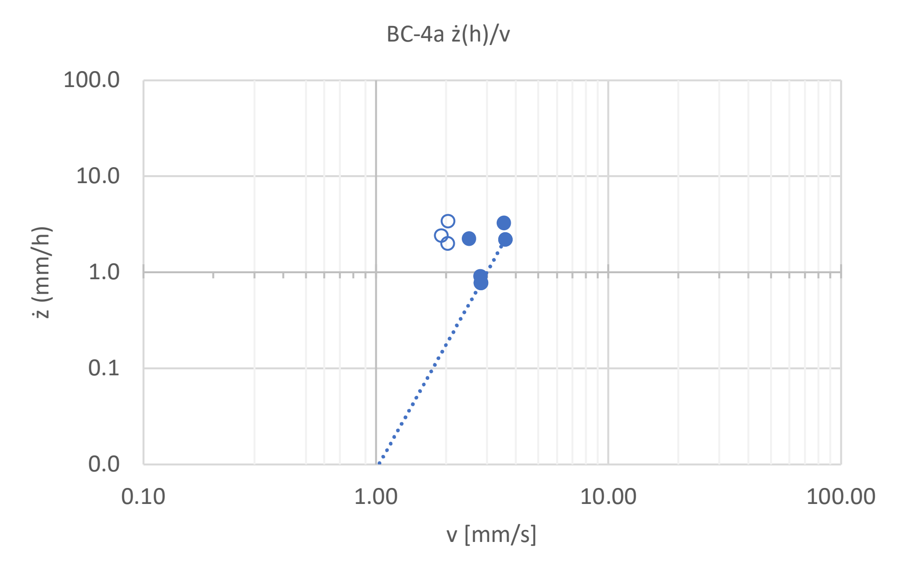

BC-4a EFA 4				
ρd	1.40	g/cm3	**v [m/s]**	**1.91**
W0	27.00	%	**τ [Pa]**	**9.36**
ρ	1.78	g/cm3	**Freq [Hz]**	**21.77**
IL	0.18	-		8.35
m1	45.01	g	mass	before
m1d	35.44	g	dry mass	the test
m2	41.43	g	mass	after the
m2d	31.47	g	dry mass	test
dm	**3.97**	**g**	**mass loss**	
t	44	min		
	0.73			
ż	**5.41**	**g/h**	2.42	mm/h

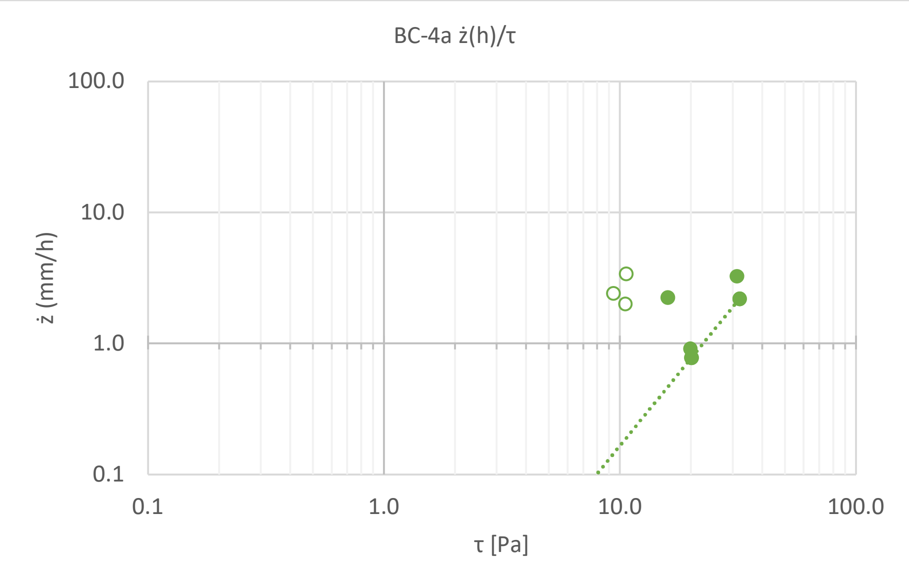

BC-4a EFA 5				
ρd	1.38	g/cm3	**v [m/s]**	**2.03**
W0	27.00	%	**τ [Pa]**	**10.54**
ρ	1.75	g/cm3	**Freq [Hz]**	**25.14**
IL	0.18	-		9.33
m1	44.16	g	mass	before
m1d	34.77	g	dry mass	the test
m2	41.43	g	mass	after the
m2d	31.47	g	dry mass	test
dm	**3.30**	**g**	**mass loss**	
t	45	min		
	0.75			
ż	**4.40**	**g/h**	2.01	mm/h

BC-4a EFA 6				
ρd	1.40	g/cm3	**v [m/s]**	**2.51**
W0	27.00	%	**τ [Pa]**	**15.93**
ρ	1.78	g/cm3	**Freq [Hz]**	**30.04**
IL	0.18	-		
m1	44.90	g	mass	before
m1d	35.35	g	dry mass	the test
m2	40.62	g	mass	after the
m2d	31.60	g	dry mass	test
dm	**3.75**	**g**	**mass loss**	
t	45	min		
	0.75			
ż	**5.01**	**g/h**	2.24	mm/h

		BC-4a EFA 7		
ρd	1.42	g/cm3	**v [m/s]**	**2.81**
W0	27.00	**%**	**τ [Pa]**	**19.84**
ρ	1.80	g/cm3	**Freq [Hz]**	**35.10**
IL	0.18	-		
m1	45.54	g	mass	before
m1d	35.86	g	dry mass	the test
m2	44.11	g	mass	after the
m2d	34.24	g	dry mass	test
dm	**1.62**	**g**	**mass loss**	
t	47	min		
	0.78			
ż	**2.07**	**g/h**	0.91	mm/h
		BC-4a EFA 8		
ρd	1.44	g/cm3	**v [m/s]**	**3.55**
W0	27.00	**%**	**τ [Pa]**	**31.26**
ρ	1.83	g/cm3	**Freq [Hz]**	**45.63**
IL	0.18	-		
m1	46.23	g	mass	before
m1d	36.40	g	dry mass	the test
m2	39.16	g	mass	after the
m2d	30.40	g	dry mass	test
dm	**6.00**	**g**	**mass loss**	
t	48	min		
	0.80			
ż	**7.50**	**g/h**	3.26	mm/h
τ_C	**8.40**	**Pa**	**SRICOS Model**	
v_C	**1.05**	**m/s**	**NCHRP Report**	
τ_C	**8.00**	**Pa**	**Model**	

BC-4b EFA 1				
ρd	1.46	g/cm3	**v [m/s]**	**3.91**
W0	26.63	%	**τ [Pa]**	**37.72**
ρ	1.85	g/cm3	**Freq [Hz]**	**50.00**
IL	0.17	-		
m1	46.77	g	mass	before
m1d	36.93	g	dry mass	the test
m2	34.46	g	mass	after the
m2d	28.57	g	dry mass	test
dm	**8.36**	**g**	**mass loss**	
t	45	min		
	0.75	h		
ż	**11.15**	**g/h**	4.80	mm/h

BC-4b EFA 2				
ρd	1.46	g/cm3	**v [m/s]**	**1.84**
W0	26.28	**%**	**τ [Pa]**	**8.70**
ρ	1.84	g/cm3	**Freq [Hz]**	**22.38**
IL	0.16	-		
m1	46.51	g	mass	before
m1d	36.83	g	dry mass	the test
m2	42.69	g	mass	after the
m2d	34.42	g	dry mass	test
dm	**2.41**	**g**	**mass loss**	
t	72	min		
	1.20	h	3.71	
ż	**2.01**	**g/h**	0.87	mm/h

BC-4b EFA 3				
ρd	1.40	g/cm3	**v [m/s]**	**3.67**
W0	26.73	**%**	**τ [Pa]**	**33.35**
ρ	1.77	g/cm3	**Freq [Hz]**	**46.21**
IL	0.17	-		
m1	44.87	g	mass	before
m1d	35.41	g	dry mass	the test
m2	40.39	g	mass	after the
m2d	28.07	g	dry mass	test
dm	**7.34**	**g**	**mass loss**	
t	60	min		
	1.00	h		
ż	**7.34**	**g/h**	3.29	mm/h

τ_c	**6.21**	**Pa**	**SRICOS Model**
v_c	**0.60**	**m/s**	**NCHRP Report Model**
τ_c	**0.98**	**Pa**	

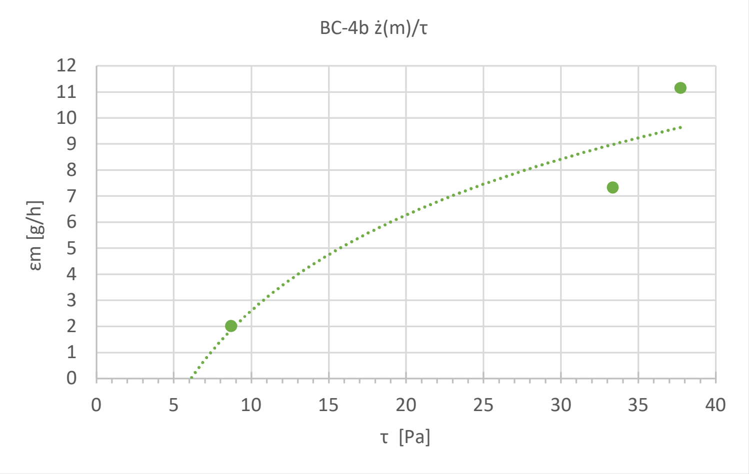

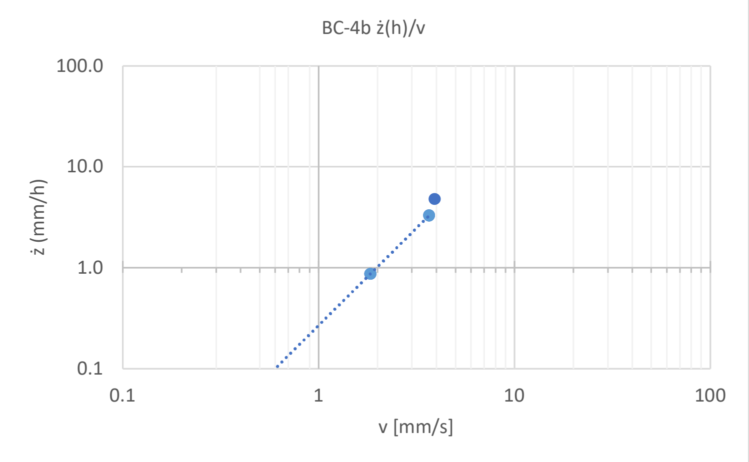

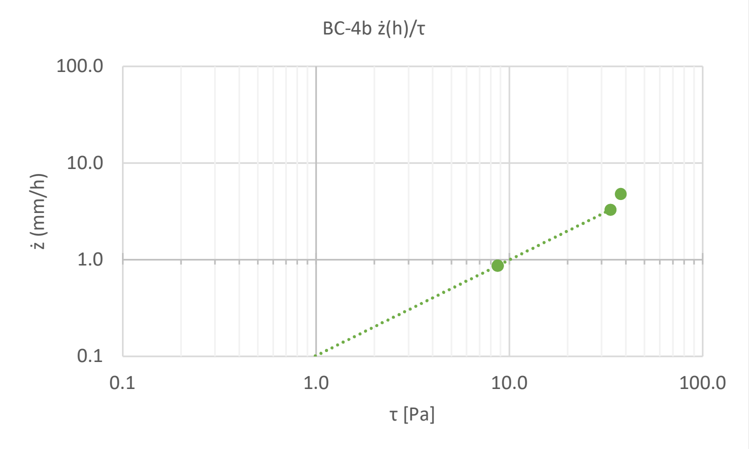

BC-5a EFA 1				
ρd	1.42	g/cm3	**v [m/s]**	**2.02**
W0	25.70	%	**τ [Pa]**	**10.44**
ρ	1.78	g/cm3	**Freq [Hz]**	**24.69**
IL	0.14	-		
m1	45.09	g	mass	before
m1d	35.87	g	dry mass	the test
m2	46.15	g	mass	after the
m2d	35.36	g	dry mass	test
dm	**0.51**	**g**	**mass loss**	
t	66	min		
	1.1	h		
ż	**0.46**	**g/h**	0.21	mm/h

BC-5a EFA 2				
ρd	1.43	g/cm3	**v [m/s]**	**2.82**
W0	25.70	**%**	**τ [Pa]**	**19.98**
ρ	1.80	g/cm3	**Freq [Hz]**	**35.04**
IL	0.14	-		
m1	45.53	g	mass	before
m1d	36.22	g	dry mass	the test
m2	44.78	g	mass	after the
m2d	34.05	g	dry mass	test
dm	**2.17**	**g**	**mass loss**	
t	68	min		
	1.1	h		
ż	**1.92**	**g/h**	0.85	mm/h

BC-5a EFA 3				
ρd	1.42		**v [m/s]**	**3.62**
W0	25.70	**%**	**τ [Pa]**	**32.47**
ρ	1.78	g/cm3	**Freq [Hz]**	**45.00**
IL	0.14	-		
m1	44.99	g	mass	before
m1d	35.79	g	dry mass	the test
m2	44.61	g	mass	after the
m2d	33.28	g	dry mass	test
dm	**2.51**	**g**	**mass loss**	
t	64	min		
	1.07	h		
ż	**2.35**	**g/h**	1.05	mm/h

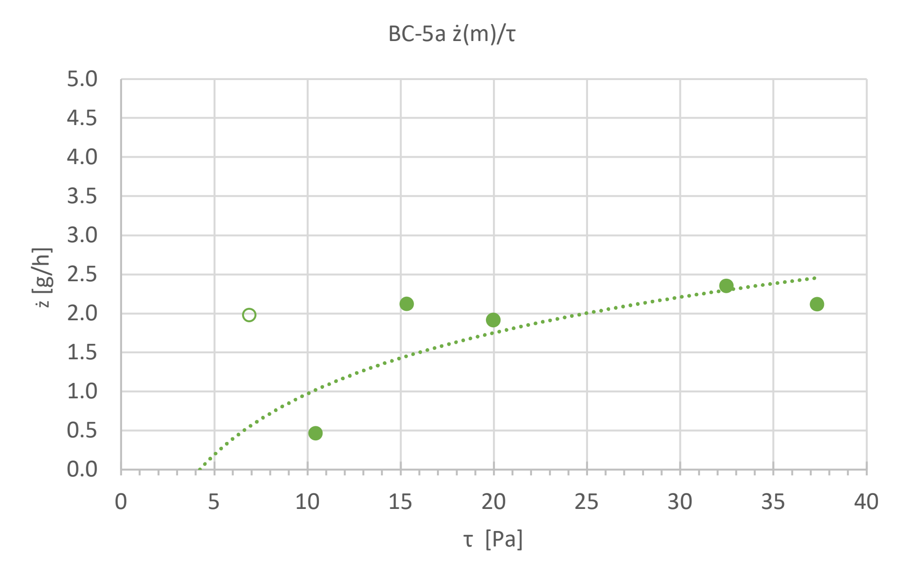

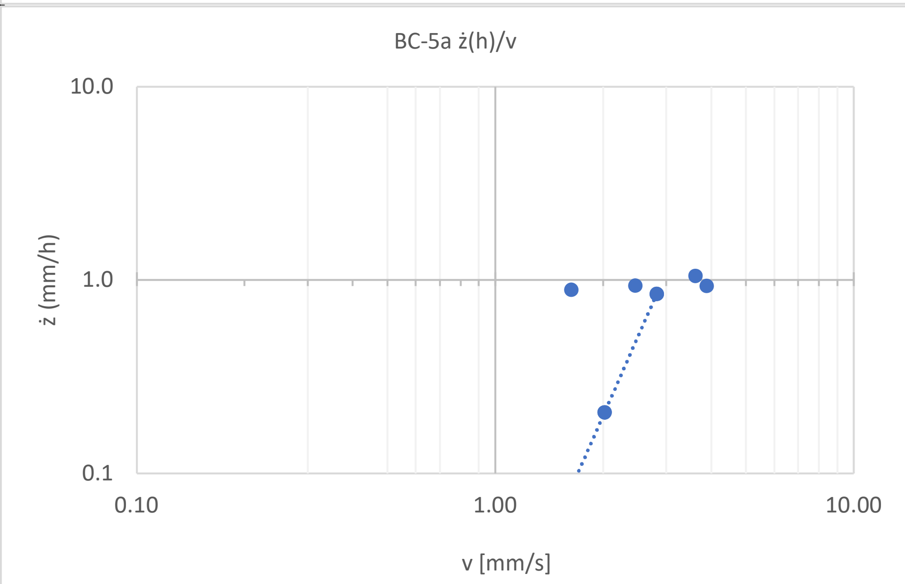

		BC-5a EFA 4		
ρd	1.41	g/cm3	**v [m/s]**	**1.63**
W0	25.70	%	**τ [Pa]**	**6.87**
ρ	1.77	g/cm3	**Freq [Hz]**	**20.22**
IL	0.14	-		
m1	44.72	g	mass	before
m1d	35.58	g	dry mass	the test
m2		g	mass	after the
m2d	33.43	g	dry mass	test
dm	**2.15**	**g**	**mass loss**	
t	65	min		
	1.08	h		
ż	**1.98**	**g/h**	0.89	mm/h
		BC-5a EFA 5		
ρd	1.43	g/cm3	**v [m/s]**	**2.46**
W0	25.70	%	**τ [Pa]**	**15.32**
ρ	1.80	g/cm3	**Freq [Hz]**	**30.52**
IL	0.14	-		
m1	45.56	g	mass	before
m1d	36.25	g	dry mass	the test
m2	46.21	g	mass	after the
m2d	34.09	g	dry mass	test
dm	**2.16**	**g**	**mass loss**	
t	61	min		
	1.02	h		
ż	**2.12**	**g/h**	0.94	mm/h
		BC-5a EFA 6		
ρd	1.44	g/cm3	**v [m/s]**	**3.89**
W0	25.70	%	**τ [Pa]**	**37.35**
ρ	1.81	g/cm3	**Freq [Hz]**	**50.00**
IL	0.14	-		
m1	45.73	g	mass	before
m1d	36.38	g	dry mass	the test
m2	45.03	g	mass	after the
m2d	33.52	g	dry mass	test
dm	**2.86**	**g**	**mass loss**	
t	81	min		
	1.35	h		
ż	**2.12**	**g/h**	0.93	mm/h
τ_C	**4.22**	**Pa**		
v_C	**1.70**	**m/s**	**NCHRP Report**	
τ_C	**7.42**	**Pa**	**Model**	

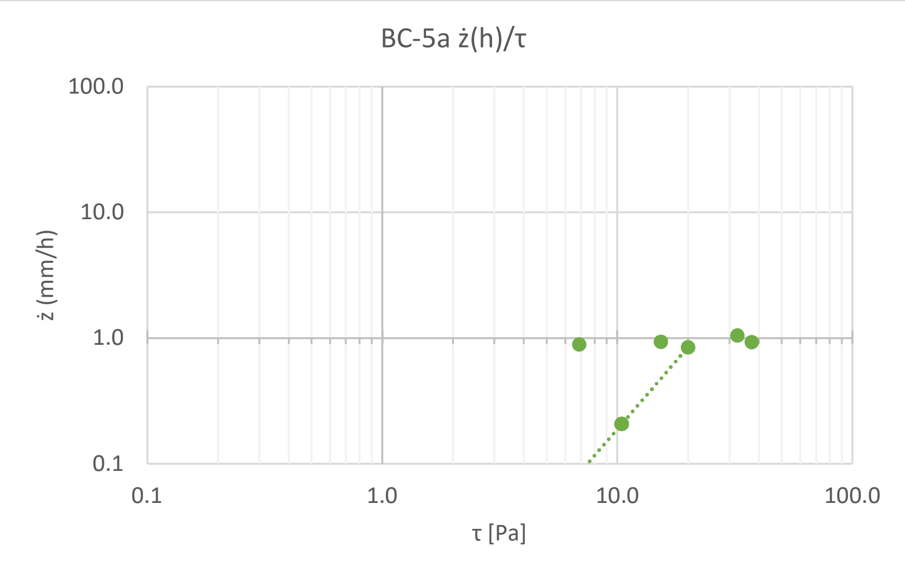

BC-5b EFA 1				
ρd	1.47	g/cm3	**v [m/s]**	**1.98**
W0	29.04	%	**τ [Pa]**	**10.04**
ρ	1.89	g/cm3	**Freq [Hz]**	**22.00**
IL	0.23	-		
m1	47.89	g	mass	before
m1d	37.11	g	dry mass	the test
m2	41.81	g	mass	after the
m2d	32.26	g	dry mass	test
dm	**4.85**	**g**	**mass loss**	
t	63	min		
	1.1	h		
ż	**4.62**	**g/h**	1.94	mm/h
BC-5b EFA 2				
ρd	1.43	g/cm3	**v [m/s]**	**2.10**
W0	29.54	%	**τ [Pa]**	**11.26**
ρ	1.86	g/cm3	**Freq [Hz]**	**26.01**
IL	0.24	-		
m1	46.91	g	mass	before
m1d	36.21	g	dry mass	the test
m2	43.60	g	mass	after the
m2d	33.12	g	dry mass	test
dm	**3.09**	**g**	**mass loss**	
t	78	min		
	1.3	h		
ż	**2.38**	**g/h**	1.02	mm/h
BC-5b EFA 3				
ρd	1.54	g/cm3	**v [m/s]**	**2.43**
W0	29.30	%	**τ [Pa]**	**14.96**
ρ	1.99	g/cm3	**Freq [Hz]**	**30.05**
IL	0.23	-		
m1	50.23	g	mass	before
m1d	38.85	g	dry mass	the test
m2	40.01	g	mass	after the
m2d	30.56	g	dry mass	test
dm	**8.29**	**g**	**mass loss**	
t	63	min		
	1.05	h		
ż	**7.89**	**g/h**	3.16	mm/h

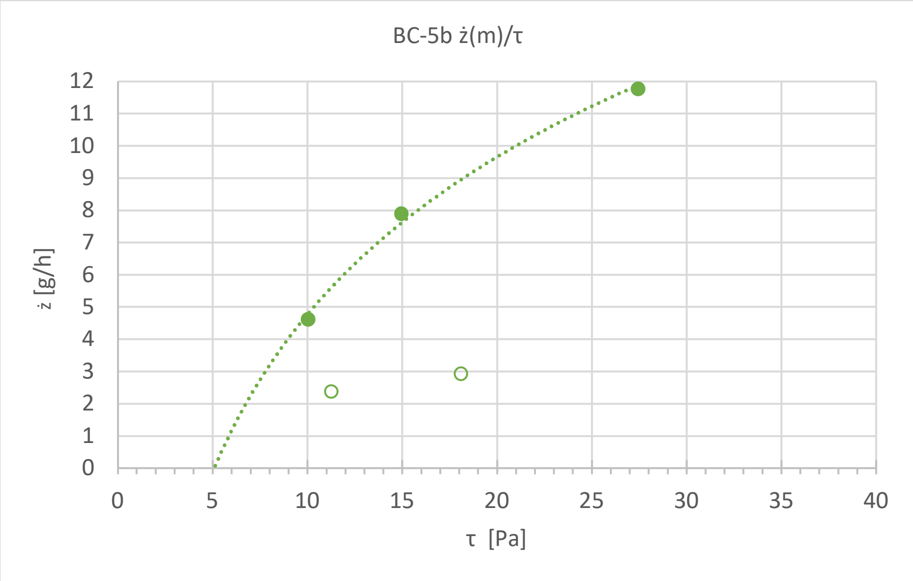

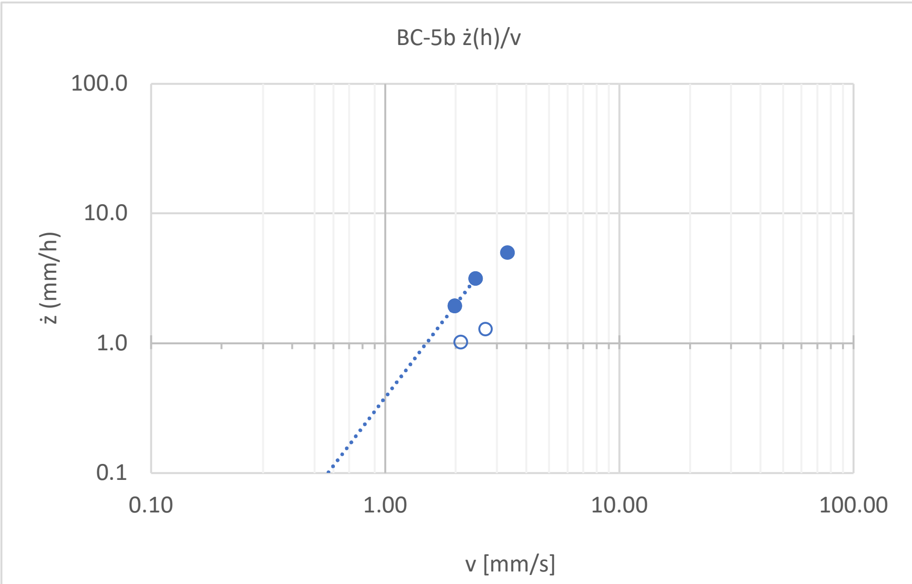

BC-5b EFA 4				
ρd	1.45	g/cm3	**v [m/s]**	**3.32**
W0	29.34	%	**τ [Pa]**	**27.45**
ρ	1.87	g/cm3	**Freq [Hz]**	**40.09**
IL	0.23	-		
m1	47.29	g	mass	before
m1d	36.56	g	dry mass	the test
m2	37.01	g	mass	after the
m2d	28.52	g	dry mass	test
dm	**8.04**	**g**	**mass loss**	
t	41	min		
	0.68	h		
ż	**11.77**	**g/h**	5.01	mm/h
BC-5b EFA 5				
ρd	1.41	g/cm3	**v [m/s]**	**2.68**
W0	28.05	%	**τ [Pa]**	**18.10**
ρ	1.81	g/cm3	**Freq [Hz]**	**37.34**
IL	0.20	-		
m1	45.80	g	mass	before
m1d	35.77	g	dry mass	the test
m2	42.70	g	mass	after the
m2d	32.79	g	dry mass	test
dm	**2.98**	**g**	**mass loss**	
t	61	min		
	1.02	h		
ż	**2.93**	**g/h**	1.29	mm/h
τ_C	**5.08**	**Pa**		
v_C	**0.57**	**m/s**	**NCHRP Report**	
τ_C	**0.89**	**Pa**	**Model**	

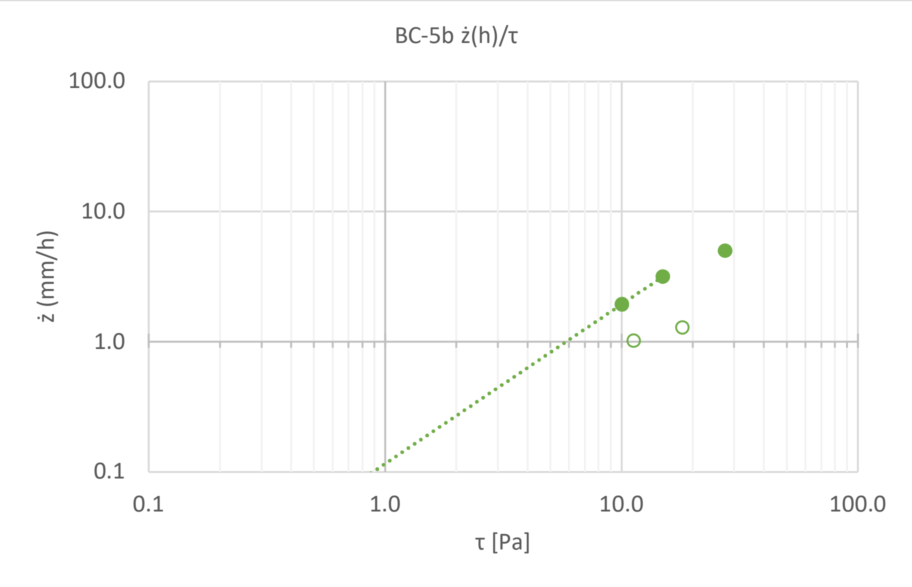

A.2 EFA Tests Logbook: Kleirijperij Clay

CR-4a EFA 1				
ρd	1.03	g/cm^3	**v [m/s]**	**1.77**
W0	41.20	%	**τ [Pa]**	**8.07**
ρ	1.52	g/cm^3	**f [Hz]**	**21.83**
IL	0.02	-		
m1	38.53	g	mass	before
m1d	27.29	g	dry mass	the test
m2	37.55	g	mass	after the
m2d	22.98	g	dry mass	test
dm	**4.31**	**g**	**mass loss**	
t	65	min		
	1.1	h		
ε(m)	**3.98**	**g/h**	2.08	mm/h

CR-4a EFA 2				
ρd	1.03	g/cm^3	**v [m/s]**	**2.11**
W0	41.20	**%**	**τ [Pa]**	**11.36**
ρ	1.57	g/cm^3	**f [Hz]**	**26.05**
IL	0.02	-		
m1	39.73	g	mass	before
m1d	28.14	g	dry mass	the test
m2	38.37	g	mass	after the
m2d	22.06	g	dry mass	test
dm	**6.08**	**g**	**mass loss**	
t	72	min		
	1.2	h		
ε(m)	**5.06**	**g/h**	2.56	mm/h

CR-4a EFA 3				
ρd	1.03	g/cm^3		
W0	41.20	**%**	**v [m/s]**	**2.43**
ρ	1.51	g/cm^3	**τ [Pa]**	**14.96**
IL	0.02	-	**f [Hz]**	**30.00**
m1	38.21	g	mass	before
m1d	27.06	g	dry mass	the test
m2	34.67	g	mass	after the
m2d	20.08	g	dry mass	test
dm	**6.98**	**g**	**mass loss**	
t	55	min		
	0.9	h		
ε(m)	**7.62**	**g/h**	4.01	mm/h

τ_c	**4.26 Pa**	**SRICOS Model**
v_c	**0.14 m/s**	**NCHRP Report Model**
τ_c	**0.06 Pa**	

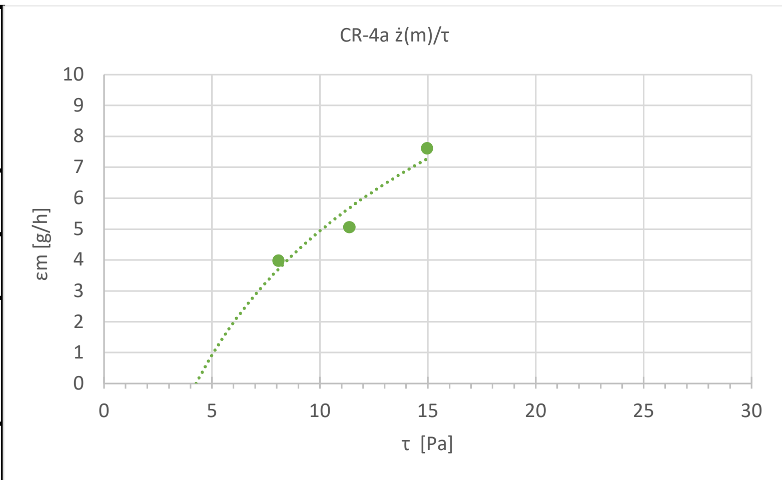

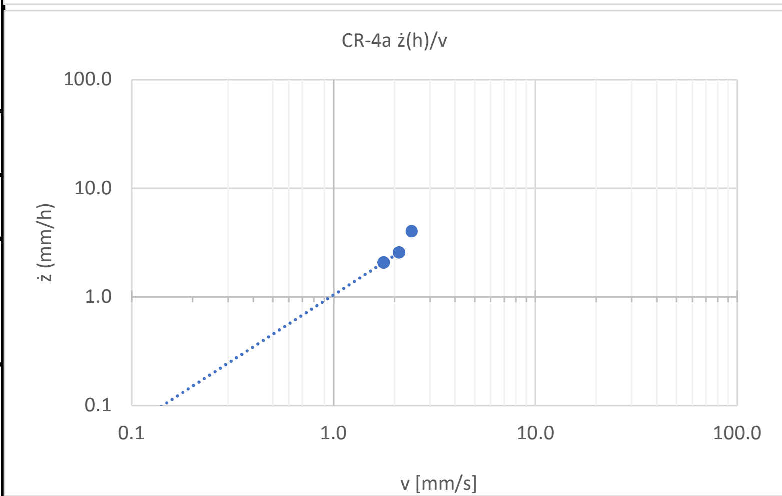

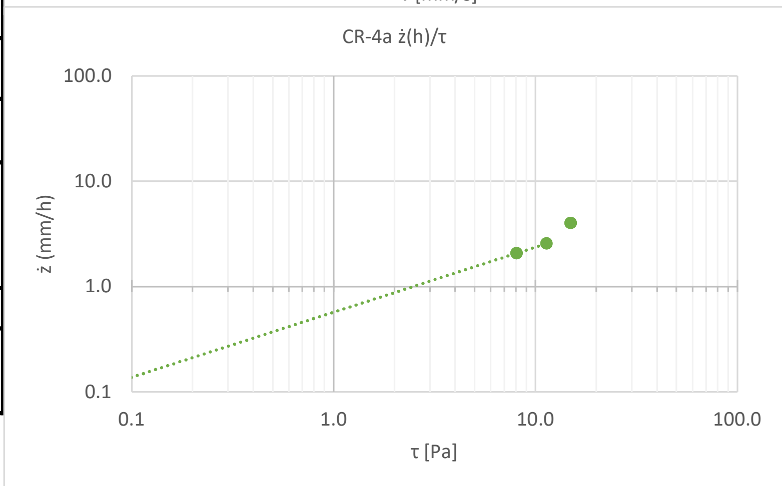

A.3 Laboratory Report: Verslag bezoek groeve Schelle 21/02/2023 BKE-MMD

hoogheemraadschap Hollands Noorderkwartier
ALLIANTIE MARKERMEERDIJKEN

MEMO

Aan

Van Rob Faas

Kopie aan BKE Lab

Onderwerp	**Documentnummer**	**Datum**
Groeve Schelle, Belgie conclusies nav bezoek en analyses	UvM-000399	5-10-2022

1. Inleiding

Op het project Markermeerdijken moet circa 400.000 m^3 erosieklasse klei worden aangebracht op de nieuwe dijk. Deze klei zal voor het grootste gedeelte worden geleverd uit 2 groeves in België. Als voorbereiding op de eerste leveringen in juli en augustus 2022 is een bezoek gebracht aan beide groeves met als doel om de kwaliteit vast te stellen van de klei en de daarbij behorende karakteristieken.

2. Bezoek groeve

Op 21 juni is er een bezoek gebracht aan de Groeve schelle door Patrick van der Tas, Harry Hovenkamp en Rob Faas van het laboratorium van het project Markermeerdijken. De groeve is gelegen nabij de Tuinlei in Schelle, Antwerpen, België.

Tijdens dit bezoek zijn er 15 handboringen gezet tot verschillende dieptes. De boringen waren verspreid over het gedeelte van de groeve waar, volgens de eigenaar, komende periode de klei uit ontgraven gaat worden.

Wat opviel tijdens doen van de boringen was dat de klei zeer hard was waardoor het op veel plekken niet mogelijk was om met de handboor dieper dan 1 m te boren.

In bijlage 1 zijn de boorbeschrijvingen en de locatie kaart weergegeven. Helaas was het niet mogelijk om de hoogte van de boorlocaties nauwkeurig te bepalen (geen bereik met GPS / correctiebestanden). De hoogte ten opzichte van elkaar is dan ook geschat en staat onderaan de boring weergegeven.

Tijdens het veldwerk viel op dat er 2 duidelijke stoorlagen aanwezig zijn in de groeve. De eerste stoorlaag is circa 10 cm dik en bevind zich 2 m beneden het bestaande maaiveld. De stoorlaag bestaat uit siltige klei en laat daardoor beter water door. Op circa 3 m beneden maaiveld bevindt zich een stoorlaag van maximaal 30 cm met siltige klei. Doordat beide lagen makkelijker water doorlaten dan de boven en onderliggende kleilagen zijn ze zeer goed te onderscheiden in de wanden van de put. Tevens viel op dat ze dikker lijken in de wanden van de put. Bij nadere inspectie bleek dit echter visueel te zijn en is de stoorlaag zelf aanzienlijk dunner dan dat deze van een afstand lijkt.

Figuur 1 geeft een doorsnede van de put want met de betreffende stoorlagen erin.

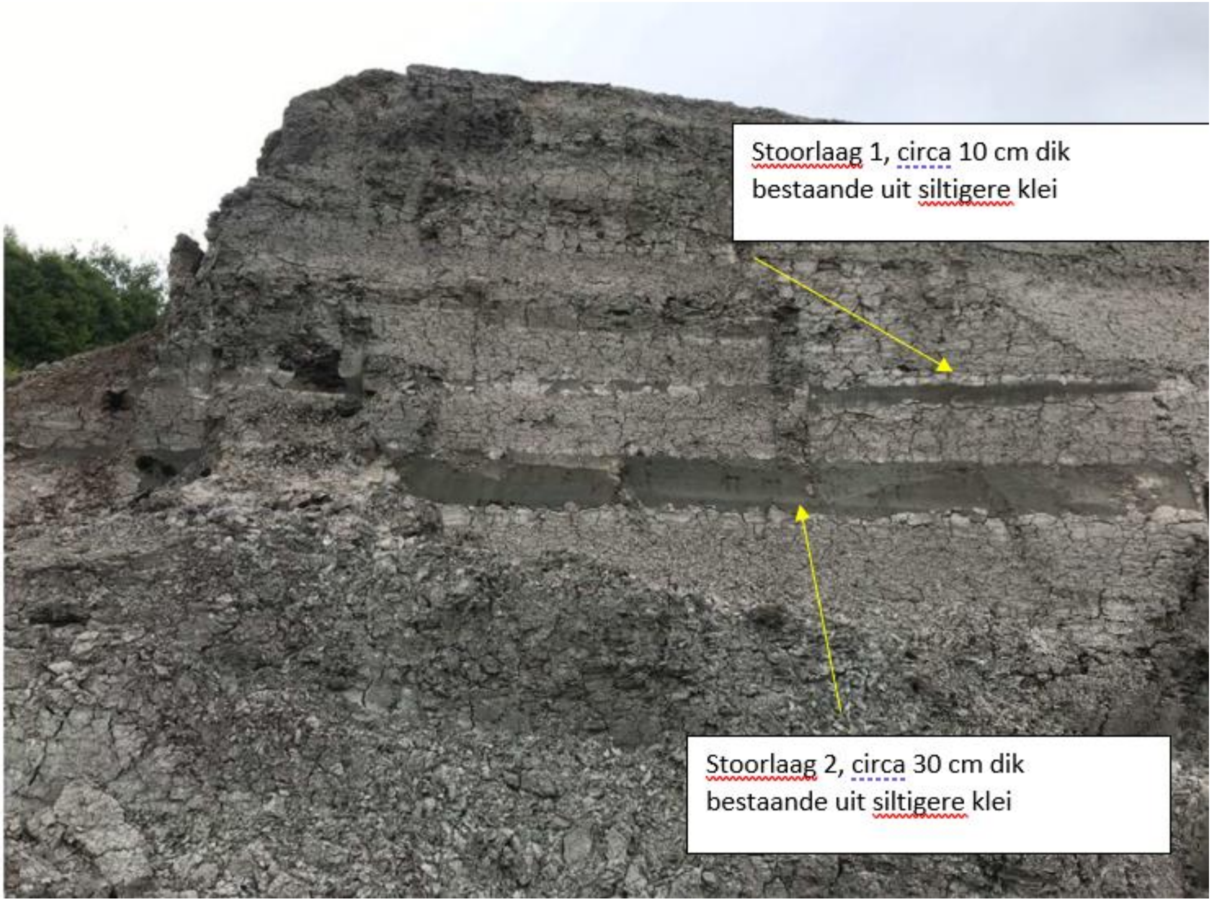

Figuur 1 putwand met de stoorlagen

Op de 2 stoorlaagjes na kan de klei uit de put het beste omschreven worden als zeer harde (vette) klei.

3. Laboratorium onderzoek

Van de boringen en de daarbij behorende monsters is een selectie gemaakt om de klei karakteristieken te bepalen. In totaal zijn er 18 monsters onderzocht waarvan voor 14 monsters de complete erosieklasse is bepaald en voor alle monsters het huidige vochtgehalte.

In bijlage 2 is de rapportage en bijbehorende samenvattingstabel van de laboratorium analyses weergegeven.

Uit het onderzoek blijkt dat alle monsters behalve monster 15 voldoen aan erosieklasse 1 klei. Monster 15 betreft een monster welke gestoken is in de stoorlaag van circa 30 cm met siltige klei en het was dus al visueel de verwachting dat deze van mindere kwaliteit zou zijn.

Op het project markermeerdijken geld ook dat de klei moet voldoen aan een juist vochtgehalte wanneer deze verwerkt wordt. Het minimum vochtgehalte van de klei is gegeven door:

$$Min\ Vochtgehalte = 0.9 * rolgrens$$

het maximum vochtgehalte is gegeven door:

$$Max\ vochtgehalte = vloeigrens - (0.75 * plasticiteitsindex)$$

Wanneer de verkregen vochtgehaltes worden getoetst aan de bovenstaande grenzen voldoen bijna alle monsters. Uitzondering hierop zijn de monsters 4 en monster 15. Deze zijn beide te nat.

Monster 15 betreft een monster welke gestoken is in de stoorlaag van 30 cm met siltige klei. Deze laag is juist de “natte” laag en het was dus al de verwachting het vochtgehalte binnen deze laag mogelijk te hoog zou zijn. Dat monster 4 te nat is, is niet direct te verklaren. Vermoedelijk betreft dit een analyse fout danwel dat er vervuiling in het monster is gekomen tijdens het bemonsteren zelf. De verkregen waarde wordt als uitschieter behandeld en als niet representatief beschouwd.

Wat verder opvalt is dat van deze klei de rol en de vloeigrenzen bijna identieke zijn tussen de verschillende monsters. Het is daarom goed mogelijk om een gemiddelde vloeigrens en rolgrens te bepalen en daaruit de grenzen van het vochtgehalte van tevoren te berekenen.

Voor het bepalen van de gemiddelde vloei-, en rolgrens zijn alle monsters gebruikt behalve monster 15 aangezien dit de stoorlaag betrof. In tabel 1 zijn deze waardes weergegeven.
Op basis van de gegevens in tabel 1 kan nu ook de minimum en maximumwaarde worden vastgesteld waaraan de klei uit Groeve Schelle dient te voldoen om goed verwerkbaar te zijn op Markermeerdijken. Dit is ook weergegeven in onderstaande tabel.

Tabel 1 Gemiddelde vloei- en rolgrenzen met daarbij behorende min/max vochtgehalte

Herkomst locatie	**Vloeigrens**	**Rolgrens**	**Plasticiteitsindex**	**Min. vochtgehalte**	**Max Vochtgehalte**
Schelle, Belgie	69	21	48	19	33

4. Conclusies

De klei welke aanwezig is in de Groeve Schelle is van uniforme en homogene kwaliteit. Op 2 kleine stoorlaagjes na bestaat het materiaal uit zwak siltige (zeer) harde klei.

Tijdens het ontgraven wordt de wand van boven naar beneden in 1 keer ontgraven. Daardoor worden de twee stoorlaagjes ongemengd en zijn ze niet meer terug te vinden in de klei welke wordt aangevoerd naar Markermeerdijken. De stoorlaagjes zijn tevens zo klein in omvang dat deze geen negatief effect hebben op de algemene kwaliteit van de klei.

Aangezien het materiaal dusdanig homogeen is, is het mogelijk om een gemiddelde waarde te bepalen voor de vloeigrens en rolgrens. Met deze waarde is het tevens mogelijk om vooraf een minimum en maximumwaarde te berekenen waaraan de klei moet voldoen om deze goed te kunnen verwerken op Markermeerdijken. Dit is in tabel 1 weergegeven.

Schelle resultaten lab onderzoek

Monster		Laboratorium analyse						Toetsing	
Sample	**Beschrijving uit boring**	**Erosieklasse**	**Plasticiteitsindex**	**Vloeigrens**	**Rolgrens**	**Fractie <63 um**	**Vochtgehalte**	**min vocht (= 0.9*rol)**	**max vocht (= vloei * 0.75-Pi)**
01, B1 0.5-2.0 m	klei, zwak siltig, neutraal grijs, zwart	Cat 1	47.50%	67%	20%	93.3	28.3%	18.0%	31.4%
02, B2 1.0-3.8 m	klei, zwak siltig, neutraal grijs, zwart, hard	Cat 1	47.9%	70.0%	22.0%	98.6	28.9%	19.8%	34.1%
03, B3 1.0 - 3.8 m	klei, zwak siltig, neutraal grijs, zwart, resten zand, hard	Cat 1	53.9%	73.0%	19.0%	93.1	27.1%	17.1%	32.6%
04, B4 0.0-1.0 m	klei, zwak siltig, sporen puin/kiezel laagje op 90 cm, matig hard	Cat 1	52.4%	72.0%	19.0%	91.6	38.1%	17.1%	32.7%
05, B4 1.0-3.0 m	klei, zwak siltig, hard	Cat 1	50.3%	73.0%	23.0%	94.3	30.3%	20.7%	35.3%
06, B5 0.0-1.75 m	klei, zwak siltig, zeer hard	Cat 1	39.7%	59.0%	19.0%	93.4	25.9%	17.1%	29.2%
07, B5 1.9-2.1 m	klei, uiterst siltig, zwak humeus, neutraal grijs, zwart, matig zand	Cat 1	37.0%	59.0%	22.0%	83	26.9%	19.8%	31.3%
08, B6 0.0-1.0 m	klei, zwak siltig, neutraal grijs, zwart, extreem hard	Cat 1	47.6%	72.0%	24.0%	98	30.2%	21.6%	36.3%
09, B7 0.3-1.0 m	klei, zwak siltig, neutraal zwart, groen, klei zeer hard					99.2	30.2%	18.9%	33.0%
10, B8 0.0-0.5 m	klei, zwak siltig, neutraal grijs, groen, zeer hard					99	30.6%	18.9%	33.0%
11, B8 0.5-1.0 m	klei, zwak siltig, neutraal grijs, groen	Cat 1	50.9%	72.0%	22.0%	96.7	29.2%	19.8%	33.8%
12, B9 0.0-1.0 m	klei, zwak siltig, neutraal grijs, groen					99.2	29.8%	18.9%	33.0%
13, B11 0.0-1.0 m	klei, zwak siltig, neutraal grijs, groen, zeer hard	Cat 1	52.9%	74.0%	21.0%	96.8	30.2%	18.9%	34.3%
14, B13 0.0-1.5 m	klei, zwak siltig, neutraal groen, grijs		51.0%	71.5%	21.5%	97.9	29.3%	19.4%	33.3%
15, B14 2.5-3.0 m	klei, uiterst siltig, neutraal groen, grijs, matig hard	Cat 3	17.4%	41.0%	24.0%	99.8	29.9%	21.6%	28.0%
16, B14 3.0-4.0 m	klei, zwak siltig, neutraal grijs, grijs	Cat 1	46.5%	67.0%	21.0%	96.6	29.7%	18.9%	32.1%
17, B15 0.0-1.0 m	klei, zwak siltig, neutraal grijs, groen, zeer hard	Cat 1	50.5%	70.0%	20.0%	87.8	28.8%	18.0%	32.1%
18, B15 2.0-2.5 m	klei, zwak siltig, neutraal grijs, groen, zeer hard	Cat 1	50.5%	71.0%	21.0%	84.6	27.1%	18.9%	33.1%

Bijlage 2B, Lab rapportage erosieklasse

Boskalis Environmental

Project: Versterking Markermeerdijken
Deelgebied:AMMD Noord

Unie van Marken V.O.F.

Sublocatie : MMD deelgebied Noord

KTA nummer :

Vak : Bezoek groeve Schelle juni 2022

Overzicht van resultaten

Monster	Dijkpaal / Coordinaten	Laag	Datum	Eis	Resultaat	Toetsing
		(diepte tov laag)			(%)	
01, B1 0.5-2.0 m		83001()	21-6-2022	U-34, Erosieklasse Vochtgehalte gemeten U-38, Minimum vochtgehalte U-38, Maximum vochtgehalte	Cat 1 28,3 17,7 31,6	Voldoet Voldoet Voldoet
02, B2 1.0-3.8 m		83007()	21-6-2022	U-34, Erosieklasse Vochtgehalte gemeten U-38, Minimum vochtgehalte U-38, Maximum vochtgehalte	Cat 1 28,9 20,3 34,5	Voldoet Voldoet Voldoet
03, B3 1.0 - 3.8 m		83042()	21-6-2022	U-34, Erosieklasse Vochtgehalte gemeten U-38, Minimum vochtgehalte U-38, Maximum vochtgehalte	Cat 1 27,1 17,1 32,5	Voldoet Voldoet Voldoet
04, B4 0.0-1.0 m		83040()	21-6-2022	U-34, Erosieklasse Vochtgehalte gemeten U-38, Minimum vochtgehalte U-38, Maximum vochtgehalte	Cat 1 38,1 17,6 32,6	Voldoet Voldoet Voldoet niet
05, B4 1.0-3.0 m		83040()	21-6-2022	U-34, Erosieklasse Vochtgehalte gemeten U-38, Minimum vochtgehalte U-38, Maximum vochtgehalte	Cat 1 30,3 20,5 35,4	Voldoet Voldoet Voldoet
06, B5 0.0-1.75 m		83030()	21-6-2022	U-34, Erosieklasse Vochtgehalte gemeten U-38, Minimum vochtgehalte U-38, Maximum vochtgehalte	Cat 1 25,9 17,4 29,2	Voldoet Voldoet Voldoet
07, B5 1.9-2.1 m		83030()	21-6-2022	U-34, Erosieklasse Vochtgehalte gemeten U-38, Minimum vochtgehalte U-38, Maximum vochtgehalte	Cat 1 26,9 20,0 31,5	Voldoet Voldoet Voldoet
08, B6 0.0-1.0 m		83032()	21-6-2022	U-34, Erosieklasse Vochtgehalte gemeten U-38, Minimum vochtgehalte U-38, Maximum vochtgehalte	Cat 1 30,2 22,1 36,4	Voldoet Voldoet Voldoet
09, B7 0.3-1.0 m		83052()	21-6-2022	Vochtgehalte gemeten U-38, Minimum vochtgehalte U-38, Maximum vochtgehalte	30,2 18,9 33,0	Voldoet Voldoet
10, B8 0.0-0.5 m		83051()	21-6-2022	Vochtgehalte gemeten U-38, Minimum vochtgehalte U-38, Maximum vochtgehalte	30,6 18,9 33,0	Voldoet Voldoet
11, B8 0.5-1.0 m		83051()	21-6-2022	U-34, Erosieklasse Vochtgehalte gemeten U-38, Minimum vochtgehalte U-38, Maximum vochtgehalte	Cat 1 29,3 19,4 34,3	Voldoet Voldoet Voldoet

Boskalis Environmental

Project: Versterking Markermeerdijken
Deelgebied:AMMD Noord

Unie van Marken V.O.F.

Monster	Dijkpaal / Coordinaten	Laag	Datum	Eis	Resultaat	Toetsing
12, B9 0.0-1.0 m		83073()	21-6-2022	Vochtgehalte gemeten U-38, Minimum vochtgehalte U-38, Maximum vochtgehalte	29,8 18,9 33,0	Voldoet Voldoet
13, B11 0.0-1.0 m		83015()	21-6-2022	U-34, Erosieklasse Vochtgehalte gemeten U-38, Minimum vochtgehalte U-38, Maximum vochtgehalte	Cat 1 30,2 18,9 34,2	Voldoet Voldoet Voldoet
14, B13 0.0-1.5 m		83023()	21-6-2022	Vochtgehalte gemeten U-38, Minimum vochtgehalte U-38, Maximum vochtgehalte	29,3 18,9 33,0	Voldoet Voldoet
15, B14 2.5-3.0 m		83006()	21-6-2022	U-34, Erosieklasse Vochtgehalte gemeten U-38, Minimum vochtgehalte U-38, Maximum vochtgehalte	Cat 3 29,9 21,4 28,1	Voldoet niet Voldoet Voldoet niet
16, B14 3.0-4.0 m		83006()	21-6-2022	U-34, Erosieklasse Vochtgehalte gemeten U-38, Minimum vochtgehalte U-38, Maximum vochtgehalte	Cat 1 29,7 18,9 32,6	Voldoet Voldoet Voldoet
17, B15 0.0-1.0 m		83063()	21-6-2022	U-34, Erosieklasse Vochtgehalte gemeten U-38, Minimum vochtgehalte U-38, Maximum vochtgehalte	Cat 1 28,8 18,0 32,6	Voldoet Voldoet Voldoet
18, B15 2.0-2.5 m		83063()	21-6-2022	U-34, Erosieklasse Vochtgehalte gemeten U-38, Minimum vochtgehalte U-38, Maximum vochtgehalte	Cat 1 27,1 18,9 33,6	Voldoet Voldoet Voldoet

A.4 Proctor Compaction: Boom Clay

Modified Proctor Compaction															
Number	Sample	Mould	Mould+Soil	OVEN Sample	Dry OVEN Sample	W	V Mold	ρ	ρ_d	ρ_s	e	n	Sr	PI	LI
	[g]					[%]	[cm³]	g/cm³						[%]	
BC-1	1793.00	3176.00	4969.00	146.20	110.50	32.3	967.1	1.85	1.40	2.65	0.89	0.47	0.96	48	0.24
BC-2	1758.00	3160.00	4918.00	183.30	141.10	29.9	967.1	1.82	1.40	2.65	0.89	0.47	0.89	48	0.19
BC-4	1764.60	3160.00	4924.60	111.85	88.27	26.6	967.1	1.82	1.44	2.65	0.84	0.46	0.84	41	0.11
ST-2	1678.00	3098.80	4776.80	61.10	57.16	6.9	967.1	1.74	1.62	2.65	0.63	0.39	0.29	48	-0.29
ST-3	1745.20	3098.80	4844.00	144.95	105.15	37.9	967.1	1.80	1.31	2.65	1.02	0.51	0.98	48	0.35
ST-4	1764.00	3160.00	4924.00	126.40	96.70	30.7	967.1	1.82	1.40	2.65	0.90	0.47	0.91	48	0.20

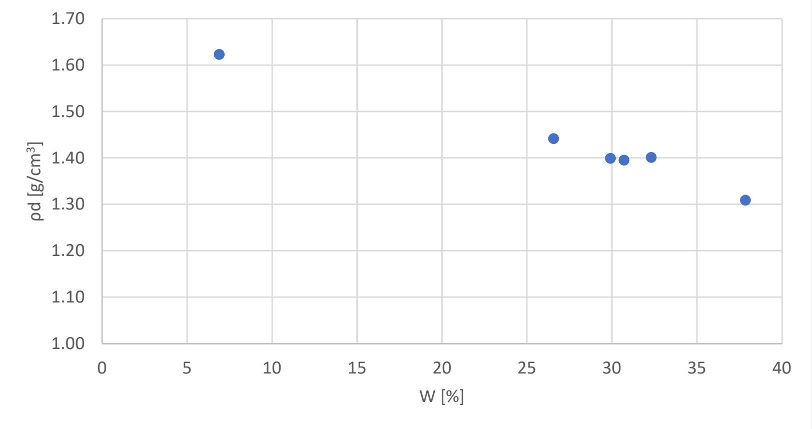

A.5 Proctor Compaction: Kleirijperij Clay

Proctor Compaction															
Number	Sample	Mould	Mould+Soil	OVEN Sample	Dry OVEN Sample	W	V Mold	ρ	ρ_d	ρ_s	e	n	Sr	PI	LI
	[g]					[%]	[cm³]	g/cm^3						[%]	
CR-1	1729.0	3160.0	4889.0	161.0	123.6	30.3	967.1	1.79	1.37	2.68	0.95	0.49	0.85	65	-0.15
CR-2	1757.0	3165.0	4922.0	153.0	115.5	32.5	967.1	1.82	1.37	2.68	0.95	0.49	0.91	65	-0.12
CR-4	1411.0	3165.0	4576.0	52.0	36.8	41.2	967.1	1.46	1.03	2.68	1.59	0.61	0.69	65	0.02

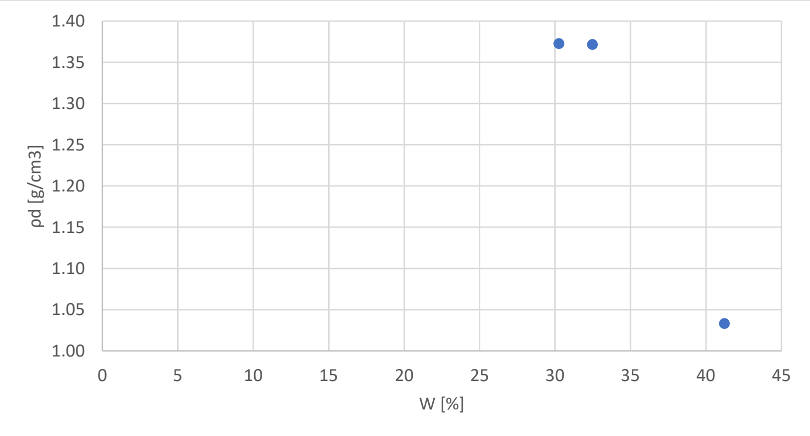

B List of Specimens

Prepared Specimens Properties

Method	Wet/Dry	Specimen	W	ρ	ρ_d	ρ_s	e	Sr	W_L	W_P	PI	LI	Test	Valid result
			%	g/cm3			-		%			-		
Boom clay														
Simulated Construction	N	ST-4bE1	30.71	1.82	1.40	2.65	0.90	0.91	69	21	48	0.20	Y	N
	N	BC-1aE1	32.30	1.85	1.40	2.65	0.90	0.96	69	21	48	0.24	Y	N
	N	BC-1aE2	32.30	1.85	1.40	2.65	0.90	0.96	69	21	48	0.24	Y	N
	Y	BC-1bE1	32.09	1.85	1.40	2.65	0.89	0.95	69	21	48	0.23	Y	N
	Y	BC-1bE2	32.09	1.85	1.40	2.65	0.89	0.96	69	21	48	0.23	Y	N
	N	BC-2aE1	25.61	1.84	1.46	2.65	0.81	0.84	69	21	48	0.10	Y	Y
	N	BC-2aE2	25.61	1.61	1.28	2.65	1.07	0.64	69	21	48	0.10	Y	Y
	N	BC-2aE3	25.61	1.83	1.46	2.65	0.82	0.83	69	21	48	0.10	Y	Y
	Y	BC-2bE1	26.32	1.81	1.43	2.65	0.85	0.82	69	21	48	0.11	Y	Y
	Y	BC-2bE2	26.32	1.83	1.45	2.65	0.83	0.84	69	21	48	0.11	Y	Y
	Y	BC-2bE3	26.32	1.83	1.45	2.65	0.83	0.84	69	21	48	0.11	Y	Y
Homogenized Reconstitution	N	BC-4aE1	25.70	1.83	1.45	2.65	0.82	0.83	63	22	41	0.09	Y	Y
	N	BC-4aE2	25.70	1.79	1.42	2.65	0.86	0.79	63	22	41	0.09	Y	Y
	N	BC-4aE3	25.70	1.79	1.43	2.65	0.86	0.79	63	22	41	0.09	Y	Y
	N	BC-4aE4	27.00	1.78	1.40	2.65	0.89	0.80	63	22	41	0.12	Y	Y
	N	BC-4aE5	27.00	1.75	1.38	2.65	0.93	0.77	63	22	41	0.12	Y	Y
	N	BC-4aE6	27.00	1.78	1.40	2.65	0.89	0.80	63	22	41	0.12	Y	N
	N	BC-4aE7	27.00	1.80	1.42	2.65	0.87	0.82	63	22	41	0.12	Y	N
	N	BC-4aE8	27.00	1.83	1.44	2.65	0.84	0.85	63	22	41	0.12	Y	N
	Y	BC-4bE1	27.00	1.85	1.46	2.65	0.82	0.87	63	22	41	0.12	Y	Y
	Y	BC-4bE2	27.00	1.84	1.45	2.65	0.83	0.86	63	22	41	0.12	Y	Y
	Y	BC-4bE3	27.00	1.77	1.40	2.65	0.90	0.80	63	22	41	0.12	Y	Y
In-situ Retrieval	N	BC-5aE1	25.70	1.78	1.42	2.65	0.87	0.78	69	21	48	0.10	Y	Y
	N	BC-5aE2	25.70	1.80	1.43	2.65	0.85	0.80	69	21	48	0.10	Y	Y
	N	BC-5aE3	25.70	1.78	1.42	2.65	0.87	0.78	69	21	48	0.10	Y	Y
	N	BC-5aE4	25.70	1.77	1.41	2.65	0.88	0.77	69	21	48	0.10	Y	Y
	N	BC-5aE5	25.70	1.80	1.43	2.65	0.85	0.80	69	21	48	0.10	Y	Y
	N	BC-5aE6	25.70	1.81	1.44	2.65	0.84	0.81	69	21	48	0.10	Y	N
	Y	BC-5bE1	29.04	1.89	1.47	2.65	0.81	0.96	69	21	48	0.17	Y	Y
	Y	BC-5bE2	29.54	1.86	1.43	2.65	0.85	0.92	69	21	48	0.18	Y	Y
	Y	BC-5bE3	29.30	1.99	1.54	2.65	0.72	1.07	69	21	48	0.17	Y	Y
	Y	BC-5bE4	29.34	1.87	1.45	2.65	0.83	0.93	69	21	48	0.17	Y	N
	Y	BC-5bE5	28.05	1.81	1.41	2.65	0.87	0.85	69	21	48	0.15	Y	N

Method	Wet/Dry	Specimen	W	ρ	$ρ_d$	$ρ_s$	e	Sr	W_L	W_P	PI	LI	Test	Valid result
			%	g/cm3			-		%			-		
Kleirijperij clay														
Simulated Construction	N	CR-1aE1	30.26	1.79	1.37	2.68	0.95	0.85	105	40	65	-0.15	Y	N
	N	CR-1aE2	30.26	1.79	1.37	2.68	0.95	0.85	105	40	65	-0.15	Y	N
	N	CR-1aE3	30.26	1.79	1.37	2.68	0.95	0.85	105	40	65	-0.15	Y	N
	Y	CR-1bE1	31.07	1.79	1.36	2.68	0.96	0.86	105	40	65	-0.14	Y	N
	Y	CR-1bE2	31.07	1.79	1.36	2.68	0.96	0.86	105	40	65	-0.14	Y	N
	Y	CR-1bE3	31.07	1.79	1.36	2.68	0.96	0.86	105	40	65	-0.14	Y	N
	N	CR-2aE1	32.47	1.82	1.37	2.68	0.95	0.91	105	40	65	-0.12	Y	N
	N	CR-2aE2	32.47	1.82	1.37	2.68	0.95	0.91	105	40	65	-0.12	Y	N
	N	CR-2aE3	32.47	1.82	1.37	2.68	0.95	0.91	105	40	65	-0.12	Y	N
	N	CR-4aE1	41.22	1.52	1.08	2.68	1.48	0.69	105	40	65	0.02	Y	N
	N	CR-4aE2	41.22	1.57	1.11	2.68	1.41	0.69	105	40	65	0.02	Y	N
	N	CR-4aE3	41.22	1.51	1.07	2.68	1.50	0.69	105	40	65	0.02	Y	N
	Y	CR-4bE1	33.46	1.52	1.14	2.68	1.36	0.69	105	40	65	-0.10	N	N
	Y	CR-4bE2	35.89	1.55	1.14	2.68	1.36	0.69	105	40	65	-0.06	N	N
	Y	CR-4bE3	39.85	1.55	1.11	2.68	1.42	0.69	105	40	65	0.00	N	N

C Cyclic Wetting and Drying Logbook

ST-4a

Properties					W [%]		Mass [g]			
Initial W.C.	W, %	30.7			W0	30.70	750.32	m0	0	
Bulk density	ρ, g/cm³	1.82			Wd1	10.67	635.32	md1	Dry	Cycle 1
Dry Density	ρd, g/cm³	1.40			Ww1	38.61	795.70	mw1	Wet	
Specific grav	ρs, g/cm³	2.65			Wd2	7.86	619.20	md2	Dry	Cycle 2
Void ratio	e	0.90			Ww2	26.99	729.00	mw2	Wet	
Porosity	n	0.47			Wd3	12.18	644.00	md3	Dry	Cycle 3
Degree of sat	Sr	0.91			Ww3	29.77	745.00	mw3	Wet	
Liq Lim	Wl, %	69.0			Wd4	9.5	628.6	md4	Dry	Cycle 4
Plast Lim	Wp, %	21.0			Ww4	28.7	738.7	mw4	Wet	
Plast Index	Ip, %	48.0	md, g	574.07						
Liq. Index.	Il	0.20								

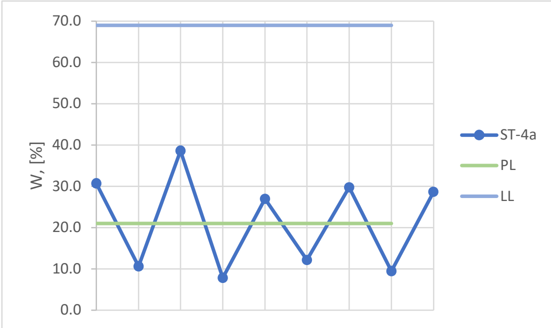

BC-1b E1, E2

Properties					W [%]		Mass [g]			
Initial W.C.	W, %	30.7			W0	32.30	978.02	m0	0	
Bulk density	ρ, g/cm³	1.82			Wd1	13.83	841.50	md1	Dry	Cycle 1
Dry Density	ρd, g/cm³	1.40			Ww1	30.26	963.00	mw1	Wet	
Specific grav	ρs, g/cm³	2.65			Wd2	18.23	874.00	md2	Dry	Cycle 2
Void ratio	e	0.90			Ww2	35.81	1004.00	mw2	Wet	
Porosity	n	0.47			Wd3	12.68	833.00	md3	Dry	Cycle 3
Degree of sat	Sr	0.91			Ww3	32.09	976.50	mw3	Wet	
Liq Lim	Wl, %	69.0								
Plast Lim	Wp, %	21.0								
Plast Index	Ip, %	48.0	md, g	748.28						
Liq. Index.	Il	0.20								

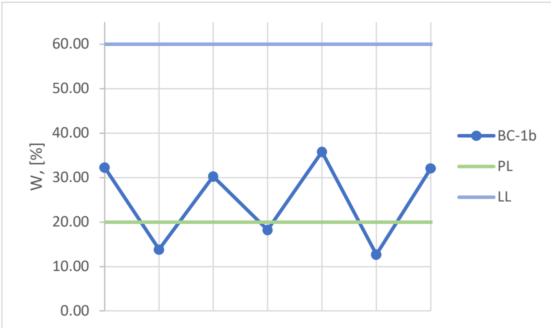

BC-2b E1, E2, E3

Properties					W [%]		Mass [g]			
Initial W.C.	W, %	29.9			W0	29.91	885.00	m0	0	
Bulk density	ρ, g/cm³	1.82			Wd1	17.52	800.60	md1	Dry	Cycle 1
Dry Density	ρd, g/cm³	1.40			Ww1	35.93	926.00	mw1	Wet	
Specific grav	ρs, g/cm³	2.65			Wd2	13.82	775.40	md2	Dry	Cycle 2
Void ratio	e	0.89			Ww2	30.48	888.90	mw2	Wet	
Porosity	n	0.47			Wd3	12.34	765.30	md3	Dry	Cycle 3
Degree of sat	Sr	0.89			Ww3	27.50	868.60	mw3	Wet	
Liq Lim	Wl, %	69.0								
Plast Lim	Wp, %	21.0								
Plast Index	Ip, %	48.0	md, g	681.25						
Liq. Index.	Il	0.19								

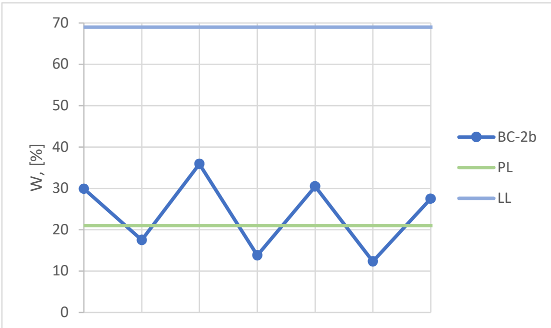

BC-4b E1

Properties			Measurements			W [%]		Mass [g]			
Initial W.C.	W, %	26.5	m₀, g	50.02	**44.72**	W0	32.31	44.72	m0	0	
Bulk density	ρ, g/cm³	1.85	md1	46.07	**40.77**	Wd1	20.62	40.77	md1	Dry	Cycle 1
Dry Density	ρd, g/cm³	1.46	mw1	51.98	**46.68**	Ww1	38.11	46.68	mw1	Wet	
Specific grav	ρs, g/cm³	2.65	md2	45.57	**40.27**	Wd2	19.14	40.27	md2	Dry	Cycle 2
Void ratio	e	0.81	mw2	51.60	**46.30**	Ww2	36.98	46.30	mw2	Wet	
Porosity	n	0.45	md3	46.03	**40.73**	Wd3	20.50	40.73	md3	Dry	Cycle 3
Degree of sat	Sr	0.86	mw3	48.10	**42.80**	Ww3	26.63	42.80	mw3	Wet	
Liq Lim	Wl, %	69.0									
Plast Lim	Wp, %	21.0									
Plast Index	Ip, %	48.0	md, g	35.35							
Liq. Index.	Il	0.11									

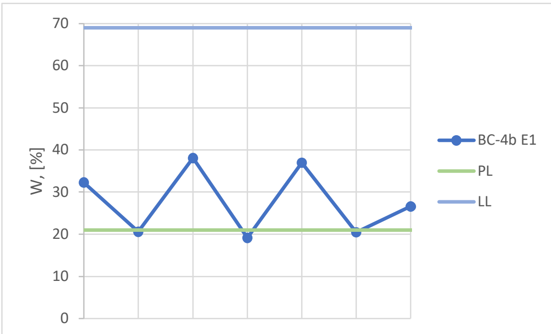

BC-4b E2

Properties			Measurements			W [%]		Mass [g]			
Initial W.C.	W, %	26.5	m₀, g	49.89	**44.59**	W0	32.31	44.59	m0	0	
Bulk density	ρ, g/cm³	1.84	md1	44.96	**39.66**	Wd1	17.68	39.66	md1	Dry	Cycle 1
Dry Density	ρd, g/cm³	1.45	mw1	51.20	**45.90**	Ww1	36.19	45.90	mw1	Wet	
Specific grav	ρs, g/cm³	2.65	md2	45.67	**40.37**	Wd2	19.79	40.37	md2	Dry	Cycle 2
Void ratio	e	0.82	mw2	49.95	**44.65**	Ww2	32.49	44.65	mw2	Wet	
Porosity	n	0.45	md3	44.46	**39.16**	Wd3	16.20	39.16	md3	Dry	Cycle 3
Degree of sat	Sr	0.85	mw3	47.86	**42.56**	Ww3	26.28	42.56	mw3	Wet	
Liq Lim	Wl, %	69.0									
Plast Lim	Wp, %	21.0									
Plast Index	Ip, %	48.0	md, g	35.25							
Liq. Index.	Il	0.11									

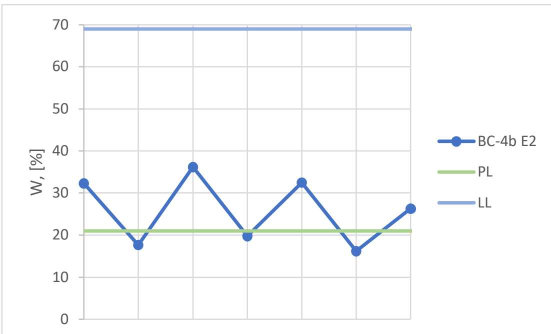

BC-4b E3

Properties			Measurements			W [%]		Mass [g]			
Initial W.C.	W, %	26.5	m_0, g	51.08	**45.78**	W0	32.31	45.78	m0	0	
Bulk density	ρ, g/cm^3	1.81	md1	46.37	**41.07**	Wd1	18.70	41.07	md1	Dry	**Cycle 1**
Dry Density	ρd, g/cm^3	1.43	mw1	51.31	**46.01**	Ww1	32.97	46.01	mw1	Wet	
Specific grav	ρs, g/cm^3	2.65	md2	45.98	**40.68**	Wd2	17.57	40.68	md2	Dry	**Cycle 2**
Void ratio	e	0.85	mw2	52.01	**46.71**	Ww2	35.00	46.71	mw2	Wet	
Porosity	n	0.46	md3	46.09	**40.79**	Wd3	17.89	40.79	md3	Dry	**Cycle 3**
Degree of sat	Sr	0.83	mw3	49.15	**43.85**	Ww3	26.73	43.85	mw3	Wet	
Liq Lim	Wl, %	69.0									
Plast Lim	Wp, %	21.0									
Plast Index	Ip, %	48.0	md, g	36.19							
Liq. Index.	Il	0.11									

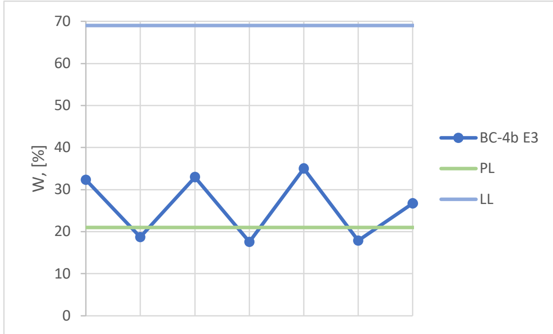

BC-5b E1

Properties			Measurements			W [%]		Mass [g]			
Initial W.C.	W, %	25.7	m_0, g	51.95	**46.65**	W0	25.70	46.65	m0	0	
Bulk density	ρ, g/cm^3	1.85	md1	45.87	**40.57**	Wd1	9.32	40.57	md1	Dry	**Cycle 1**
Dry Density	ρd, g/cm^3	1.47	mw1	53.87	**48.57**	Ww1	30.87	48.57	mw1	Wet	
Specific grav	ρs, g/cm^3	2.65	md2	46.27	**40.97**	Wd2	10.39	40.97	md2	Dry	**Cycle 2**
Void ratio	e	0.81	mw2	53.47	**48.17**	Ww2	29.79	48.17	mw2	Wet	
Porosity	n	0.45	md3	47.25	**41.95**	Wd3	13.04	41.95	md3	Dry	**Cycle 3**
Degree of sat	Sr	0.85	mw3	53.19	**47.89**	Ww3	29.04	47.89	mw3	Wet	
Liq Lim	Wl, %	69.0									
Plast Lim	Wp, %	21.0									
Plast Index	Ip, %	48.0	md, g	37.11							
Liq. Index.	Il	0.10									

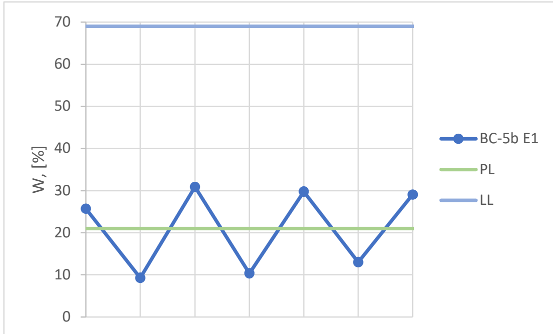

BC-5b E2

Properties			Measurements			W [%]		Mass [g]			
Initial W.C.	W, %	25.7	m_0, g	50.82	**45.52**	W0	25.70	45.52	m0	0	
Bulk density	ρ, g/cm^3	1.80	md1	45.02	**39.72**	Wd1	9.68	39.72	md1	Dry	**Cycle 1**
Dry Density	ρd, g/cm^3	1.43	mw1	53.30	**48.00**	Ww1	32.55	48.00	mw1	Wet	
Specific grav	ρs, g/cm^3	2.65	md2	46.34	**41.04**	Wd2	13.33	41.04	md2	Dry	**Cycle 2**
Void ratio	e	0.85	mw2	52.78	**47.48**	Ww2	31.11	47.48	mw2	Wet	
Porosity	n	0.46	md3	46.44	**41.14**	Wd3	13.60	41.14	md3	Dry	**Cycle 3**
Degree of sat	Sr	0.80	mw3	52.21	**46.91**	Ww3	29.54	46.91	mw3	Wet	
Liq Lim	Wl, %	69.0									
Plast Lim	Wp, %	21.0									
Plast Index	Ip, %	48.0	md, g	36.21							
Liq. Index.	Il	0.10									

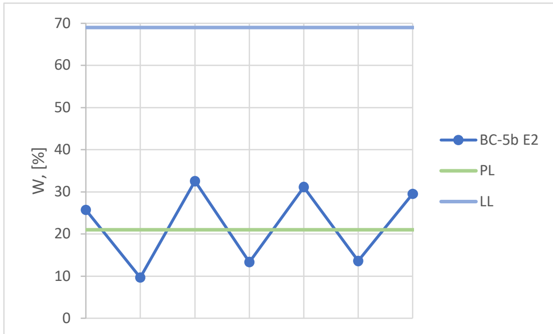

BC-5b E3

Properties			Measurements			W [%]		Mass [g]			
Initial W.C.	W, %	25.7	m_0, g	54.13	**48.83**	W0	25.70	48.83	m0	0	
Bulk density	ρ, g/cm^3	1.93	md1	47.59	**42.29**	Wd1	8.86	42.29	md1	Dry	**Cycle 1**
Dry Density	ρd, g/cm^3	1.54	mw1	53.24	**47.94**	Ww1	23.41	47.94	mw1	Wet	
Specific grav	ρs, g/cm^3	2.65	md2	47.87	**42.57**	Wd2	9.58	42.57	md2	Dry	**Cycle 2**
Void ratio	e	0.72	mw2	54.18	**48.88**	Ww2	25.83	48.88	mw2	Wet	
Porosity	n	0.42	md3	48.52	**43.22**	Wd3	11.26	43.22	md3	Dry	**Cycle 3**
Degree of sat	Sr	0.94	mw3	55.53	**50.23**	Ww3	29.30	50.23	mw3	Wet	
Liq Lim	Wl, %	69.0									
Plast Lim	Wp, %	21.0									
Plast Index	Ip, %	48.0	md, g	38.85							
Liq. Index.	Il	0.10									

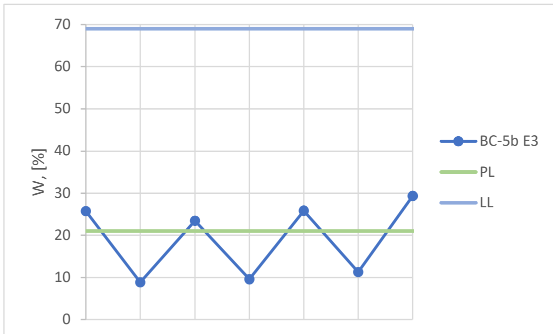

BC-5b E4

Properties			Measurements			W [%]		Mass [g]			
Initial W.C.	W, %	25.7	m_0, g	51.26	**45.96**	W0	25.70	45.96	m0	0	
Bulk density	ρ, g/cm^3	1.82	md1	45.34	**40.04**	Wd1	9.51	40.04	md1	Dry	**Cycle 1**
Dry Density	ρd, g/cm^3	1.45	mw1	53.58	**48.28**	Ww1	32.04	48.28	mw1	Wet	
Specific grav	ρs, g/cm^3	2.65	md2	46.52	**41.22**	Wd2	12.74	41.22	md2	Dry	**Cycle 2**
Void ratio	e	0.83	mw2	52.97	**47.67**	Ww2	30.38	47.67	mw2	Wet	
Porosity	n	0.45	md3	46.31	**41.01**	Wd3	12.16	41.01	md3	Dry	**Cycle 3**
Degree of sat	Sr	0.82	mw3	52.59	**47.29**	Ww3	29.34	47.29	mw3	Wet	
Liq Lim	Wl, %	69.0									
Plast Lim	Wp, %	21.0									
Plast Index	Ip, %	48.0	md, g	36.56							
Liq. Index.	Il	0.10									

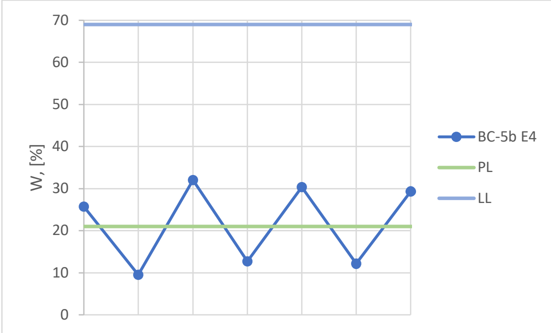

BC-5b E5

Properties			Measurements			W [%]		Mass [g]			
Initial W.C.	W, %	25.7	m_0, g	50.26	**44.96**	W0	25.70	44.96	m0	0	
Bulk density	ρ, g/cm^3	1.78	md1	44.03	**38.73**	Wd1	8.28	38.73	md1	Dry	**Cycle 1**
Dry Density	ρd, g/cm^3	1.41	mw1	51.52	**46.22**	Ww1	29.22	46.22	mw1	Wet	
Specific grav	ρs, g/cm^3	2.65	md2	45.73	**40.43**	Wd2	13.03	40.43	md2	Dry	**Cycle 2**
Void ratio	e	0.87	mw2	50.96	**45.66**	Ww2	27.66	45.66	mw2	Wet	
Porosity	n	0.47	md3	44.99	**39.69**	Wd3	10.97	39.69	md3	Dry	**Cycle 3**
Degree of sat	Sr	0.78	mw3	51.1	**45.80**	Ww3	28.05	45.80	mw3	Wet	
Liq Lim	Wl, %	69.0									
Plast Lim	Wp, %	21.0									
Plast Index	Ip, %	48.0	md, g	35.77							
Liq. Index.	Il	0.10									

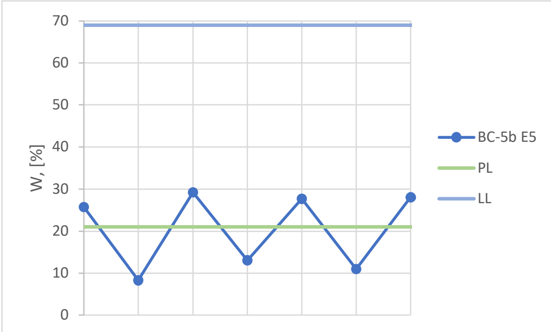

CR-1b E1, E2

Properties					W [%]		Mass [g]			
Initial W.C.	W, %	30.3			W0	30.26	801.00	m0	0	
Bulk density	ρ, g/cm^3	1.79			Wd1	18.39	728.00	md1	Dry	**Cycle 1**
Dry Density	ρd, g/cm^3	1.37			Ww1	30.91	805.00	mw1	Wet	
Specific grav	ρs, g/cm^3	2.68			Wd2	14.00	701.00	md2	Dry	**Cycle 2**
Void ratio	e	0.95			Ww2	30.75	804.00	mw2	Wet	
Porosity	n	0.49			Wd3	14.81	706.00	md3	Dry	**Cycle 3**
Degree of sat	Sr	0.85			Ww3	31.07	806.00	mw3	Wet	
Liq Lim	Wl, %	105.0								
Plast Lim	Wp, %	40.0								
Plast Index	Ip, %	65.0	md, g	614.93						
Liq. Index.	Il	-0.15								

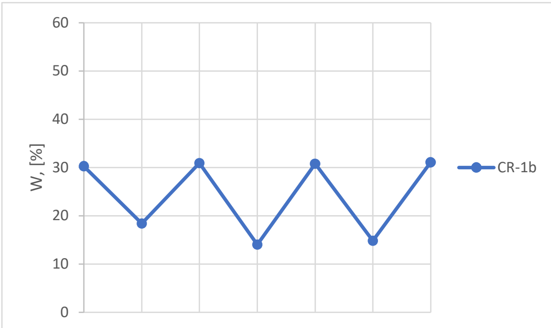

D Shear stress

Shear stress (or hydraulic shear stress) τ is the force per unit area exerted by the moving water on the soil or sediment surface and is typically expressed in Pa. In erosion processes, this hydraulic shear stress handles detaching soil particles and initiating erosion.

The initial approach to measuring hydraulic shear stress at the soil-water interface involved taking pressure readings before and after the soil sample, for example using standpipe manometers. However, due to the small and fluctuating differences in water levels caused by turbulent flow, these were replaced by a sensitive differential transducer for more accurate measurements. The method was accurate for coarse-grained soils, but the presence of a small protrusion during the testing of fine-grained soils on an Erosion Function Apparatus (EFA) introduced significant errors in the calculations as it induced a roughness much larger than the natural roughness of the soil. An experiment conducted with an aluminum cylinder replacing the soil sample in the EFA showed the considerable influence of the protrusion on the calculated shear stress (Briaud et al. [2001]). Currently, the following methods are used within various lab and in-situ tests to assess the value of shear stress during the experiment:

1. Calculation from the flow velocity: As water flows over a surface, it exerts a force tangential to that surface. This force, divided by the surface area over which it's applied, results in a shear stress. Changes in pressure or velocity can indicate changes in this force, and hence in the shear stress. (Briaud et al. [2001])
2. Differential Pressure Transducer: To overcome the limitations of direct pressure measurements, a sensitive differential pressure transducer can be used. This method supplies more accurate measurements of the small and fluctuating differences in water levels caused by turbulent flow.
3. Computational Fluid Dynamics (CFD): CFD can also be used to estimate the shear stress on the soil sample. This method involves the numerical solution of the Navier-Stokes equations, which govern fluid flow, to predict the stress distribution on the soil surface. While this method can provide highly accurate results, it is computationally intensive and requires specialized knowledge and software.

1. Flow velocity The shear stress applied to soil samples can be derived from the flow velocity using the friction factor. The formula to represent this relationship is given as

$$\tau = 1/8 f \rho v^2 \tag{D.1}$$

With:

τ - shear stress $[Pa]$.

f - friction factor obtained from the Moody diagram $[-]$.

ρ - mass density of water $[kg/m^3]$.

v - mean flow velocity in the pipe $[mm/sec]$.

The equation is derived from the Darcy-Weisbach equation, which conveys the concept of head loss due to friction in fluid flow systems. It's by combining and adapting this with other foundational fluid dynamics equations that the relationship for shear stress in terms of velocity and friction factor is derived.

The friction factor f is determined by the Moody chart. First, the Reynolds number is calculated as follows:

$$R_e = \frac{\rho V D}{\mu} \tag{D.2}$$

With:

ρ - fluid density $[g/cm^3]$.

V - average flow velocity $[m/sec]$.

μ - dynamic viscosity $[Pas]$.

Relative roughness is the dimensionless ratio of roughness height ε, to the fume hydraulic radius. Based on these two parameters the value of the friction factor is determined on the Moody chart that incorporates both laminar and turbulent flow regimes, ensuring accuracy across a broad spectrum of flow conditions. In EFA tests the value of effective roughness (ε [mm], is typically estimated as $D_{50}/2$.

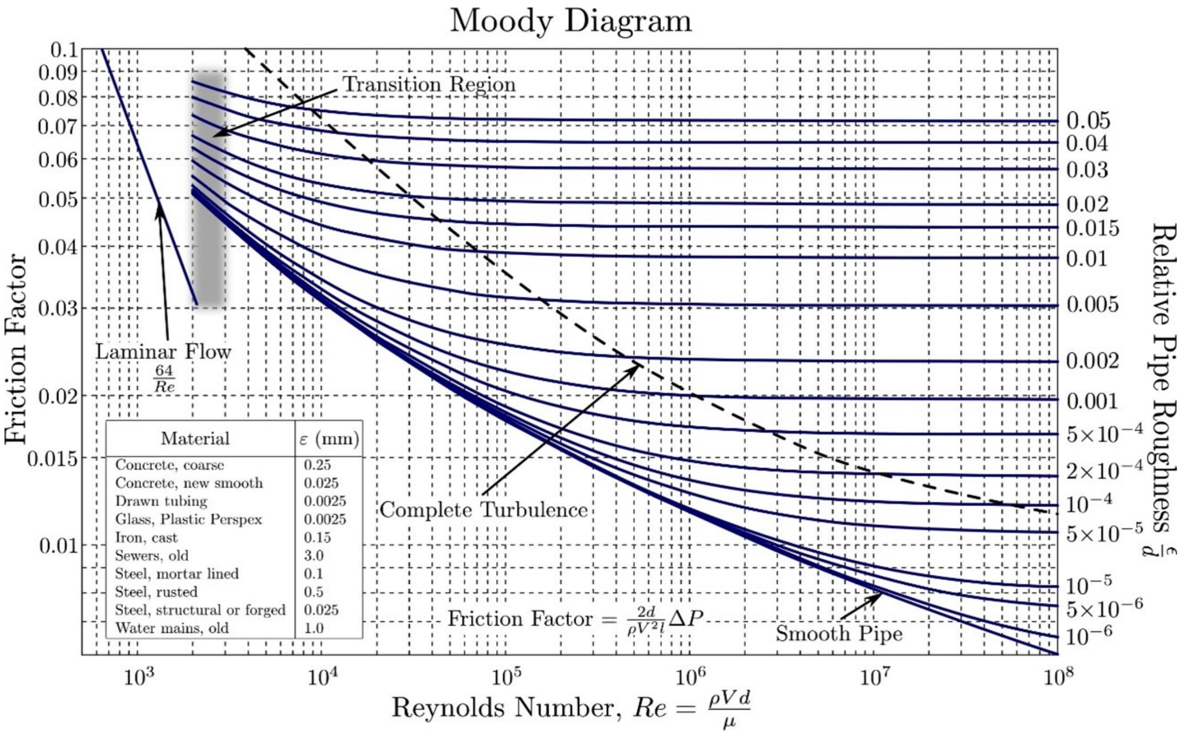

Figure D.1: Moody diagram showing the Darcy–Weisbach friction factor f plotted against Reynolds number Re for various relative roughness ε/D

The use of $D_{50}/2$ as a representative value for effective roughness height is based on the assumption that the average grain or particle size largely determines the surface roughness. This assumption holds well for initial conditions, especially when the soil surface is relatively undisturbed, and the particles are relatively uniform in their distribution on the surface. However, as erosion progresses, the surface morphology can change considerably. This has been observed through all tests since erosion forces can lead to the selective removal of certain particles and aggregates, create depressions or pits, lead to the formation of micro-rills, or even expose larger, more cohesive soil aggregates. In these evolved conditions, relying solely on to describe roughness can indeed be an oversimplification, particularly for surfaces that have undergone substantial erosive changes. To address this limitation, an alternative approach was explored to quantify effective roughness directly from side-view photographs of the eroded samples. Using the **ImageJ** software, a calibrated baseline was drawn on each photograph, representing the original surface level. Deviations from this baseline, both peaks and valleys, were then measured across the sample's profile. The effective roughness was then calculated as follows:

$$\varepsilon = \frac{1}{N}\sum_{i=1}^{N}|y_i - y_b| \tag{D.3}$$

With:

ε - effective roughness $[mm]$.

N - total number of profile points [-].

y_i - height of the $i-th$ point $[mm]$.

y_b - height of the baseline $[mm]$.

Figure D.2 below demonstrates the calculation procedure for the sample BC-4aE6. First, the photo of the side-view of the sample after the erosion test is given, followed by the processed image used for calculation in *Imagej* software. At the bottom of the figure, the roughness profile is shown.

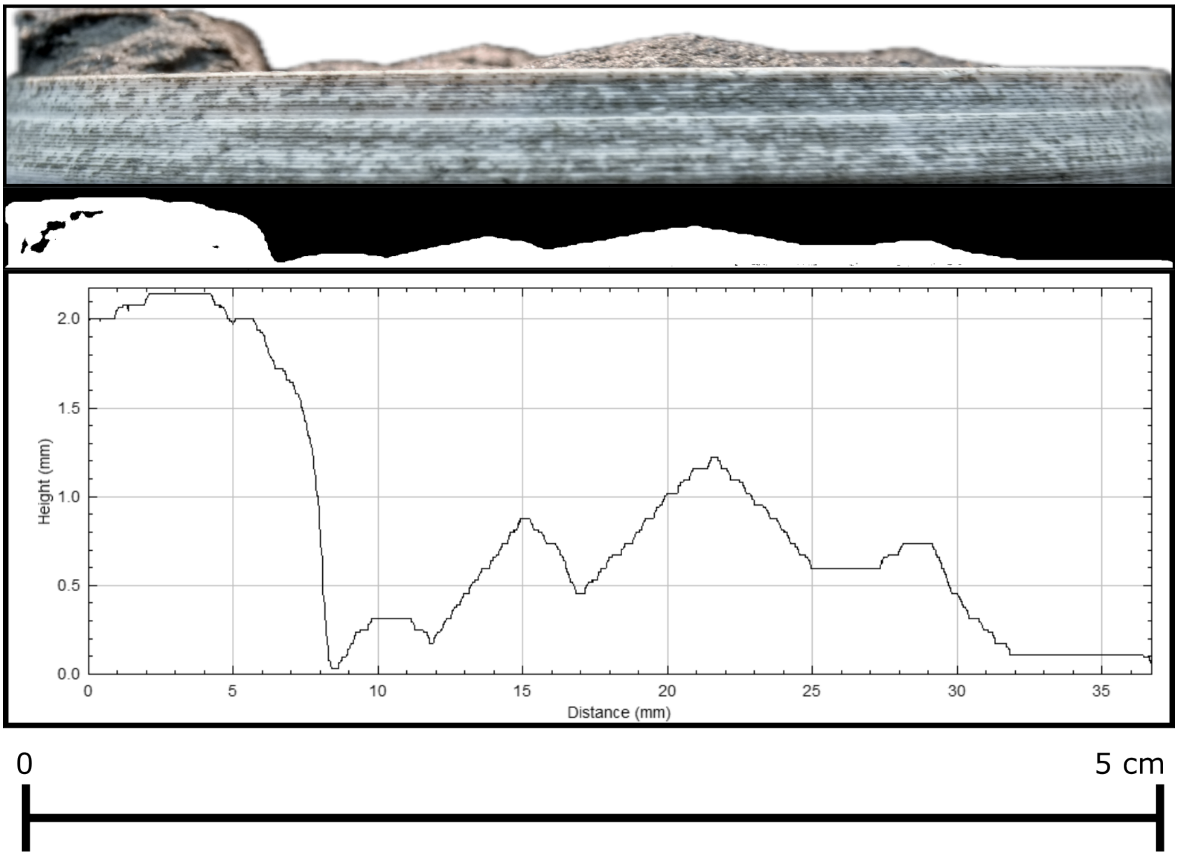

Figure D.2: calculation procedure for the sample BC-4aE6.

The obtained value was then used for the calculation of relative roughness and obtaining the value of friction ratio. The calculated value of shear stress is relevant to the end of the test, so the average of the shear stress calculated using D_{50} and the approach described above is taken as the reliable value. The derived values for shear stress, when utilizing a more detailed analysis of surface roughness, yielded results higher than those calculated solely with D_50. The comparison of shear stress for three different samples at three different flow speeds is given in Table D.1 below.

v [m/s]	ε [mm]						
	$D_{50}/2$, $2\mu m$	0.18		0.21		0.52	
	τ [Pa]						
		max	aver	max	aver	max	aver
1.5	**5.29**	7.94	**6.61**	8.23	**6.76**	10.55	**7.92**
2.5	**13.30**	21.65	**17.47**	22.51	**17.90**	29.07	**21.18**
3.5	**24.53**	42.09	**33.31**	43.79	**34.17**	56.79	**40.66**

Table D.1: Shear stress calculation results.

The side view of three samples used for calculation is shown in Figure D.3below.

While this approach offers a potentially more accurate representation, it is rather time-consuming in the current application. The average value of calculated shear stress at the beginning and conclusion of the test is used, which is based on the assumption that the sample's surface incrementally increases in roughness. This generalization, however, doesn't align with the EFA test observations, introducing an additional uncertainty. Consequently, due to the complexities and potential variances, it was resolved to use the friction ratio calculation based on D_{50} for all the tests.

However, this approach potentially allows a better understanding of the development of shear stress

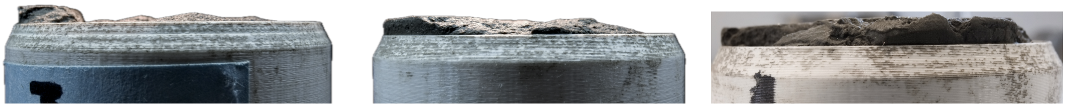

(a) BC-4aE6; $\varepsilon = 0.53mm$ (b) BC-4aE7; $\varepsilon = 0.18mm$ (c) BC-5aE1; $\varepsilon = 0.21mm$

Figure D.3: Boom Clay samples were used for relative roughness calculation.

during the tests and leads to a more accurate estimation of erodibility. The following improvements may be made to make the whole process less time-consuming and more efficient:

1. Implementing an automated photo-capturing system during tests would help with gathering consistent data on surface roughness over time. With several photos analyzed through the test, the simplification of even change of roughness will be mitigated.
2. Obtained photos might be analyzed with the specially designed script, that would aggregate all captured images, conduct an in-depth analysis, and automatically calculate the roughness, saving both time and effort.
3. Another potential improvement could be integrating real-time 3D surface scanning technology, which could provide a more detailed representation of the sample's surface at any given moment.
4. Employing machine learning algorithms might aid in predicting the progression of surface changes based on initial data, leading to more accurate shear stress calculations.

2. Pressure drop. The second method allows the calculation of shear stress from the pressure drop measurements taken immediately before and after the sample. This method uses the Darcy–Weisbach equation to derive the formula as follows (for a rectangular channel):

$$\tau = \frac{(\Delta P \times A)}{(2a + 2b) \times L} \tag{D.4}$$

With

- τ - shear stress[Pa];
- ΔP - pressure drop [Pa];
- A - cross-section area of the channel [m^2];
- $2a + 2b$ - hydraulic radius of the channel;
- L - distance between pressure reading spots [m].

The EFA set-up was equipped with two sensors that allowed the reading of the pressure drop over the sample during the test. However, due to sensor sensitivity, the fluctuations in the readings were very high. Also, after performing all tests a comparative analysis of the shear stress calculated by these two methods and the data obtained by L. Rook during the calibration of the set-up was carried out. Figure D.4 below gives a correlation of shear stress and flow velocity. The results obtained during the calibration run were compared to relevant calibration performed by L. Rook in his study and ultimately compared to the values of shear stress on a relevant speed that were calculated according to the method described above.

Based on this analysis it seems that the value of shear stress calculated from the readings of pressure drop is systematically higher than values obtained by calculation from flow velocity and data of L. Rook (Rook [2020]). Based on this and the significant fluctuations of the pressure drop readings it was decided to use the value of shear stress calculated from the flow velocities. The other advantage is that this method of obtaining shear stress is typical for EFA tests, which makes obtained results comparable with other available data.

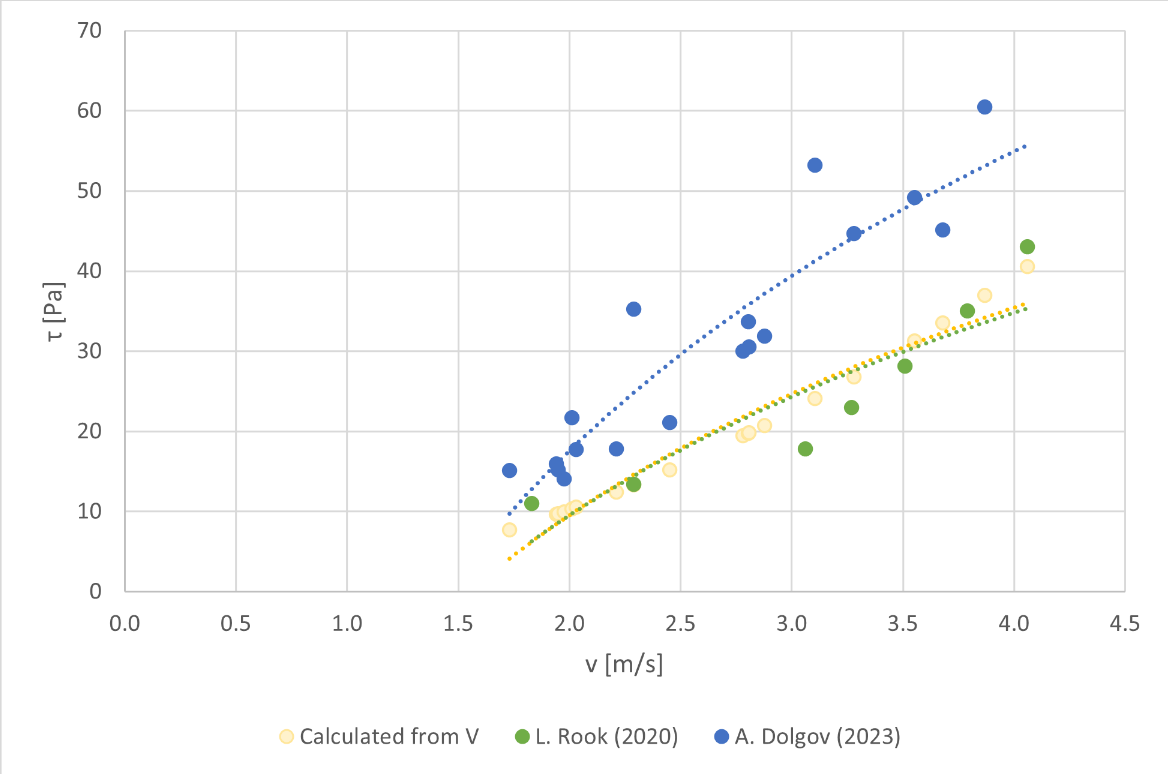

Figure D.4

3. CDF Computational Fluid Dynamics (CFD) offers a powerful approach for determining the shear stress on surfaces in fluid flow scenarios, like those in Erosion Function Apparatus (EFA) tests. By solving the Navier-Stokes equations, which describe fluid motion, CFD allows for the numerical analysis of the fluid's behavior and its interaction with surfaces. In the context of shear stress (τ) calculations, CFD provides a detailed spatial distribution of velocity and pressure fields. The wall shear stress can be directly extracted from these simulations and is given by:

$$\tau = \mu(\frac{\partial u}{\partial y})_{y=0} \tag{D.5}$$

With

- τ - shear stress[Pa];
- μ - dynamic viscosity of the fluid [Pa s];
- $\frac{\partial u}{\partial y}$ - velocity gradient at the wall [s^{-1}];

This numerical approach offers the advantage of gaining a detailed insight into flow structures, turbulence effects, and their consequent impact on shear stress distributions over complex geometries. However, it's essential to use appropriate boundary conditions, turbulence models, and grid resolution to ensure the reliability of the results. Moreover, validation against experimental data is crucial to confirm the accuracy of CFD-derived shear stress values. This kind of modeling was not carried out during the current research.

Colophon

This document is a Master Thesis for the completion of the Master of Applied Earth Science at the Delft University of Technology, Delft, The Netherlands.

Title	Effect of wetting and drying cycles on soil erodibility
Version	
Date	
Author	Alexey Dolgov s/n: 5600200
University	Delft University of Technology Civil Engineering and Geosciences
Supervisor	Prof. Cristina Jommi
Supervisor	Dr.ir. Anne-Catherine Dieudonné
Supervisor	Prof. Juan Pablo Aguilar-López
Host Company	Royal Boskalis N.V.
Supervisor	ir. Patricia Ammerlaan
Supervisor	Dr. ir. Buu-Long Nguyen

TU Delft